NATIONAL INSTITUTE OF PUBLIC HEALTH AND THE ENVIRONMENT
BILTHOVEN, THE NETHERLANDS

Report no. 722201 010

Modelling gas-phase and heterogeneous conversions of nitrogen oxides in the exhaust plume of an aircraft

A parameterization for global models

E.W. Meijer, J.P. Beck and G.J.M. Velders

December 1996

This investigation has been performed by order and for the account of the Directorate-General for Environmental Protection (DGM/GV) within the framework of project 722201: "Global Air Pollution and Climate Forcing".

National Institute of Public Health and the Environment (RIVM), P.O. Box 1,
3720 BA Bilthoven, The Netherlands
Telephone: +31 - 30 - 274 91 11, Telefax: +31 - 30 - 274 29 71

Ministerie van Volkshuisvesting, Ruimtelijke Ordening en Milieubeheer, DGM/GV, Postbus 30945, 2500 GX Den Haag

MAILING LIST

1 Directeur Geluid en Verkeer, Ir. A.J. Baayen
2 Plv. Directeur-Generaal Milieubeheer, Dr. Ir. B.C.J. Zoeteman
3 Plv. Directeur Geluid en Verkeer, Drs. H.C.G.M. Brouwer
4 Ir. J.H.A.M. Peeters, DGM/GV
5 Dr. L.A. Meyer, DGM/LE
6 Drs. J.B. Weenink, DGM/LE
7 Dr. K.R. Krijgsheld, DGM/LE
8 Ir. S.M. Smeulders, DGM/LE

9 Dr. S. Bekki, University of Cambridge (UK)
10 Dr. G. Billet, ONERA, Chatillon (F)
Dr. G. Brasseur, NCAR (USA)
Dr. ir. B. Bregman, IMAU, Utrecht
Dr. H. ten Brink, ECN, Petten
Ir. P. Brok, NLR, Amsterdam
15 Prof. dr. ir. P.J.H. Builtjes, TNO-IMW, Delft; IMAU, Utrecht
Prof. dr. P. Crutzen, MPI, Mainz (D)
Dr. F. Deidewig, DLR, Köln (D)
Dr. H. van Dop, IMAU, Utrecht
Ir. R. van Drimmelen, NLR, Amsterdam
20 Dr. R.M. Gardner, DERA, Farnborough (UK)
Dr. T. Gerz, DLR, Oberpfaffenhofen (D)
Ir. H. ten Have, NLR, Amsterdam
Dr. O. Hov, NILU, Kjeller (N)
Dr. C. Johnson, UK Met. Office, Reading (UK)
25 Dr. B. Kärcher, Universität Munchen (D)
Dr. R. Kawa, NASA/GSFC, Greenbelt, MD (USA)
Prof. dr. I.L. Karol, St. Petersburg (Russia)
Dr. H. Kelder, KNMI, De Bilt
Dr. D.E. Kinnison, LLNL, Livermore, CA (USA)
30 Dr. P. Konopka, DLR, Oberpfaffenhofen (D)
Dr. A.G. Kraabol, NILU, Kjeller (N)
Dr. M. Krol, IMAU, Utrecht
Dr. M. Kuhn, KFA, Jülich (D)
Dr. K.S. Law, University of Cambridge (UK)
35 Dr. D. Lee, AEA Technology, Harwell (UK)
Prof. dr. J. Lelieveld, IMAU, Utrecht
Dr. D. Lister, DRA, Farnborough (UK)
Dr. N. Louisnard, ONERA, Meudon (F)

Dr. P. Mirabel, Université de Strassbourg, Strassbourg (F)
Mw. C. Peletier, RLD, Den Haag
Dr. K. Pleijel, IVL, Göteborg (Zwe)
Ir. F. M. Post, RLD, Den Haag
Ir. J.W. Pulles, RLD, Den Haag
Dr. J.A. Pyle, University of Cambridge (UK)
Dr. R. Ramaroson, ONERA, Meudon (F)
Drs. M.G.M. Roemer, TNO-IMW, Delft
Dr. R. Sausen, DLR, Oberpfaffenhofen (D)
Ing. P. Scheeper, RLD, Den Haag
Prof. dr. U. Schumann, DLR, Oberpfaffenhofen (D)
Prof. dr. J. Slanina, LUW, Wageningen; ECN, Petten
Dr. A. Strand, University of Bergen, Bergen (N)
Dr. A.M. Thompson, NASA/GSFC, Greenbelt (USA)
Dr. P.F.J. van Velthoven, KNMI, De Bilt
Drs. K. Vringer, Universiteit Utrecht
Dr. A. Wahner, KFA, Jülich (D)
Dr. W.M.F. Wauben, KNMI, De Bilt

Directie RIVM
Dr. R.M. van Aalst
Ir. H.S.M.A. Diederen
Prof. ir. N.D. van Egmond
Dr. L.H.J.M. Janssen
Ir. F. Langeweg
Dr. F.A.A.M. de Leeuw
Dr. ir. D. van Lith
Drs. J.G.J. Olivier
Dr. D. Onderdelinden
Dr. R.J. Swart
Dr. R.A. Thomas
Ir. P.J.M. Valks

70 Depot Nederlandse publicaties en Nederlandse bibliografie
71-73 Auteurs
74-75 Bibliotheek RIVM
76-81 Bibliotheek LLO
82 SBD/Voorlichting en Public Relations
83 Bureau Rapportenregistratie
84-110 Bureau Rapportenbeheer

PREFACE

The research described in this report was performed as part of the Netherlands AIRFORCE project focusing on the effects of subsonic aircraft emissions on the chemical composition and subsequent radiative forcing of the atmosphere. It includes the modelling of exhaust plumes of aircraft, large-scale global effects and measurements around the tropopause. The project represents a coorperative effort of the Royal Netherlands Meteorological Institute (KNMI), the Institute of Marine and Atmospheric Research (IMAU) of the University of Utrecht, and the National Institute of Public Health and the Environment (RIVM).

The RIVM contribution to the project can be divided in two parts. In the first part, completed with this report, the chemical processes in the plume of an aircraft were studied, and a parameterization converting the aircraft emissions from the exhaust of the engines to modified emissions, representative for the aircraft plume after approximately one day, derived. In the second part, these converted emissions will be used directly as input for global models to study the impact of aircraft emissions on the composition of the atmosphere. At the end of the project, a joint report describing the current state of knowledge of atmospheric effects of aircraft emissions will be brought out by the three participating institutes.

ABSTRACT

The gas-phase and heterogeneous chemical conversion of nitrogen compounds occurring in the plume of an aircraft in the first two days after emission were investigated with a newly developed aircraft plume model. A parameterization was developed for global chemical transport models to account for the subgrid chemical processes taking place in the plume of an aircraft. The role of different plume dynamics, heterogeneous chemistry, ambient temperatures and concentrations, and different aircraft types in the chemical conversions in the plume were studied. The calculated parameters, relating the aircraft emissions to effective emissions of the aircraft plume after two days, were found to be largely dependent on season, latitude and altitude. In the North Atlantic flight corridor approximately 30% to 70%, depending on the season, of the emitted nitrogen oxides are converted to other oxides of nitrogen in the plume within the first two days.

TABLE OF CONTENTS

SUMMARY

Aircraft emissions can influence the global environment by contributing to the enhanced greenhouse effect and other large-scale atmospheric disturbances. Emitted nitrogen oxides contribute to the production of ozone at a cruise altitude of the aircraft of between 8 and 12 km. This happens in the tropopause region where changes in ozone have the largest effect on the temperature in the troposphere. The common approach to studying these effects is to use global chemistry transport models. In an early stage (shortly after emission) nitric oxide and nitrogen dioxide are efficiently converted into other reactive nitrogen compounds due to the high concentrations; this results in a diminished potential to form ozone. Since these effects cannot be taken into account in global models due to their low resolution, a plume model has been developed to study the gas-phase and heterogeneous chemical conversions in the aircraft plume occurring in the first few days after emission. The calculations with the plume model yield altitude, latitude and season-dependent conversion factors relating the NO_x (= NO + NO_2) aircraft emissions to effective emissions of reactive nitrogen compounds from the aircraft plume. From these converted emissions, accounting as they do for the subgrid plume processes, a parameterization has been developed which can be used directly for aircraft emissions in global 3D models. The parameterization is made under the assumption of discrete exhaust plumes, so corridor effects are not taken into account.

Plume model calculations have shown that the conversion of NO_x into other reactive nitrogen compounds depends highly on temperature and photochemical activity. In the North Atlantic flight corridor approximately 30% to 70%, depending on the season, of the emitted nitrogen oxides are converted to other reactive nitrogen compounds in the plume within the first two days. In summer, NO_x is much more rapidly converted to other reactive nitrogen compounds than in winter. Under typical summer conditions the converted nitrogen compounds consist mainly of HNO_3, HO_2NO_2 and N_2O_5, relative to NO_x, with increasing fractions at higher altitudes. Under typical winter conditions the main nitrogen compound is almost only N_2O_5. The formation of other species is suppressed by the low temperatures and low photochemical activity in winter. Since the concentration in the plume of other reactive nitrogen compounds (PAN, NO_3 and the organic nitrates) is low they can be ignored as an effective emission product of the aircraft plume.

In studying the role of heterogeneous reactions on sulphate aerosols, and ice and soot particles in the plume, the heterogeneous reaction of N_2O_5 on sulphate aerosols can be important since it can increases the HNO_3 concentration in the plume by a factor of 5. The influence of heterogeneous reactions of N_2O_5 on ice particles under moderate conditions is very small due to the short lifetimes of contrails. Little is known about heterogeneous reactions on soot particles. A sensitivity calculation showed that when soot particles are treated like sulphate aerosols to account for the possible binary heterogeneous nucleation of sulphate on soot particles, the heterogeneous reaction of N_2O_5 on soot can strongly influence the conversion of nitrogen oxides in the aircraft plume.

Uncertainties in the background temperatures have a large effect on the conversion of the nitrogen oxides. Preliminary sensitivity simulations show that a temperature variation of 10% at cruise altitude in summer results in a variation of 0.28 in the nitrogen oxide fraction to the sum of all reactive nitrogen compounds. The uncertainties in the concentrations of species in the ambient air around the aircraft exhaust also have a large influence. A variation in the background concentrations of 25% at cruise altitude in summer resulted in a variation of 0.20 in the nitrogen oxide fraction to the sum of all reactive nitrogen compounds. Variations in the

dispersion rates of the plume can change the volume of the plume and thereby affect the chemical reactions inside it. We found that the plume dispersion could in all cases be adequately described with constant diffusion parameters for a stably stratified atmosphere with weak turbulence without distinguishing between different levels of stratification.

The usage of different emission data for specific aircraft will clearly have some effect on the conversion processes, but proved to have only few implications for the selected cases where emission data differed between the Boeing 747-400, 767-300 and Airbus 310-200.

SAMENVATTING

Emissies van vliegtuigen kunnen bijdragen aan het versterkt broeikaseffect en aan andere grootschalige verstoringen in de atmosfeer. Geëmitteerde stikstofoxiden kunnen bijdragen aan de productie van ozon op de kruisvluchthoogte van vliegtuigen tussen 8 en 12 km. Dit is in het tropopause gebied waarin veranderingen in ozon het grootste effect hebben op de temperatuur in de troposfeer. Vaak worden deze effecten bestudeerd met mondiale chemie-transportmodellen. Door de hoge concentratie worden stikstofoxide en stikstofdioxide, direct na te zijn geëmitteerd, efficiënt omgezet in verschillende andere oxiden van stikstof, waardoor het potentieel om ozon te kunnen produceren wordt beperkt. Mondiale modellen kunnen door hun grove resolutie deze subgrid-effecten niet beschrijven. Een pluimmodel is daarom ontwikkeld om de gasfase en heterogene chemische omzettingen in de pluim van een vliegtuig direct na de emissie van uitlaatgassen te kunnen bestuderen. De pluimmodel-berekeningen resulteren in hoogte, breedtegraad en seizoensafhankelijke omzettingsfactoren waardoor de NO_x (= NO + NO_2) emissies van vliegtuigen kunnen worden vertaald in effectieve stikstofoxide-emissies van de vliegtuigpluim. Uit deze omzettingsfactoren is een parameterisatie afgeleid die de subgrid-effecten in de vliegtuigpluim verdisconteert. De parameterisatie kan direct gebruikt worden voor de emissiefactoren van vliegtuigen in mondiale 3D-modellen. In de pluimparameterisatie zijn geen corridoreffecten meegenomen.

Pluimberekeningen laten zien dat de omzetting van NO_x in andere stikstofoxiden sterk afhangt van de temperatuur en fotochemische activiteit. In the Noord-Atlantische vliegcorridor wordt, afhankelijk van het seizoen, ongeveer 30% tot 70% van de geëmitteerde NO_x binnen twee dagen in de pluim omgezet in andere stikstofverbindingen. NO_x wordt in de zomer veel sneller in NO_y omgezet dan in de winter. Onder typische zomercondities bestaan de omgezette stikstofoxiden voornamelijk uit HNO_3, HO_2NO_2 en N_2O_5, waarbij de bijdrage van deze stoffen toeneemt met toenemende hoogte, ten opzichte van NO_x. Onder karakteristieke winteromstandigheden bestaat de NO_y fractie voornamelijk uit N_2O_5. Door de lage temperatuur en fotochemische activiteit in de winter wordt de vorming van andere stoffen onderdrukt. De concentratie in de pluim van andere stikstofoxiden (PAN, NO_3 en de organische nitraten) is klein en verwaarloosbaar als een effectief emissieproduct van de vliegtuigpluim.

De bijdrage van heterogene reacties op sulfaataërosolen, ijsdeeltjes en roetdeeltjes is bestudeerd. De heterogene reactie van N_2O_5 op sulfaataërosolen kan belangrijk zijn bij lage temperaturen aangezien hierdoor de HNO_3-concentratie in de pluim een factor vijf groter kan worden. De invloed van de heterogene reactie van N_2O_5 op ijsdeeltjes is erg klein onder normale omstandigheden, door de geringe leeftijd van vliegtuigcontrails. Over heterogene reacties op roetdeeltjes is erg weinig bekend. In een gevoeligheidsberekening zijn reacties op roetdeeltjes hetzelfde behandeld als op sulfaataërosolen om mogelijke binaire heterogene vorming van sulfaataërosolen op roetdeeltjes in rekening te brengen. Deze berekening toonde aan dat de heterogene omzetting van N_2O_5 op roetdeeltjes een grote invloed kan hebben op de omzetting van stikstofoxiden in de vliegtuigpluim.

Onzekerheden in de achtergrondtemperatuur hebben een groot effect op de omzetting van stikstofoxiden. Voorlopige gevoeligheidsstudies laten zien dat variatie in temperatuur in de zomer op kruisvluchthoogte van 10% een variatie van 0,28 in de stikstofoxide fractie tot gevolg heeft, t.o.v. de som van alle stikstofverbindingen. De onzekerheden in de achtergrond concentraties van stoffen rond de vliegtuigpluim kan ook een groot effect hebben. Variatie van 25% in de achtergrondconcentraties op kruisvluchthoogte in de zomer geeft een variatie

van 0,20 in de stikstofoxidefracties, t.o.v. de som van alle stikstofverbindingen. Variaties in de dispersiesnelheid van de pluim veranderen het pluimvolume waardoor de chemische reacties in de pluim worden beïnvloed. Pluimdispersie blijkt voor alle gevallen adequaat te kunnen worden beschreven door constante diffusieparameters voor een stabiele gestratificeerde atmosfeer met zwakke turbulentie, zonder onderscheid te maken tussen het niveau van stratificatie.

Het gebruik van emissiegegevens van verschillende vliegtuigen zal zeker een effect hebben op de omzettingsprocessen, maar het gebruik van emissiegegevens van een Boeing 747-400, een Boeing 767-300 en een Airbus 310-200 resulteerde slechts in kleine verschillen in de berekende stikstoffracties.

1. INTRODUCTION

Aircraft have an effect on the composition of the atmosphere through their emission of nitrogen oxides NO_x (= NO + NO_2), CO_2, CO, hydrocarbons, water vapour, soot and sulphur oxides. An important effect is an increase in the ozone concentration, causing an enhanced greenhouse effect. This contribution of aircraft to ozone concentrations is caused mainly by the emission of nitrogen oxides. Usually, this effect is studied with global chemistry transport models. However, these global chemistry transport models have relatively coarse grids and cannot properly take into account processes on smaller spatial scales. For this reason, aircraft exhaust plume models have been developed to study the chemical conversions of aircraft emissions in the high troposphere and low stratosphere shortly after injection of the emissions. The chemical regime in the plume of an aircraft directly after the exhaust gas emissions differs completely from that of the background atmosphere in which the aircraft flies. Errors will be made when the aircraft exhaust emissions are used directly as emissions in 3D global models. One objective of plume models is to study subgrid effects of aircraft emissions to make parameterizations for global 3D models by converting the exhaust emissions of the engines to effective emissions of the exhaust plume.

The first RIVM aircraft exhaust model was developed by Veenstra *et al.* (1995). It consisted of a simple box model approach, implemented in Facsimile - a pseudo language, specially developed for box models with extensive chemistry sets (Curtis and Sweetenham, 1985). Several sensitivity runs were performed; this led to a first parameterization of the aircraft emissions used in the global 3D model, Moguntia. The model results showed an important contribution of the plume-effects: The increases in NO_x on cruising altitudes due to aircraft were for the incorporated plume effects 30-60% less than simulations without plume effects. However, the sensitivity runs showed the necessity for a more detailed simulation of the plume effects, with better descriptions of the plume chemistry and dynamics, and of the dependency on altitude, latitude and season.

Extensive sensitivity studies demand a flexible and easy-to-modify computer code. For this reason, a new aircraft exhaust model - PARANOX - has been developed in FORTRAN for the HP workstations. The model allows sequential plume calculations for different altitudes, latitudes, seasons and emission times. The main improvements of PARANOX are the use of a more up-to-date chemical scheme with additional heterogeneous reactions, height dependent photolysis rates and the implementation of the Gaussian elliptic ring structure in preference to the single box approach.

This report contains a scientific model description of PARANOX (Chapter 2) and a technical description of the software (Chapter 3). The general model results are described in Chapter 4. Chapter 5 discusses different possible descriptions of the plume dynamics, Chapter 6, the influence of heterogeneous chemistry and Chapter 7, the implications of using emission data for different types of aircraft. Finally, the main findings and conclusions are given in Chapter 8.

2. MODEL DESCRIPTION

2.1. Introduction

The model describes the chemical processes and dispersion of the exhaust plume of an aircraft at cruising altitude for different conditions by varying the time of emission, season, latitude and altitude. These variations cover most of the parameters determining the results of the model. The type of aircraft can be a Boeing 747-400, a Boeing 767-300 or an Airbus 310-200. The default is a B747-400, with a JT9D-7R4D engine, used in most studies and consequently having the best known properties.

For each situation the conversion fractions of the originally emitted nitrogen oxides NO and NO_2 (=NO_x) into other reactive nitrogen compounds are calculated for the period of typically one day. The sum of all reactive nitrogen compounds minus NO_x is defined here as NO_y (N_2O_5 is counted twice for NO_y). Calculated fractions are defined as the concentration of a specific nitrogen compound divided by the total amount of reactive nitrogen compounds (= NO_x + NO_y). This approach makes it possible to determine a differentiated nitrogen oxide emission for the global atmosphere for different seasons. Since global chemistry transport models have grids too coarse to account for these plume effects, the results of this plume model can be used to modify the NO_x emission into emissions of other reactive nitrogen compounds in the global chemistry transport model, distributed according to calculations by the plume model and taking the plume effects into account.

2.2. Dynamics of the exhaust plume

2.2.1. General description

The aircraft plume can be conveniently subdivided into three regimes (Schumann, 1994): the jet, the vortex and the dispersion regimes. These regimes correspond to the flow dynamics that control the structure and growth of the plume. In the jet regime, the plume consists of separate turbulent flows from each exhaust jet. At the end of the jet phase the flows merge and are entrained in the so-called roll-up vortex, which is caused by the airflow around the aircraft. The following vortex persists for a while, becomes unstable and breaks up, after which the dispersion regime is entered, in which the further mixing of the plume depends on the atmospheric conditions. Typical time intervals are 10 seconds for the jet regime, 100 seconds for the vortex regime and several hours up to 48 hours for the dispersion regime.

For the first two regimes of a Boeing 747-400 simple analytical calculations, performed by Miake-Lye *et al.* (1993), resulted in cross-sections in the jet regime of 3 m^2 at the beginning to about 3600-4500 m^2 at the end over a period of 10 seconds. In the following vortex, which lasted 2-3 minutes, the cross-sections increased to 21000-52000 m^2. A downward motion of the double vortex of 2.3 ± 0.2 ms^{-1} is found due to the lift of the aircraft, which is consistent with the lidar measurements of Baumann *et al.* (1993); these showed a downward motion of 2.4 ± 0.6 ms^{-1}. A statistical analysis of emitted gases along the flight path of an aircraft (Schumann and Reinhardt, 1991) showed a vertical distribution of the emitted species with a standard deviation σ_z (of the Gaussian distribution function), of 0.729 km at the time of the release. This was caused by the variations in flight altitudes: 0.860 km after 12 h, 1.014 km

after 1 day and 1.194 km after 2 days. The horizontal distribution had standard deviations σ_y, of 496, 638, 854, 1303 km after 0, 12, 24 and 48 h, respectively.

2.2.2. Gaussian plume theory for chemically reactive gases

Model calculations (Louisnard *et al.*, 1995) and measurements (Fahey *et al.*, 1995a and 1995b) have shown that NO_x conversions are negligible for the first two regimes (within 1-2 minutes). Furthermore, the detailed dynamics of the jet and the vortex regimes are far too complicated for the objectives of this model, i.e. calculating the conversion ratios of the emitted nitrogen oxides. The dynamics of this plume model (PARANOX) are described by the Gaussian plume theory for all three regimes. Although the Gaussian plume theory is strictly speaking only valid for the dispersion regime, it is also applied to the earlier stages of the exhaust gas dynamics. However, this will introduce a negligible error because of the short time span of the first two regimes.

The approach is to follow the fate of species emitted at a certain time. When defining the *x*-coordinate parallel to the flight direction, the *y*-coordinate horizontally and perpendicular to the flight direction and the *z*-coordinate in the vertical direction, this approach results in modelling a two-dimensional expanding plume cross-section in the *yz*-plane. The horizontal dispersion is much faster than the vertical, resulting in an elliptic plume cross-section. Shear is also a process that influences the plume dynamics, but its values, assumed small, for different meteorological situations are not well known. Measurements by Schumann *et al.* (1995) showed a very weak mean shear of 0.002 s^{-1}, confirming this assumption. For this reason, shear is not implemented in this model.

For a good description of a Gaussian plume with reactive gases it is necessary to divide the plume into different rings because of the non-linearity of chemical equations. Between the rings, fluxes have to be applied to describe the dispersion and the turbulent mixing caused by the chemically induced concentration fluctuations. The mathematical description of this approach was suggested by Freiberg (1976) and completed by Melo *et al.* (1978). For a chemically reactive species in ring *i*, the concentration c_i can be conveniently written in the following form:

$$\frac{dc_i}{dt} = \lambda\left(\alpha_i c_{i-1} + \beta_i c_i + \gamma_i c_{i+1}\right) + r_i \tag{1}$$

where $i=1,...,N$, with N the number of rings and r_i the net chemical formation rate. The coefficient λ is given in terms of the dispersion coefficients σ_y and σ_z by the following equation:

$$\lambda = \frac{d}{dt}\left(\ln \sigma_y \sigma_z\right) \tag{2}$$

The so-called Lusis coefficients α, β, γ are constants which depend only on the number i of the particular ring considered and the total number of rings N:

$$\alpha_i = \frac{1}{\varphi_i} \frac{\varphi_{i-1}}{\varphi_i - \varphi_{i-1}} \sum_{m=1}^{i-1} \varphi_m \tag{3}$$

$$\gamma_i = \frac{1}{\varphi_i} \frac{\varphi_{i+1}}{\varphi_{i+1} - \varphi_i} \sum_{m=1}^{i} \varphi_m \tag{4}$$

$$\beta_i = -(\alpha_i + \gamma_i) \tag{5}$$

with

$$\varphi_i = \ln\left[\frac{N-i+1}{N-1}\right] \tag{6}$$

The inner and outermost rings require special consideration. Equations 1 to 6 apply, with the following exceptions:

$$\alpha_1 = \gamma_N = 0 \tag{7}$$

$$\beta_N = \alpha_N - \frac{1}{\varphi_N}\sum_{m=1}^{N}\varphi_m \tag{8}$$

$$\varphi_N = 2\varphi_{N-1} \tag{9}$$

The effect of chemical interactions with reactive species entrained in the plume from the ambient air are taken into account by replacing r_i for the outside ring in Eq. 1 with

$$r_i = r_N + c^a \frac{\ln 4N}{\ln N} \tag{10}$$

Here c^a is the concentration in the ambient air. The surfaces of the elliptic rings can also be expressed using the above-mentioned coefficients. The surface of ring i is:

$$A_i = 2\pi\sigma_y\sigma_z\varphi_i \tag{11}$$

2.2.3. Dispersion coefficients

Traditionally, the time evolution of the dispersion coefficient σ_y and σ_z are modelled using the mixing theories based on turbulent diffusion. However, observations and regional turbulence statistics at cruising altitudes over oceans show that strong turbulence seldom occurs; the atmospheric flow is described by weak, anisotropic and decaying turbulence in a stably stratified environment, as pointed out by Dürbeck and Gerz (1995). In this case, the mixing is caused by large-scale turbulences. Practically speaking, this implies that the time evolution of the dispersion coefficient σ_y and σ_z can still be described with Eq. 12, derived from the Gaussian plume theory:

$$\sigma^2 = 2Dt + \sigma_{ini}^2 \tag{12}$$

with t (s) the elapsed time, D (m^2s^{-1}) the diffusion coefficient and σ_{ini} (m) the initial dispersion coefficient. Only the actual values of the diffusion coefficients are affected by the meteorological conditions. Two stages are distinguished in the model: before the dispersion regime (t < 100 s) and in the dispersion regime (t > 100 s).

For the dispersion regime, the diffusion constants are D_y = 20 m^2s^{-1} for the horizontal direction and D_z = 0.15 m^2s^{-1} for the vertical direction. The initial dispersion coefficients are $\sigma_{y,100}$ = 117 m and $\sigma_{z,100}$ = 83 m for a Boeing 747-400. These values are based on the results of large eddy simulations of Dürbeck and Gerz (1995). For the other types or aircraft, it is assumed that the initial horizontal dispersion coefficient is proportional to the wingspan. The initial vertical

dispersion coefficient can be derived from Eq. 13 for the maximum vertical displacement h_s (m) at a given stratification (Hoshizake *et al.*, 1975) because $\sigma_{z,100} \approx 2.2\ h_s$.

$$h_s = \frac{8W}{\pi^3 \rho_{air} N B^2 v} \tag{13}$$

In this equation, W (kg) is weight of the aircraft, ρ_{air} (kgm^{-3}) the air density, N (s^{-1}) the Brunt-Väisälä frequency, which defines the level of stratification, B (m) the wing-span width of the aircraft and v (ms^{-1}) the velocity of the aircraft. So, with a given weight, velocity and wing-span width, the initial dispersion coefficients can be calculated relative to the values for the Boeing 747-400. Table 1 gives the values for the three aircraft at cruising conditions.

Table 1. *Weight, speed and wing-span width for different aircraft at cruising conditions.*

Aircraft type	Weight (kg)	Speed (ms^{-1})	Wing-span width (m)
Boeing 747-400	3.0x10^5	250	64
Boeing 767-300	1.6x10^5	235	48
Airbus 310-200	1.3x10^5	235	44

Before the dispersion regime, the initial dispersion coefficients are estimated from an initial total cross-section of the plume of 50 m^2 for all types of aircraft. Both the vertical and horizontal initial dispersion coefficients are assumed to be equal for the initial plumes, since the jets are circular. This results in initial dispersion coefficients of $\sigma_{y,0} = \sigma_{z,0} = 2.82$ m. The diffusion coefficients for t < 100 s are estimated from Eq. 12, using the initial dispersion coefficients for t < 100 s and for t > 100 s.

2.3. Chemical mechanism

2.3.1. General

The net chemical formation rate r_i in Eq. 1 is described with the common continuity equation for chemistry for one species j:

$$\frac{dc_j}{dt} = P(t,C) - L(t,C)c_j \tag{14}$$

with P and L being the production and loss term, C the concentration vector and c_j the concentration of species j. This equation is also applied to the ambient air species in the initialization time in order to describe the diurnal fluctuations of the concentrations.

2.3.2. Gas-phase chemistry

The chemical mechanism used here is based on a scheme, very similar to the EMEP scheme (Simpson, 1992). It is adapted for the free troposphere by Strand and Hov (1994). Here, the chemistry of the radicals O(^{3}P) and O(^{1}D) is made implicit. Furthermore, the oxidation of SO_2 is incorporated in the gas-phase mechanism. Heterogeneous chemical reactions have also been added to the scheme. The chemical mechanism contains 44 species and 103 reactions, of

which 16 are photochemical, 20 inorganic and 9 heterogeneous. An overview of all gas-phase and heterogeneous reactions is given is Appendix A. All gas-phase reactions rates are updated according to DeMore *at al.* (1994). The photolysis rates are derived from calculations by Van Weele and Duynkerke (1993). The calculations were done for a mid-latitude standard atmosphere (324 DU Ozone) with clear sky conditions, a ground albedo of 0.05 and a background aerosol concentration (optical thickness of 0.2). Rainout of species is not taken into account.

2.3.3. Heterogeneous chemistry

The formation of aerosols is enhanced by the emissions from aircraft. Emitted SO_2 is partly oxidized to H_2SO_4, which enables the formation of wetted sulphate aerosols. Emitted H_2O can cause a state of supersaturation, which will possibly lead to the formation of ice particles in the plume. The sulphate aerosols formed can play a role as nucleation nuclei in the formation of ice particles; however a study by Busen and Schumann (1995) did not show any influence of emitted sulphur on the formation of contrails. Further, soot can contribute to the formation of ice particles and sulphate aerosols. In order to estimate the soot contribution to aerosol formation, it is assumed that wetted soot behaves like wetted sulphate aerosol. So, this model considers heterogeneous reactions on three types of particles: reactions on wetted sulphate aerosols, ice particles and wetted soot particles.

The fastest and therefore most important heterogeneous reaction is that of N_2O_5 on aerosols, in particular, on wetted sulphate aerosols. This reaction also represents a sink for NO_x and ozone, which is an additional important property for aircraft emission studies. Distinguishing between the different types of particles, three heterogeneous reactions with N_2O_5 are modelled:

1	$N_2O_5 + H_2O$(sulphate aerosol)	$\rightarrow$	$2HNO_3$(liquid)
2	$N_2O_5 + H_2O$(soot aerosol)	$\rightarrow$	$2HNO_3$(liquid)
3	$N_2O_5 + H_2O$(ice particle)	$\rightarrow$	$2HNO_3$(solid)

The liquid HNO_3 evaporates and contributes to the HNO_3 in the gas phase. The reaction rate constants of heterogeneous reactions are traditionally modelled with the relationship:

$$K_{het} = \frac{\gamma v S}{4} \tag{15}$$

with K_{het} (s^{-1}) the rate constant, γ the reaction probability or sticking coefficient, v (ms^{-1}) the mean absolute molecular velocity of air particles and S (m^2m^{-3}) the aerosol surface-area density. The mean absolute molecular velocity of air is given by the kinetic gas theory as:

$$v = \sqrt{\frac{8RT}{\pi M_{air}}} \tag{16}$$

with R = 8.31 $JK^{-1}mol^{-1}$ the gas constant, T (K) the temperature and M_{air} = 28.97x10^{-3} kg mol^{-1} the molar weight of air.

The reaction probability of the reaction with sulphate aerosols has been widely investigated, resulting in values in a range of 0.06 to 0.14. In tropospheric conditions with a temperature above 200 K, the reaction probability is 0.1, independent of the water content of the aerosols (DeMore *et al.*, 1994 and Fried *et al.*, 1994). So, for the reaction with sulphate aerosol a value

of 0.1 is used. The surface-area density of sulphate aerosols for background conditions is set at 0.6×10^{-8} cm^{-1}, adopted from Danilin *et al.* (1994). Measurements of exhaust plumes from a Concorde (Fahey *et al.* , 1995a) showed that at least 12% to 45% of the emitted sulphur was oxidized to H_2SO_4. Model calculations (Fahey *et al.*, 1995a) based on these results predicted 70% wetted sulphate aerosols with an initial mean diameter of 0.016 μm and an initial surface-area density of 8.0×10^{-8} cm^{-1}. Normally, coagulation would rapidly diminish the total surface-area density, as shown by Fahey *et al.* (1995a). However, coagulation in an aircraft exhaust can be neglected by assuming that the growth of the plume nullifies the collision frequencies of the particles. So, in this case the mean particle radius and the initial surface-area density is used to calculate an initial sulphate aerosol concentration. This which will diminish in time only by growth of the plume, resulting in a declining sulphate aerosol surface-area density inside the plume.

Experimental data on the reaction probability of the reaction on wetted soot aerosols is not available and therefore taken the same as on sulphate aerosols, that is 0.1. This value is probably an upper limit for the reaction probability. The aerosol surface-area density of wetted soot S_s is modelled according to Danilin *et al.* (1994):

$$S_s = 4\pi r_s^2 \, c_s \, (\mathrm{CCN/CN}) \tag{17}$$

with r_s the mean particle radius of soot, c_s the concentration of soot particles and CCN/CN the ratio of cloud condensation nuclei over condensation nuclei. The radius is set to 0.5 μm and corresponds to Danilin *et al.* (1994). The soot particle concentration and CCN/CN have a large variety of values. Danilin adopted the largest possible values (CCN/CN=0.4 and $c_s = 10^6$ cm^{-3}), although the lower values are more realistic: Hudson *et al.* (1991) mentions values for CCN/CN of 0.008 and 0.01, with a soot particle concentration of approximately 5×10^3 cm^{-3} for jet fuel. Zhao and Turco (1995) report CCN/CN values less than a few per cent, Rosen and McGreegor (1974) measured a soot particle concentration of about 2.5×10^4 cm^{-3} and Hallet *et al.* (1989) measured a CCN/CN of 0.01. Extremely low values were used by Louisnard *et al.* (1995), namely a soot particle concentration of about 5×10^2 cm^{-3} and radii of less than 0.2μm. Based on the intermediate values found in several studies, the initial soot particle concentration is set at 10^4 cm^{-3} and CCN/CN to 0.01.

A reaction probability of 0.03 is used for the reaction on ice particles, this value corresponding with that of DeMore *et al.* (1994). Large aircraft emissions of water vapour at high altitudes can result in a supersaturated water vapour concentration inside the plume, allowing the formation of contrail ice particles. A general criterion is stated by Appleman (1953), defining the meteorological state of the atmosphere. A more detailed criterion was derived by Iribarne and Godson (1992). The occurrence of contrails are predicted whenever the ambient pressure p_{amb} exceeds a critical pressure p_{cr}, defined by:

$$p_{amb} > p_{cr} = \frac{M_{air}\sigma^2 p^{sat} L_v}{C_p R T^2} \frac{Q}{EI_{H_2O}} \left(1 + \sqrt{2(1 - S_a)}\right) \tag{18}$$

In this equation, $M_{air} = 28.97 \times 10^{-3}$ kg mol^{-1} is the molar weight of dry air, $\sigma = 0.622$ a constant (molar weight of water vapour divided by molar weight of dry air), p^{sat} (Pa) the saturation vapour pressure over water, L_v (J kg^{-1}) the specific latent heat, C_p = 1005 J kg^{-1}K^{-1} the specific heat capacity of water, R = 8.31 J K^{-1}mol^{-1} the gas constant, T (K) the temperature, Q = 4.2×10^6 J kg^{-1} the specific heat of combustion of the jet engine, EI_{H_2O}= 1.26 kg kg^{-1} the

emission index of water vapour emitted by the jet engine and S_a the relative humidity in the ambient air, given as a fraction. The saturation pressure, depending on the temperature T (K), was derived by Marti and Mauersberger (1993):

$$p^{sat} = 10^{-2663.5/T+12.537} \tag{19}$$

The latent heat also depending on the temperature, is given by the empirical relationship of Pruppacher and Klett (1980):

$$L_v = 2.497x10^6\left(\frac{273.15}{T}\right)^{0.167+3.67x10^{-4}T} \tag{20}$$

If this criterion (Eq. 18) is satisfied, it is assumed that all the water vapour exceeding the saturation concentration is frozen, which is in agreement with the measurement of Knollenberg (1972). The water vapour saturation H_2O^{sat} (molec cm^{-3}) concentration is directly related to the saturation pressure:

$$H_2O^{sat} = \frac{p^{sat}}{k_B T} \tag{21}$$

with T the temperature (K), k_B Boltzmann's constant and p^{sat} the saturation pressure (Pa). Field measurements in persistent contrails by Knollenberg (1972) showed ice particles with bullet-like shapes. These can be regarded as cylindrical particles with a mean diameter of 0.1 mm and a height of 0.5 mm. Using the equations for volume and surface of a cylinder and the above-mentioned assumption, the following equation for the surface-area density of ice S_{ice} (m^2m^{-3}) can be derived:

$$S_{ice} = \left(\frac{2}{h}+\frac{4}{d}\right)\frac{M_{ice}\left(H_2O - H_2O^{sat}\right)}{\rho_{ice} N_a} \tag{22}$$

with h (cm) and d (cm) the mean height and diameter of the cylindrical ice part, M_{ice} = 18x10^3 kg the molar weight of ice, ρ_{ice} = 0.928x10^{-3} kg cm^{-3} the density of ice, H_2O (molec cm^{-3}) the water vapour concentration and N_A the Avogadro number.

Other heterogeneous reactions in the troposphere occur but much slower. Under background conditions all other reactions are found to be proportional to the reaction of N_2O_5 on sulphate aerosol (Isaksen and Rodhe, 1978 and Dentener and Crutzen, 1993). The proportionality factors have been estimated in order to model the other heterogeneous reactions, listed per species in Table 2.

Table 2. *Proportionality factors of the heterogeneous reactions on sulphate aerosols relative to reaction of N_2O_5 on sulphate aerosols (Appendix A, nh1 under "heterogeneous reactions"). Values derived from Isaksen and Rodhe (1978).*

Species	Proportionality factor ($x10^{-4}$)
HNO_3	9.16
H_2O_2	30.58
CH_3OOH	30.58
HCHO	18.31
ethanal	18.31
PAN	1.83

2.4. Emissions

2.4.1. The Boeing 747- 400

The model considers three types of aircraft: a B747-400 airliner, a B767-300 and an A310-200. The best studied aircraft is the B747-400, with engine JT9D-7R4D, for which emissions were derived from studies by Schumann (1994) and Olivier (1991). The emissions are treated as concentrations C_{em} (molec cm^{-3}) in the initial plume cross-section A_{ini} of 50 m^2, and depend on the emission indices EI (g kg^{-1}), the speed of the aircraft and fuel use f (kg s^{-1}):

$$C_{em} = \frac{fEI}{M_w A_{ini}} N_a \tag{23}$$

In this equation M_w is the molar weight of the emitted species and N_a, Avogadro's number. Table 3 illustrates the emission data of a B747-400, according to Schumann (1994) and Olivier (1991).

Table 3. *Emissions from a B747-400 at flight altitude with a speed of 250 ms^{-1} and a fuel use of 2.9 kg s^{-1}.*

Species	EI (g kg^{-1})	Margin	Emission(g s^{-1})	Molar weight
CO_2	3150		9135	44
H_2O	1260		3654	18
NO_x (as NO_2)	16	7-20	46.4	46
CO	1.5	1.5-10	4.35	28
Hydrocarbons	0.6	0.2-3	1.73	
soot	0.015	±0.014	0.043	12
SO_2	1	0.02-6	2.88	64

The emissions of the different hydrocarbons are based on the total emissions and the measured distribution of hydrocarbons (Shareef *et al.*, 1988). The distribution profile is displayed as hydrocarbon fractions in Table 4.

Table 4. *Hydrocarbon fractions of the total emitted hydrocarbons per species per molecule according to Shareef et al. (1988).*

Hydrocarbon	Emitted fraction
CH_4	0.268248
C_2H_6	0.013750
C_2H_4	0.216896
C_3H_6	0.167908
n-C_4H_{10}	0.013497
HCHO	0.184800
CH_3CHO	0.086150
HCOCHO	0.017129
CH_3COCHO	0.009899
C_8H_{10}	0.021723
total	1.000000

Other emission data were derived from the aircraft emission model FLEM of the Dutch Civil Aviation Department (Pulles *et al.,* 1995) for a B747-400, a B767-300 and an Airbus 310-200. This model predicts somewhat lower emission indices; the data can be used for sensitivity calculations. The same hydrocarbon profile is applied.

2.5. Meteorological data and background concentrations

The model uses meteorological data and background concentrations derived from the TNO version of the global two-dimensional model of Isaksen and Rodhe (1978). The meteorological data consists of seasonally varying temperatures and air densities for 90^0S to 90^0N in gradations of 10^0 for vertical layers of 1 km from sea level to 16 km. The TNO model calculated monthly global concentrations of all inorganic species and most of the hydrocarbons. The monthly concentrations are used as input for the background concentrations.

2.6. Numerical method

The combined Eqs. 1 and 14 were solved using the two-step method (Verwer, 1993). The method is specially designed to solve ordinary differential equations (ODEs) from atmospheric chemistry, providing fast convergence with reasonable accuracy in the order of 1%, depending on the stiffness of the equations. The method is based on the second-order backward differentiated equation, commonly used in high-precision implicit solvers, but is instead applied to a straightforward Gauss-Seidel iteration.

3. TECHNICAL DESCRIPTION

3.1. General description

The model is written in FORTRAN for HP workstations and is not tested for other environments. The source code has been tested with the utility LINTFOR (part of the HP-UX system) and the programs QAF and FORCHECK. All variables are declared explicitly with an explanation. All source code files are equal to the routine name with extension "f", except for the output routines, which are placed in the file "output.f". A list of source-code files and input files is given in Appendix B.

3.2. Description of the source code

3.2.1. Main structure

The main routine is called “PARANOX”. The relationships between the subroutines and the main routine are shown in Scheme 1.

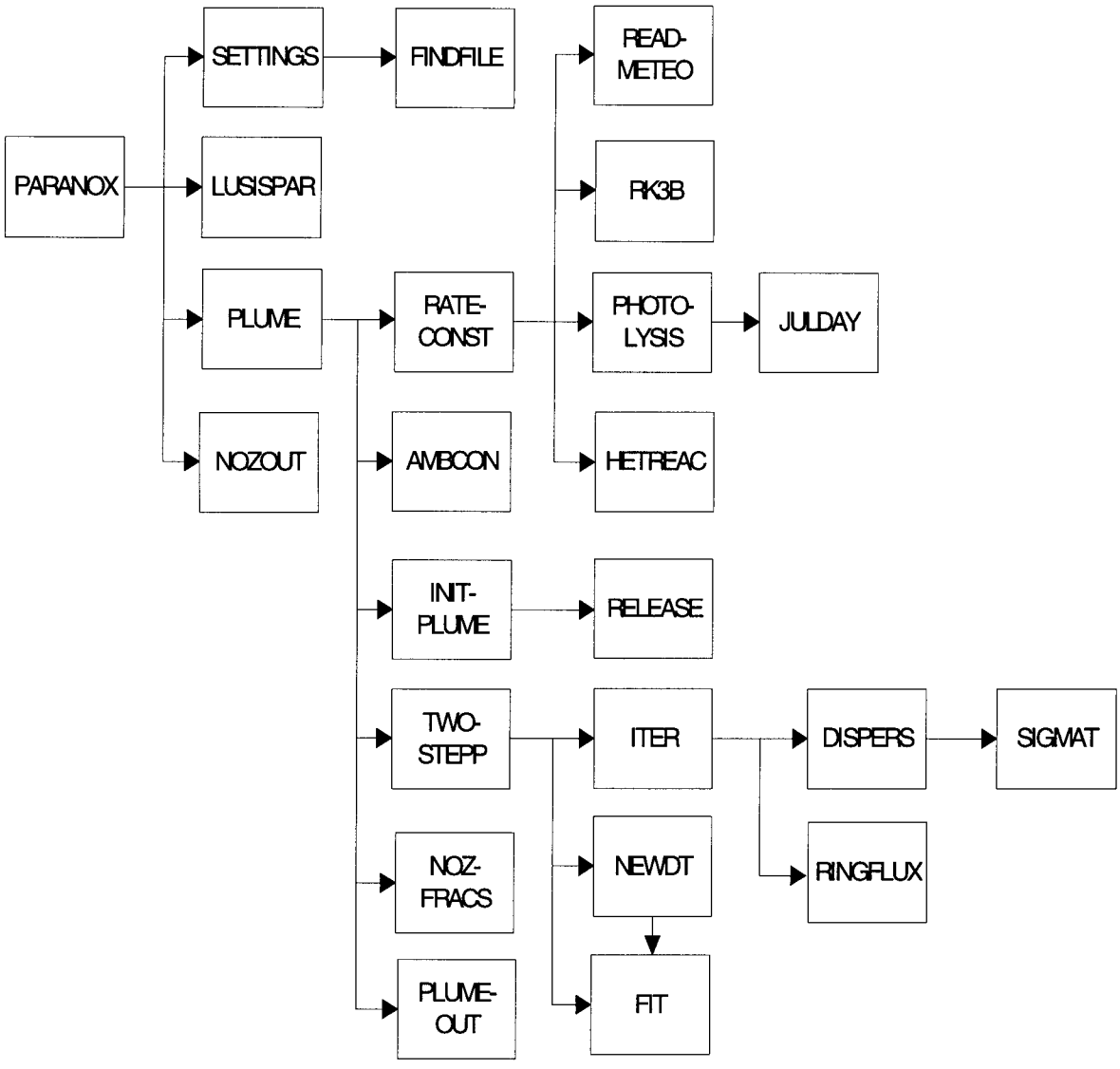

Scheme 1. The relationships between the subroutines and the main routine in PARANOX 1.4. The level of the program from left to right is and the order in time of execution from top to bottom are given. Repetition of calls due to loops are not represented in this scheme.

The function and role of each routine in alphabetical order:

- AMBCON: Initializes the concentrations (molec cm^{-3}) of the ambient reactive species and water vapour per month, latitude and altitude. The data is derived from the TNO 2D model.
- DISPERS: Calculates the dispersion coefficient λ in Eq. 1 by taking a linear approximation of the derivative in Eq. 2.
- FINDFILE: Function for opening files with a given filename and unit number.
- HETREAC: Calculates the rate constants of the heterogeneous reactions.
- INITPLUME: Initializes the concentrations (molec cm^{-3}) in the plume per elliptic ring for a given number of rings and the emission given as mean initial concentrations.

- ITER: Defines the production and loss terms of Eqs. 1 and 13 to evaluate the gas-phase and heterogeneous chemistry, and the dispersion and mixing of the plume for each elliptic ring of the plume. The evaluation takes place in routine TWOSTEPP.
- JULDAY: Function for calculating the Julian day number of the first day of a given month.
- LUSISPAR: Initializes the ring structure for a plume divided into a given number of elliptic rings. Calculation of the Lusis coefficients, α, β and γ, as defined with Eqs. 3, 4 and 6 and the squared radii in y- and z-coordinates of each ring.
- NOZFRACS: Calculates the fractions of remaining NO and NO_2 and all other reactive nitrogen compounds produced from the emitted nitrogen oxides in the plume.
- NOZOUT: Output of the remaining reactive nitrogen fractions at the end of a single-plume simulation.
- PARANOX: Main routine. Contains the loops over the grid, and over time and releases.
- PHOTOLYSIS: Calculates the photolysis rate coefficients as a function of height and solar zenith angle, based on data by Van Weele and Duynkerke (1993).
- PLUME: Main routine for the plume calculation and the ambient air chemistry.
- PLUMEOUT: Detailed output at given time intervals of the concentrations of the major species for each ring in the plume in ppbv and the reactive nitrogen fractions.
- RATECONST: Initialization of the reaction-rate constants and some stoichiometric constants that appear in the reaction scheme.
- READMETEO: Reads meteorological data from the output of the TNO 2D-model; the temperature (K), the air density (molec cm^{-3}) and the water vapour concentration (molec cm^{-3}).
- RELEASE: Initialization of the emissions from B747-400 airliner at cruising altitude with a fuel use of 2.9 kg s^{-1}. The emissions are given as mean plume concentrations (molec cm^{-3}).
- RINGFLUX: Calculates the fluxes into and out of all species in a given elliptic ring of the plume. The total in-flux of a species in ring i is defined as $\lambda(\alpha c_{i-1}+\gamma c_{i+1})$ and the total out-flux as $\lambda\beta c_i$.
- RK3B: Function for calculating the rate constant of a termolecular reaction according to the definition given in the LACTOZ report (Wirtz *et al.*, 1994), also stated in Eq. 19 in Appendix A.
- SETTINGS: Reads the user-defined run parameters from the input file "PARAM" and opens all data input files.
- SIGMAT: Calculation of the dispersion coefficient of given coordinate direction by solving Eq. 12 with given parameters depending on the dynamics regime ($t < 100$ s or $t > 100$ s).
- TWOSTEPP: Implementation of the two-step method of Verwer (1993) for solving the combined Eqs. 1 and 14.

3.2.2. Basic run description

The main routine PARANOX contains the loops over the plume per latitude, altitude, months, emission times and time-loop. These loops are user-defined in input file "PARAM" (see 3.2.1). So, the routine starts with the initialization of the user-defined parameters and enters the above-mentioned loops. The loops contain only a reset of the time variables and a call to routine PLUME, which is the routine for the actual plume simulation of a plume at a given latitude, altitude, month, emission time and actual lifetime of the plume. At the end of the time-loop the basic output of the remaining reactive nitrogen compounds is complete.

3.3. Input and output

3.3.1. Input of user-defined parameters

The user of the model defines the parameters of each run using of the input file "PARAM". An example of this file is given below:

```
PARAMETER FILE FOR PARANOX $Revision: 1.4 $
-----------------------------------------------------------------------
START LATITUDE    = -90
LAST LATITUDE     = 90
STEPSIZE LAT.     = 10
START HEIGHT(km)  = 5
STOP HEIGHT (km)  = 12
STEPSIZE HGT(km)  = 1
FIRST MONTH       = 1
LAST MONTH        = 10
STEPSIZE MONTH    = 3
RELEASES          = 4
RELEASE TIMES(hr)= 0.,6.,12.,18.
AIRCRAFT TYPE     = 1 (1=B747-400,NLR;2=B767-300,3=A310=200,4=B747-400)
TIMESTEP (s)      = 50.
STOP TIME (hr)    = 48.
INIT TIME (hr)    = 24.
RTOL    (TWOSTEP) = 0.01
DTMIN   (TWOSTEP) = .1
DTMAX   (TWOSTEP) = 50.
NUMIT   (TWOSTEP) = 2
NUMBER OF RINGS   = 10
NOZFRACS FILE     = ./fnoz.glob
DETAILED OUTPUT   = .false.
OUTPUT TIME (s)   = 3600.
AMBIENT AIR FILE = ./input/ambcon2D.dat
```

```
METEO FILE        = ./input/meteo2D.dat
PHOTOLYSIS FILE   = ./input/jvalmvw.dat
HETCHEM FILE      = ./input/hetchem.dat
```

The parameters START LATITUDE, LAST LATITUDE and STEPSIZE LAT. are integers and define the loop over the latitudes. The minimal stepsize is 10 degrees. Negative values are used for the Southern Hemisphere.

The parameters START HEIGHT, STOP HEIGHT and STEPSIZE HGT define the loop over altitudes (km). The values are integers. The minimal altitude is 5 km, the maximum altitude 12 km and the minimal stepsize 1 km.

The parameters FIRST MONTH, LAST MONTH and STEPSIZE MONTH define the loop over the months. The values are integers.

The parameters RELEASES and RELEASE TIMES (hr) define the number of releases in one day (per latitude, altitude and month). RELEASES is an integer and RELEASE TIMES is an array of real numbers. The release times are separated by a comma.

The parameters TIMESTEP (s), STOP TIME (hr) and INIT TIME (hr) define the time loop over a single plume and are given in real numbers. The STOP TIME defines the lifetime of the plume: INIT TIME is the initialization period for the ambient air chemistry. Note that the total simulation time per plume is equal to INIT TIME + RELEASE TIME + STOP TIME. The default choice of TIMESTEP is 50 s. For most simulations this value could be higher, with a maximum of 300 s; however, with the default value the model is more stable.

The parameters RTOL (real), DTMIN (s), DTMAX (s) and NUMIT (integer) are used in the two-step method (Verwer, 1993). RTOL defines the relative tolerance for all species and the absolute tolerance by making this equal to 1.0E-06 times the relative tolerance. DTMIN and DTMAX represents the real number and define the minimum and maximum time steps. NUMIT defines the number of iterations per time step. The settings RTOL=0.01, DTMIN=0.1, DTMAX=50 and NUMIT=2 are the optimal values. The two-step method is not very sensitive to the parameters RTOL, DTMIN and NUMIT, but the value of DTMAX=50 s is a maximum value. Exceeding this value causes loss of precision. Current precision lies in the range of 5%.

The NUMBER OF RINGS defines the number of elliptic rings in the Gaussian plume. Ten is a sufficient value.

NOZFRACS FILE represents the names of the output file with the fractions of the reactive nitrogen compounds per release time, month, latitude and altitude. The file must be non-existent in order to prevent accidental overwriting of older model results.

DETAILED OUTPUT is a logical parameter determining the use of detailed output generated by subroutine PLUMEOUT. The parameter OUTPUT TIME (s) is the time interval for the detailed output.

The parameters to be set in the model for the numerical integration are the minimal iteration time step DTMIN (s), the maximum DTMAX (s), the number of subdivisions of the NUMIT iterations, the absolute and relative tolerances ATOL and RTOL per species and the model time step TIMESTEP. These parameters are set by the input file PARAM (see Chapter 3). The optimal values are DTMIN = 0.1 s, DTMAX = 50 s, NUMIT = 2, RTOL = 0.01, ATOL = 10^{-7} and TIMESTEP = 50 s. With these settings an accuracy of 95% or higher is achieved, which is sufficient, given the external uncertainties.

The remaining parameters are the locations and the filenames of the input files, which are discussed below.

3.3.2. Input files

The model requires the following input files:

- **Ambient concentrations**

The default input file is AMBCON2D.DAT and contains the concentrations from the TNO 2D model.

- **Photolysis rate data**

The default input file is JVALMVW.DAT. The photolysis rates were calculated by Van Weele and Duynkerke (1993) for a mid-latitude standard atmosphere (324 DU ozone) with clear-sky conditions, a ground albedo of 0.05 and a background aerosol concentration (optical thickness of 0.2). The data contains the rates for 0 to 12 km, with intervals of 1 km.

- **Meteorological data**

The default input file is METEO2D.DAT and contains the densities (molec cm^{-3}), the temperatures (K) and the water vapour concentrations (molec cm^{-3}) from the TNO 2D model.

- **Heterogeneous chemistry data**

The default input file is HETCHEM.DAT and contains flags for activating or de-activating the heterogeneous reactions. The default settings use only the reactions of N_2O_5 on sulphate aerosol and contrail ice particles.

All reading is done by subroutine AMBCON and is specific for the above-mentioned input files, so changing the input requires changes in the computer code.

3.3.3. Output files

The major output file contains the fractions of reactive nitrogen compounds at the end of the plume simulation. The name of that file is user-defined. The file contains a header, which is a copy of the header of the input file "PARAM" and the table header. The data is labelled with the latitude, altitude, month and release time. The data is separated by commas, simplifying the import into spreadsheet software and software for graphical representation as in IDL programs.

The so-called detailed output is optional; it contains time evolution concentrations (ppbv) of the major species and the fractions of the reactive nitrogen compounds for each plume simulation. The filenames per plume have self-generated names in the form abxxyyzz, with an (absolute) latitude divided by 10; b is "n" or "s" for the Northern or Southern Hemisphere, xx the altitude, yy the month number and zz the time of release. The concentration output files have extension "con", whereas the fraction output files have the extension "noz". For example, the file "5n080712.con" contains the concentrations of a plume emitted at 50^0N at an altitude of 8 km on 1 July at 12:00.

3.3.4. Debugging information

The source code of PARANOX has additional routines for generating information for debugging and testing. These routines generate a large amount of output data. It is recommended to use this debugging information only for single-plume calculations.

Normally, these routines are not active. These routines are activated by re-compiling the source code with the option "-D" (see the HP-UX manual for more details). The following debugging routines are available:

- DEBUG1: Output of the concentration and production and loss terms per species. The filename is "chem.db1".
- DEBUG2: Output of the photolysis rates. The filename is "photol.db2".
- DEBUG3: Output of the initial ambient concentrations. The filename is "ambient.db3".
- DEBUG4: Output of the meteorological data. The filename is "meteo.db4".
- DEBUG5: Output of the rate constants and stoichiometric constants. The filename is "ratcon.db5".
- DEBUG6: Output of the initial Gaussian distribution. The filename is "initial.db6".
- DEBUG7: Output of the time evolution of all species per ring, including the inert species H_2O, soot and sulphate aerosol in order to evaluate the Gaussian-distribution evolution. The output of the concentrations is in ppbv, except for the inert species. The filename is "plume.db7".
- DEBUG8: Output of the total number of nitrogen atoms and water molecules in the plume as a test for mass conservation. The filename is "mass.db8".
- DEBUG9: Output of the time evolution of the dispersion coefficients σ_y and σ_z, and the total cross-section surface of the plume. The filename is "surf.db9".
- DEBUGA: Output of the emissions as mean concentrations in the initial plume. The filename is "emitted.dba".

4. GENERAL RESULTS

4.1. Introduction

In this chapter the version of the model PARANOX as described in Chapters 2 and 3 is used for calculation of the distribution of the emissions of an aircraft at a latitude of 50° N and at an altitude of 10 km at cruising speed, which can be regarded as a representation of an airliner in the North Atlantic Flight Corridor (NAFC), the most important flight route between the United States and Europe. Also, a full sweep through the global domain over the year with different emission times has been performed for gaining insight in the spatial and temporal dependencies. The selected aircraft is a B747-400, with emission data from Schumann (1994) and Olivier (1991) and the heterogeneous chemistry is restricted to the reaction of N_2O_5 on sulphate aerosol and contrail ice particles. The plume is divided into 10 elliptical rings and was evaluated for a period of 48 hours.

4.2. Results for an airliner in the NAFC

Some of the details of the dynamics and the chemistry of the exhaust plume were first studied. The emission took place at noon in July. Figures 1 to 5 (Appendix C) show the time evolution of the concentrations of the inner, middle and outer ring in the plume for NO, NO_2, HNO_3, HO_2NO_2 and O_3. The ambient concentrations for these species are approximately 85 ppbv for ozone, 0.05 ppbv for NO_x, 0.5 ppbv for HNO_3 and 0.1 ppbv HO_2NO_2.

Directly after the NO_x emissions their concentrations are so high that the reaction NO + O_3 causes O_3 to drop to very low values (far below the ambient concentration). The concentrations of NO and NO_2, which are much higher than those in the background atmosphere, decrease rapidly by the expansion of the plume. The destruction of O_3 by NO diminishes and O_3 is effectively produced from the oxidation of hydrocarbons and by the photolysis of NO_2, within the first few hours after emission. After approximately seven hours the decrease in sunlight (sunset) reduces the production of O_3 while in the inner rings of the plume the NO concentration is still relatively high, causing the photostationary state to tend towards the NO_2 side which reducing O_3. During the night (8-16 h) the concentration of NO_2 decreases by the formation of N_2O_5 and by the expanding volume of the plume. Since in the dark no ozone is produced the increase in concentration inside the plume arises from the influx from ambient air with higher mixing ratio. In the morning (16 h after emission) when sunlight returns, NO_2 is converted to NO and O_3 is produced again.

The elevated level of NO_2 after the emission results also in the production of HNO_3 and HO_2NO_2 by the reaction with OH and HO_2, respectively. In the first minutes after emission the lack of OH and HO_2 inhibit the production of HNO_3 and HO_2NO_2. During the night the production is stopped and the concentrations of HNO_3 and HO_2NO_2 decrease through the expansion of the plume volume.

After 24 hours the ozone concentrations in the elliptic rings exceed the background concentration of 85 ppbv. NO_x and the other reactive nitrogen compounds still exceed the background concentrations after 48 hours. However, a period of 48 hours is commonly regarded as the maximum lifetime of an aircraft exhaust plume. Combined with the fact that ozone inside the plume exceeds the background concentration after 24 hours, it can be

concluded that a 48-hour period should be sufficient to estimate the conversion ratios of the reactive nitrogen compounds inside a plume.

The conversion of emitted NO_x into other reactive nitrogen compounds, NO_y, can be expressed in fractions of the total reactive nitrogen compounds ($NO_x + NO_y = 1$). At the start of the release only NO and NO_2 are emitted, so the initial fraction of NO_x is 1. Figures 6 and 7 represent the time evolution of the reactive nitrogen compounds for emissions at noon in the NAFC for the months January (winter) and July (summer). The concentrations of the species is from now on always taken as the average over all rings in the plume model. Besides the NO_x and NO_y fractions, the fractions of the major NO_y species, namely HNO_3, HO_2NO_2 and N_2O_5, have been included in the figures. The large differences between results for January and July reveal a large temperature and photolysis dependence of the conversion processes of nitrogen oxides. In summer (July) the formation of NO_y is much higher than in winter (January). In January the NO_y fraction consists almost only of N_2O_5, whereas the main contributor of NO_y in July is HNO_3. The formation of HNO_3 from N_2O_5 and NO_2 depends apparently very much on the temperature. The main processes in the formation of NO_y starts with the formation of N_2O_5 from NO_2 and NO_3. Since the NO_3 concentrations inside the plume are very low, it can be concluded that this reaction is immediate. In July the formation of HNO_3 from the reaction of NO_2 and OH is important, but is suppressed in January by the lower temperature. In July N_2O_5 is formed during the night and photodissociated to NO_2 and NO_3, while N_2O_5 is also directly converted to HNO_3 through the reaction with water vapour and the heterogeneous reaction on sulphate aerosol.

The photodissociation of N_2O_5 and other species plays an important role in the conversion processes, implying a dependence on the release time, especially in summer. In Fig. 8, the time evolution of the fraction of reactive nitrogen compounds in July is given, with a release time at midnight. The day–night patterns are similar to those in Fig. 7. Within a period of 48 hours, there are now two nighttime periods with formation of N_2O_5 followed by photodissociation of N_2O_5 and NO_3 in the morning, which results in a lower fraction of NO_x at the end of 0.24 instead of 0.26. This small difference can be explained by the fast conversion of NO_x to NO_y during the first 24 hours, thus suppressing the influence of the different emission times.

In the model the conditions in the NAFC are determined mainly by the concentrations of the species in the ambient air and the temperatures. To estimate the influence of the background concentrations and the temperature additional simulations have been performed with estimated minimum and maximum values of these parameters. Figure 9 represents the influence of the uncertainties in the background concentrations by showing the time evolution of the reactive nitrogen compounds NO_x and NO_y for the normal background concentrations and with 25% higher and lower background concentrations for all species. In the end the fractions vary by about 0.2. Figure 10 shows the time evolution of the reactive nitrogen compounds NO_x and NO_y for normal temperature with a variation of 10%. Here the variation of the fractions is much larger: about 0.275 after 48 h and much larger differences at the first 24 hours.

4.3. Results for the global domain

To gain insight into the variation in latitudes and altitudes, simulations have been done for altitudes of 5 to 12 km and for latitudes of 90^0S to 90^0N. In Figs. 11 to 14 the fractions NO_x are given for the months January, April, July and October averaged over emission times of 0.00, 6.00, 12.00 and 18.00.

For all these reactive nitrogen compounds a similar pattern is noticed: both temperature and photochemical activity play a dominant role. At fixed latitude, the NO_x fractions decrease with increasing altitude, due to the temperature and pressure dependency of the formation of HNO_3 from OH and NO_2, The small increase in photolysis rates with altitude does not compensate this. High temperatures and high photochemical activity result in low NO_x fractions, with minimal values in the tropics. The peaks in altitude for each isoline are located at altitudes with maximum photochemical activity, in the Southern Hemisphere in January, in the Northern Hemisphere in July, and at the Equator in April and October. The HNO_3 and HO_2NO_2 fractions are high at high temperatures and high photochemical activity, so are high around the tropics and low at altitudes. At low temperatures the formation of HNO_3 is suppressed, resulting in high fractions of N_2O_5 in the polar regions. In the tropics the N_2O_5 fraction is negligible; all N_2O_5 formed is photodissociated and converted into HNO_3. The combined influence of temperature and photolysis results in steep slopes of all iso-lines in the mid-latitudes. All these results support the findings in section 4.2.

4.4. Conclusions

Both the single-plume calculations in the NAFC and the runs for the global domain have patterns and dependencies as expected. In summer NO_x is much more rapidly converted to NO_y than in winter. In summer the converted reactive nitrogen compounds consist mainly of HNO_3, HO_2NO_2 and N_2O_5, in winter only of N_2O_5. The concentrations of the other reactive nitrogen compounds (PAN, NO_3 and the organic nitrates) are much lower, so a parameterization of aircraft emission can be sufficiently described with fractions of NO_x, HNO_3, HO_2NO_2 and N_2O_5. The results show a large dependency on temperature and photochemical activity, especially in the area of 50^0N important for aircraft.

Preliminary sensitivity simulations show that a temperature variation of 10% in the NAFC in summer results in a variation of 0.275 in the nitrogen oxide fractions and a variation in the background concentrations of 25% result in a variation of 0.2 in the fractions. Larger variations may occur under other conditions. Since these variations in temperature and concentrations can be expected, the model outcomes are implied to describe the average behaviour of the aircraft plume processes instead of the actual chemical processes at a specific time and place. For this reason, it is also advised to use the same meteorological and photochemical data as the global model for which the parameterization is done, with the same spatial and temporal resolution. For the RIVM version of Moguntia for instance, monthly parameterizations on a 10^0 x 10^0 grid, generated with ECMWF meteorology of 1987 are required. For a model with actual meteorology instead of climatology, this would imply a severe constraint to this parameterization approach. For this reason the sensitivity of the outcomes of the global model to the variation in reactive nitrogen compounds should be investigated. Low sensitivity may justify the use of a parameterization on a less detailed scale.

The parameters of other processes, for instance the diffusion coefficients and the actual emitted amount of NO_x will also affect the model's outcomes. The influence of some of these processes forms the subject of the following chapters.

5. COMPARISON OF DIFFERENT DESCRIPTIONS OF THE PLUME DYNAMICS

5.1. Introduction

This chapter compares the influence of different descriptions of the plume dynamics. The effective diffusion of aircraft emissions is most of the time dominated by weak turbulence in a stably stratified atmosphere, however, the occurrence of strong turbulence is a possibility. For both cases, a slightly different description of the plume dynamics is needed. Furthermore, the actual values of the specific parameters of each process can vary widely for different circumstances. Again, like in Chapter 4, the selected aircraft is a B747-400 using emission data of Schumann (1994) and Olivier (1991) and the heterogeneous chemistry is restricted to the reaction of N_2O_5 on sulphate aerosol and contrail ice particles.

5.2. Diffusion by large-scale turbulence

In Chapter 2 the time evolution description of the dispersion coefficients was introduced for the case with weak turbulence and a stable stratified atmosphere. The time evolution of the dispersion coefficients σ_y and σ_z are described by Eq. 12. The initial dispersion coefficients for the dispersion regime are mainly determined by the type of aircraft, so these parameters are kept constant here. The diffusion coefficients D_y and D_z are dependent on the level of stratification, as described by the Brunt-Väisälä-frequency N (s^{-1}):

$$N = \sqrt{\frac{g}{\theta_0}\frac{d\theta}{dz}} \tag{24}$$

with g (ms^{-2}) the gravitational acceleration constant, θ (K) the potential temperature with θ_0 the potential temperature at cruising altitude. Dürbeck and Gerz (1995) calculated the diffusion constants for different N. The vertical diffusion constant after 1200 seconds is estimated on D_z = 0.15 m^2s^{-1} and is almost independent of N. In the first 1200 seconds the vertical diffusion constant is slightly higher. This is ignored in the model because of the relative short time span in which this occurs. The horizontal diffusion constant is independent of time and has the value of D_y = 10.9(2.2) m^2s^{-1} for the lowest frequency (N=0.6x10^{-2} s^{-1}) and the value of D_y = 20.0(3.3) m^2s^{-1} for the highest frequency (N=3.0x10^{-2} s^{-1}).

5.3. Scale-dependent diffusion

Under the circumstances of strong turbulence, the effective diffusion of the plume depends on the size of the plume; the dispersion of the plume is dominated in the early stage by small-scale turbulence and approaches asymptotically the global diffusion coefficients that are dominated by large-scale turbulence. In this case, the time evolution of the dispersion coefficient σ_y and σ_z is based on the approach of Gelinas and Walton (1974). For both the co-ordinate directions y and z the time evolution of the dispersion coefficient σ is described with:

$$\frac{\sigma^2}{K_m} + 3\frac{\sigma^{2/3}}{b\varepsilon^{1/3}} = 2\Delta t + \frac{\sigma_0^2}{K_m} + 3\frac{\sigma_0^{2/3}}{b\varepsilon^{1/3}} \tag{25}$$

with b a constant, ε (cm^2s^{-3}) the atmospheric dissipation energy rate and K_m (m^2s^{-1}) the global diffusion constant. The elapsed time since the emission is Δt (s) and σ_0 (m) the initial dispersion coefficient at time of the emission.

In the model, the global diffusion constants are K_m^y = 4.6 km^2s^{-1} and K_m^z = 2.8 m^2s^{-1} (Schumann, 1994). For a Boeing 747-400, the initial dispersion coefficients are estimated at σ_y^0 = 28 m and σ_z^0 = 7 m. No distinction is made between the dispersion regime and the earlier stages. The atmospheric dissipation energy and the constant b are according to Gelinas and Walton (1974); ε = 0.02 cm^2s^{-3} and b=1.

5.4. Results for different descriptions of the plume dynamics

To gain insight into the consequences of using of the different approaches, as described above, three different cases have been distinguished:

(a) large-scale turbulence dominated diffusion with D_y = 10 m^2s^{-1} and D_z = 0.15 m^2s^{-1}

(b) large-scale turbulence dominated diffusion with D_y = 20 m^2s^{-1} and D_z = 0.15 m^2s^{-1}

(c) scale-dependent diffusion

Cases (a) and (b) are, the values for weak turbulence for low and high Brunt-Väisälä-frequencies, respectively, and case (c) is the description for strong turbulence. Case (b) is the default for all calculations for which the diffusion is not specified.

For all three cases a simulation has been performed for the period of 48 h, starting with the emission at 12.00, at an altitude of 10 km at 50^0N for July. Figure 15 shows the time evolution of the cross-sections of the different plumes. The cross-sections with the large-scale turbulence dominated diffusion are $1.4x10^6$ m^2 and $2.0x10^6$ m^2 after 48 h for the cases (a) and (b), respectively. The cross-section for case (c) with scale-dependent diffusion is $1.2x10^9$ m^2. Clearly, case (c) will have much lower concentrations inside the plume than cases (a) and (b). To show the consequences on the distribution of reactive nitrogen compounds, the time evolution of the fractions of NO_x and NO_y is given in Fig. 16. Despite the large differences in cross-sections between the cases with large-scale diffusion and scale-dependent diffusion, the time evolution of the fractions of reactive nitrogen compounds are fairly similar. The variation of the fractions of reactive nitrogen compounds is maximally 0.2 and about 0.1 after 48 h. The differences between both cases with large-scale diffusion are negligible. Figure 17 shows the fractions of NO_x, NO_y, HNO_3, HO_2NO_2 and N_2O_5 for these two cases. The time evolution of all reactive nitrogen compounds have negligible differences. The chemical conversion processes are not affected by the large differences in the concentrations of the emitted species.

However, temporal and spatial variation of the temperature and photochemical intensity change the behaviour of the chemical processes and can result in a larger sensitivity to the actual plume concentrations. For this reason, plume calculations over the global domain have been performed for January and July with emissions at 0.00, 6.00, 12.00 and 18.00 h for the cases (b) and (c) to examine the difference between large-scale diffusion and scale-dependent diffusion. The fractions NO_x and HNO_3, HO_2NO_2 and N_2O_5 for January and July for the case with scale-dependent diffusion given in Fig. 18, can be compared with Figs. 11 to 14. The differences in the fractions NO_x and HNO_3, HO_2NO_2 and N_2O_5 for January and July between the two cases are shown in Fig. 19. For the NO_x fractions the difference are small at high temperatures and low photochemical activity, with negligible differences in the tropics at low

altitudes and a maximum difference of about 0.15 in the outermost parts of the polar regions. However, in most parts of the domain the difference varies from -0.02 to 0.1. The differences in the fractions HNO_3 are negligible in July, but are maximally about -0.1 for relative high temperatures in January, meaning that in the case of scale-dependent diffusion less HNO_3 is formed. The differences for the fractions of HO_2NO_2 and N_2O_5 are negligible.

5.5. Conclusions

Different descriptions of the aircraft plume dispersion results in a variation in the fractions of reactive nitrogen compounds, depending mainly on the temperature and photochemical activity. The Brunt-Väisälä-frequency N (Eq. 22) can be used to distinguish between these cases of large-scale diffusion with $D_y = 10$ m^2s^{-1} and $D_y = 20$ m^2s^{-1}, however since the differences are negligible, it is not necessary to implement this in the model. Instead, only the case with $D_y = 20$ m^2s^{-1} is modelled.

The differences between scale-dependent and large-scale diffusion are somewhat larger, but still small compared to the other uncertainties caused by the high sensitivity to the temperature. Since the occurrences of conditions for which scale-dependent diffusion is valid are not very frequent, it is not necessary to distinguish between these for the dispersion processes. Furthermore, it is not very clear what criterion should be applied.

6. INFLUENCE OF HETEROGENEOUS CHEMISTRY

6.1. Introduction

In this chapter details of the influence of the different heterogeneous reactions on the conversion of reactive nitrogen compounds is studied. The main uncertainties in the rate constants of heterogeneous reactions are determined by the particles inside the exhaust plume: the size distribution and the concentrations determine the surface-area density and the specific structure of the particles determines the sticking probabilities for the different heterogeneous reactions. By implementing the heterogeneous reactions as described in section 2.3.3, an attempt has been made to estimate a realistic maximum effect.

6.2. Results for simulations with different heterogeneous reactions

To determine the contribution to the conversion rates of the different heterogeneous reactions of reactive nitrogen compounds, different cases have been distinguished, all of them are compared with a run with only gas-phase chemistry. The cases considered:

(a) Only the reaction of N_2O_5 on wetted sulphate aerosol

(b) Only the reaction of N_2O_5 on ice particles

(c) Only the reaction of N_2O_5 on wetted soot aerosol

(d) All other reactions on wetted sulphate aerosol

6.2.1. Simulations for the NAFC

Figures 20 to 23 represent the time evolution of the fractions of reactive nitrogen compounds in the NAFC (at 50^0N and 10 km altitude) in January for the cases (a), (b), (c) and (d), compared with the results for only gas-phase chemistry. Figures 24 to 27 represent the fractions of the reactive nitrogen compounds in the NAFC for all cases for July. The major NO_y species in the NAFC in January is N_2O_5, so a maximum effect in the first three cases can be expected.

(a) The reaction of N_2O_5 on wetted sulphate aerosol

In January (Fig. 20) the formation of HNO_3 from the reaction OH + NO_2 in the NAFC is inhibited by the low temperature, so the formation of HNO_3 by the heterogeneous reaction on sulphate aerosol is the major source for this species under these circumstances. Furthermore, this heterogeneous formation benefits also from the lower loss of N_2O_5 by photolysis. Consequently, the fraction HNO_3 after 48 h is 0.10 for this case, being 0.08 higher than in the case with only gas-phase chemistry, the fraction N_2O_5 is 0.12, being 0.07 lower. In both cases the fraction HO_2NO_2 is negligible, as expected. Because HNO_3 is much more slowly photodissociated than N_2O_5, the fraction NO_x is expected to be more lower compared to the case with only gas-phase chemistry. Here a decrease of 0.02 to 0.77 of the fraction NO_x has been calculated after 48 h.

In July (Fig. 24) the major nitrogen species in the NAFC is HNO_3 (from OH + NO_2), whereas N_2O_5 is fairly unimportant. The influence of heterogeneous chemistry is therefore expected to be of minor importance with respect to the case in January. The influence of the heterogeneous reaction is based on the same processes as described above for January.

After 48 h, the fraction NO_x is 0.25 , 0.01 lower than with only gas-phase chemistry, the fraction HNO_3 is 0.68, 0.02 higher, and the fraction N_2O_5 is 0.02, 0.01 lower.

(b) The reaction of N_2O_5 on ice particles

The influence of this heterogeneous reaction is based on the same chemical processes as for case (a), only the reaction is much slower and the occurrence and lifetimes of the ice particles depend on the meteorological conditions. In July (Fig. 25) no contrails are formed in the NAFC, so there is no difference in the fractions of the reactive nitrogen compounds. In January, contrails do occur and result in the following values after 48 h (Fig. 21): 0.78 for the fraction NO_x (0.01 smaller), 0.02 for the fraction HNO_3 (negligible difference) and 0.20 for N_2O_5 (0.01 smaller).

(c) The reaction of N_2O_5 on wetted soot aerosol

To estimate a possible impact of soot emissions on the ozone chemistry in the plume, the heterogeneous reaction on wetted sooted particles is considered to behave like the one on sulphate aerosols. In January (Fig. 22), the formation of HNO_3 by the heterogeneous reaction on wetted soot is very dominant and results in a HNO_3 fraction after 48 h of 0.57, which is 0.55 higher. Consequently, the conversion of NO_x is much more efficient, resulting in a fraction of 0.35 (0.44 lower). In July (Fig. 26), the effect of the heterogeneous reaction is less dominant, caused by the presence of other channels for the formation of HNO_3. Now, the fractions are 0.193 for NO_x (0.05 lower) and 0.76 for HNO_3 (0.10 higher).

(d) The other heterogeneous reactions on sulphate aerosol

The other heterogeneous reactions do not directly affect the conversion processes of the reactive nitrogen compounds, but can have some effect by altering the radical concentrations. However, as can be seen in Figs. 23 and 27, these effects are negligible.

6.2.2. Simulations for the global domain

Figure 28 represents the fraction of NO_x, HNO_3, HO_2NO_2 and N_2O_5 after 48 hours for the case with only gas-phase chemistry for the global domain in January and July, as a reference point for Figs. 29 to 32, which represent the differences in the fractions of these species for the cases (a), (b), (c) and (d). Positive differences in Figs. 29 to 32 mean larger fractions for the case with heterogeneous chemistry.

(a) The reaction of N_2O_5 on wetted sulphate aerosol

Based on the mechanisms as described in the above section, maximum differences occur at regions with low temperatures, while differences in photochemical activity are of minor importance. Therefore maximum values occur in the Northern Hemisphere in January and in the Southern Hemisphere in July. Maximum differences (Fig. 29) in NO_x are about -0.02 and differences in HNO_3 are about 0.15. In regions with large differences the fractions NO_x are about 0.6, so the differences for the fractions NO_x are not very important. However, the fractions HNO_3 are of about the same magnitude as the differences, implying relevant differences in the regions with low temperatures. Consequently, the decrease in N_2O_5 in the regions with low temperatures is also of the same magnitude as the fractions. The HO_2NO_2 fractions are very small and have differences of the same magnitude.

(b) The reaction of N_2O_5 on ice particles

The formation of contrails can only have effect in regions of low temperatures, which can be seen in Fig. 30. The heterogeneous reaction on ice results in very small differences.

(c) The reaction of N_2O_5 on wetted soot aerosol

To estimate a possible impact of soot emissions on the ozone chemistry in the plume, the heterogeneous reaction on wetted sooted particles is considered to behave like the one on sulphate aerosols. In this modelling approach very large effects occur (Fig. 31) in regions with low temperature, resulting in larger differences than those occurring in case (a). Maximum differences in the fraction NO_x of -0.3 and 0.5 for HNO_3.

(d) The other heterogeneous reactions on sulphate aerosol

The other heterogeneous reactions (Fig. 32) do not directly affect the conversion processes of the reactive nitrogen compounds, but can have some effect by altering the radical concentrations. Temperature and photolysis do not have a large influence, so throughout the domain the differences are negligible.

6.3. Conclusions

The findings on the role of several heterogeneous reactions are summarised and discussed here.

The role of the heterogeneous reaction of N_2O_5 on sulphate aerosols is normally heavily dependent on the temperature, since this reaction becomes more important at low temperatures by suppressing formation of HNO_3 in the gas phase. Under circumstances with low temperatures, the fraction NO_x is slightly diminished by this reaction and most of the N_2O_5 is converted to HNO_3. Since N_2O_5 photodissociates very easily and HNO_3 does not, this can be regarded as an important effect. There are many uncertainties in the actual shifts in the nitrogen fractions, since there is little known about sulphur oxidation processes and subsequent formation of sulphate aerosols in the exhaust plumes of aircraft. By using the measurement of sulphur oxides by Fahey *et al.* (1995a), which showed surprisingly high oxidation rates of SO_2, most of the uncertainties in the oxidation processes are accounted for. The subsequent formation of aerosols based on these oxidation rates, is modelled according to Fahey *et al.* (1995a). By assuming that coagulation of aerosols is suppressed by the dispersion of the plume, which would diminish the surface-area density, a maximum effect has been estimated.

The formation of sulphate aerosol is based on the binary homogeneous nucleation of H_2SO_4 and H_2O. Another possibility for this formation is through heterogeneous nucleation on, for instance, soot particles. To make a crude estimation of this possible effect, wetted soot particles were treated like sulphate aerosols. At low temperatures, large effects were found, with heavily diminished NO_x fractions and an increased HNO_3 fraction. Since, the approach followed is highly speculative, it is not advised to use this reaction in future calculations. However, it does show that the conversion of reactive nitrogen compounds can be sensitive to heterogeneous reactions.

The heterogeneous reaction of N_2O_5 on ice particles plays a minor role, although it causes some shifts in the distribution of the reactive nitrogen compounds. The formation of contrails is modelled by using a criterion as described by Eq. 18 and, besides the emitted amount of water and the dispersion rate of the exhaust plume depends on the ambient pressure and temperature. By using a climatology instead of actual meteorological data, the occurrence of high pressure areas with low temperatures and high relative humidities is negligible, making the presence of persistent contrails impossible. The lifetime of contrails under moderate conditions is no longer than several minutes, whereas persistent contrails can exist for hours;

this can clearly amplify the effect of the heterogeneous reaction on ice. However, since these circumstances are not very frequent, it can be concluded that the heterogeneous reactions on ice are properly taken into account for this study. The heterogeneous reactions of non-nitrogen species proved to be insignificant with respect to the conversion of reactive nitrogen compounds emitted.

7. SIMULATIONS WITH EMISSION DATA FOR OTHER AIRCRAFT

7.1. Introduction

In this chapter the emission data of the National Aerospace Laboratory of the Netherlands (NLR) for an Airbus 310-200 (engine CF6-80A3), a B767-300 (engine PW4060) and a B747-400 (engine CF6-80C2B1F) are compared with the RIVM emission data of a B747-400. The emission indices are shown in Table 5. The comparison will reveal the sensitivity to the initial plume concentrations and, more important, it will give some insight into the usefulness of the approach followed of parameterizing aircraft emissions by an off-line plume model. A low dependency of the fractions of reactive nitrogen compounds on the selected aircraft will justify the chosen approach because all emission databases can be modified with the generated parameterization without taking the different types of aircraft into account.

Table 5. *The emission indices EI (g kg^{-1}) of the reactive species are shown for both the RIVM emission data for the B747-400, with the corresponding margins and the lowest and highest values of the emission indices as calculated by NLR.*

Species	RIVM: EI (g kg^{-1})	Margin	NLR: EI (g kg^{-1})
NO_X (as NO_2)	16	7-20	9 - 12
CO	1.5	1.5-10	1.3 - 2.0
Hydrocarbons	0.6	0.2-3	0.1 - 0.4
SO_2	1	0.02-6	0.2

7.2. Comparison of results

7.2.1. Simulation in the NAFC

First single-plume simulations in the NAFC for July are considered to reveal the time dependency of the differences between the selected emission data. The emissions occurred at noon. The time evolution of the fractions NO_x and NO_y for the different aircraft are given in Fig. 33. There are no large differences between the various engines with the largest differences in the first 12 hours. The differences between the simulations with data of NLR are almost identical. The maximum difference after 48 hours occurs between the RIVM data of the B747-400 and the B767-300 and is about 0.025. The emission data of NLR result in higher remaining NO_x fractions.

7.2.2. Comparison of results for the global domain in January and July

The comparison for the global domain is restricted to the NO_x fractions. Figures 34, 35 and 36 show the differences between NO_x fractions for January and July after 48 hours, as generated with the emission data of RIVM and NLR for, a B747-400, a B767-300 and an A310-200, respectively. Negative differences mean smaller fractions of NO_x for the case using RIVM emission data, which applies to almost the entire domain. The differences for the other

aircraft are almost the same and have maximum values in July of around -0.06. For the B747-400 the largest differences occur in July with a maximum difference of -0.035.

7.3. Conclusions

Using different emission data for different aircraft have few implications in these selected cases and are negligible in comparison with other uncertainties like the background temperature. The differences are a result of differences in initial plume concentrations caused by differences in initial plume dimensions at the start of the dispersion regime and different emission indices. The emission indices of NLR are lower than those of RIVM and explain the differences in the results. The differences in the initial plume dimensions are relatively unimportant since the differences between the results with NLR data are small.

8. DISCUSSION, CONCLUSIONS AND RECOMMENDATIONS

The model PARANOX has proved to be useful for studying aircraft exhaust processes and generating distributions of emitted reactive nitrogen compounds with temporal and spatial variations. The main objective of the calculations was to determine the main dependencies of these plume processes and make reliable parameterization of the aircraft emissions for global chemistry transport models. The parameterization is made under the assumption of discrete exhaust plumes, so corridor effects are not taken into account.

The conversion of NO_x into other reactive nitrogen compounds is highly dependent on temperature and photochemical activity. In summer NO_x is much more rapidly converted to NO_y than in winter. Under typical summer conditions the converted reactive nitrogen compounds consist mainly of HNO_3, HO_2NO_2 and N_2O_5, with a increasing fractions at higher altitudes as a result of greater photochemical activity. In typical winter conditions the main fraction is N_2O_5, with a little dependency on photochemical activity; the formation of the other species is suppressed by the low temperatures and low photochemical activity. The concentration in the plume of other reactive nitrogen compounds (PAN, NO_3 and the organic nitrates) is small and they can be neglected as an effective emission product of the aircraft plume. The conversion processes are not very dependent on the time of emission (night or day). Since temperature is an important parameter, uncertainties in the background temperatures have a large effect on the conversion processes: preliminary sensitivity simulations show that a temperature variation of 10% in the NAFC in July results in a variation of 0.275 in the nitrogen oxide fractions. Larger variations may occur under other conditions. The uncertainties in the concentrations of species in the ambient air around the aircraft exhaust also have a large influence: a variation in the background concentrations of 25% in the NAFC in July resulted in a variation of 0.2 in the fractions.

Uncertainties in the dispersion rates, studied in Chapter 5, can have an effect on the chemical reactions inside the aircraft plume. Roughly two different circumstances can be distinguished: 1) dispersion, caused by strong turbulence, described with scale-dependent diffusion and 2) dispersion in a stratified atmosphere with very weak turbulence, described with so-called large-scale diffusion. Since the latter situation is much more frequent at high altitudes, the plume dispersion can be described adequately with only large-scale diffusion. It is not necessary to distinguish between situations with different levels of stratifaction.

The heterogeneous reaction of reactive nitrogen compounds other than N_2O_5 (Chapter 6) are insignificant with respect to the conversion of reactive nitrogen compounds. There is very little influence of heterogeneous reactions of N_2O_5 on ice particles under moderate conditions due to the short lifetimes of contrails under these conditions. Since favourable conditions for persistent contrails are rare, the effect of this reaction can be regarded as unimportant. The role of the heterogeneous reaction of N_2O_5 on sulphate aerosols depends highly on the temperature, since this reaction becomes more important at low temperatures by the suppression of HNO_3 formation in the gas phase. Under circumstances with low temperatures, the NO_x fraction is slightly diminished by this reaction and most of the N_2O_5 is converted to HNO_3. Since N_2O_5 photodissociates very easily and HNO_3 does not, this can be regarded as an important effect. However, many uncertainties exist in the modelling of heterogeneous reactions. For example, when wetted soot particles are treated like sulphate aerosols to account for the possible binary heterogeneous nucleation of sulphate on soot particles, the heterogeneous reaction of N_2O_5 on soot strongly influences the conversion of reactive nitrogen compounds in the aircraft plume.

The use of different emission data for different aircraft will clearly have some effect on the conversion processes, but proved to have only small implications in the selected cases, with emission data differing depending on whether the Boeing 747-400, 767-300 or Airbus 310-200 was taken. The differences are a result of those in initial plume concentrations caused by differences in initial plume dimensions at the start of the dispersion regime and different emission indices.

Summarizing, with respect to the temperature and the background concentrations, most processes studied do not have a very large influence on the conversion processes. Roughly, the uncertainties cause a variation of about 0.2 in the nitrogen oxides. Since the major objective is to use the results of the plume model as input for global chemistry transport models, which have their own meteorological data, the best possible approach to deal with the dependency on temperature and background concentrations is to make the plume model as consistent as possible with the global model it is used for. For the RIVM version of Moguntia for instance, monthly parameterizations on a 10^0 x 10^0 grid, generated with ECMWF meteorology of 1987, are required. For analyzing specific events with a model with actual meteorology instead of climatology, this would imply a severe constraint on this approach of parameterization, since daily variation in the temperature would require an almost on-line use of the plume model. To gain insight in the dependencies of global models for the uncertainties in the reactive nitrogen compounds fractions, it would be useful to do some simulations with minimum and maximum values of the fractions of reactive nitrogen compounds.

For obtaining a good parameterization of the NO_x emissions from aircraft which can be used in 3D global models the average lifetime of the aircraft plume has to be known. A lifetime of 48 h can be regarded as a maximum for an aircraft exhaust plume. The lifetime is commonly estimated between 2 and 48 hours, which makes it very difficult to find a good criterion for the end of the plume simulations. However, at high altitudes the atmosphere very stable and stratified is most of the time, resulting in slow dispersion rates, so at those altitudes a minimal lifetime of 24 hours can be regarded as realistic. After 24 hours the chemical reactions are already producing ozone very efficiently and the decrease in the fraction NO_x relaxes, so the chemistry inside the plume is likely to be in the same state as the background chemistry. Therefore, a lifetime between 24 and 48 hours will be a realistic choice. It would be advisable to use different end times in the plume simulations in studying the consequences of the global model results.

ACKNOWLEDGEMENTS

The authors gratefully acknowledges H. ten Have (NLR) for the emissions data from different aircraft and P. Konopka (DLR) for useful information from the literature. Thanks goes to P. Valks, L. Janssen and H. Diederen for critically reading earlier versions of the manuscript and to R. de Wijs-Christensen for editorial comments.

REFERENCES

Appleman, H., The formation of exhaust condensation trails by jet aircraft, *Bull. Am. Meteorol. Soc.*, **34**, 14-20, 1953.

Baumann, R., R. Busen, H.P. Fimpel, C. Kiemle, M.E. Reinhardt, M. Quante, Measurements on contrails of commercial aircraft, Proc. 8th Symp. Meteorol. Obs. and Instrum., Am. Meteorol. Soc., Boston, 484-489, 1993.

Busen R, U. Schumann, Visible contrail formation from fuels with different sulfur contents, *Geophys. Res. Lett.*, **22**, 1357-1360, 1995.

Curtis, A.R., W.P. Sweetenham, FACSIMILE Release H User's Manual, Report AERE R-11771, 1985.

Danilin, M.Y., J.C. McConnell, Heterogeneous reactions in a stratospheric box model: A sensitivity study, *J. Geophys. Res.*, D **99**, 25681-25696, 1994.

DeMore, W.B., S.P. Sander, D.M. Golden, R.F. Hampson, M.J. Kurylo, C.J. Howard, A.R. Ravishankara, C.E. Kolb, M.J. Molina, Chemical kinetics and photochemical data for use in stratospheric modeling, 1994, Evaluation number 11. JPL-Publications **94-26**, Jet Propulsion. Laboratory, Pasadena, California, 1994.

Dentener, F.J., P.J. Crutzen, Reaction of N_2O_5 on tropospheric aerosols: impact on the global distributions of NO_x, O_3 and OH, *J. Geophys. Res.* D **98**, 7149-7163, 1993.

Dürbeck, T., T. Gerz, Large-eddy simulation of aircraft exhaust plumes in the free atmosphere: effective diffusivities and cross-sections, *Geophys. Res. Lett.*, **22**, 3203-3206, 1995.

Fahey, D.W., E.R. Keim, K.A. Boering, C.A. Brock, J.C. Wilson, H.H. Jonsson, S. Anthony, T.F. Hanisco, P.O. Wennberg, R.C. Miake-Lye, R.J. Salawitch, N. Louisnard, E.L. Woodbridge, R.S. Gao, S.G. Donelly, R.C. Wamsley, L.A. Del Negro, S. Solomon, B.C. Daube, S.C. Wofsy, C.R.Webster, R.D. May, K.K. Kelly, M. Loewenstein, J.R. Podolske, K.R. Chan, Emission Measurements of the Concorde Supersonic Aircraft in the Lower Stratosphere, *Science*, **270**, 70-74, 1995a.

Fahey, D.W., E.R. Keim, E.L. Woodbridge, R.S. Gao, K.A. Boering, B.C. Daube, S.C. Wofsy, R.P. Lohmann, E.J. Hintsa, A.E. Dessler, C.R. Webster, R.D. May, C.A. Brock, J.C. Wilson, R.C. Miake-Lye, R,C, Brown, J.M. Rodriguez, M. Loewenstein, M.H. Proffitt, R.M. Stimple, S.W.Bowen, K.R. Chan, In situ observations in aircraft exhaust plumes in the lower stratosphere at midlatitudes, *J. Geophys. Res.*, D **100**, 3065-3074, 1995b.

Freiberg, J., The iron catalyzed oxidation of SO_2 to acid sulfate in dispersing plumes, *Atmos. Environ.* **10**, 121-130, 1976.

Fried A, E.H. Bruce, J.G. Calvert, The reaction probability of N_2O_5 with sulfuric acid aerosols at stratospheric temperatures and compositions, *J. Geophys. Res.*, D **99**, 3517-3532, 1994.

Gelinas J., J.J. Walton, Dynamisc-Kinetic Evolution of a Single Plume of Interacting Species, *J. Atmos. Sci.*, **31**, 1807-1813, 1974.

Hallet, J., J.G. Hudson, C.F. Rogers, Characterization of Combustion Aerosols for Haze and Cloud Formation, *Aerosol Sci. Tech.*, **10**, 70-83, 1989.

Hoshizaki, H., L.B. Anderson, R.J. Conti, N. Farlow, J.W. Meyer, T. Overcamp, K.O. Redler, V. Watson, Aircraft wake microscale phenonemena. The Stratosphere Pertubed by Propulsion Effluents, chapter 2, CIAPm DOT-TST-75-53, Natl. Tech. Inf. Serv., Springfield, VA, 1975.

Hudson, J.G., J. Hallet, C.F. Rogers, Field and Laboratory Measurements of Cloud-Forming Properties of Combustion aerosols, *J. Geophys. Res.*, D **96**, 10847-10859, 1991.

Isaksen, I.S.A., H. Rodhe, A two dimensional model for the global distribution of gases and aerosol particles in the troposphere, University of Stockholm, report nr. AC-47, Stockholm, 1978.

Iribarne, J.V., W.L. Godson, Atmospheric Thermodynamics, D. Reidel, 2nd. ed., Norwell, Mass, 1992.

Louisnard, N., C. Baudoin, G. Billet, F. Garnier, D. Hills, T. Mentel, P. Mirabel, J.C. Petit, J.L. Schultz, D.Taleb, J. Thlibi, A. Wahnmer, P. Woods, Sub-Project 2: Physics and Chemistry in the Aircraft Wake. Aeronox report, U. Schumann (Ed.), 1995.

Knollenberg, R.G., Measurements of the growth of the ice budget in a persistent contrail, *J. Atmos. Sci.*, **29**, 1367-1374, 1972.

Marti, J., K. Mauersberger, A servey and new measurements on ive vapor pressure at temperatures between 170 and 250K, *Geophys. Res. Lett.*, **20**, 363-366, 1993.

Melo, O.T., M.A. Lusis, R.D.S. Stevens, Mathematical modelling of dispersion and chemical reactions in a plume - oxidation of NO to NO_2 in the plume of a power plant, *Atmos. Environ.*, **12**, 1231-1234, 1978.

Miake-Lye, R.C., M. Martinez-Sanchez, R.C. Brown, C.E. Kolb, Plume and wake dynamics, mixing and chemistry behind a high-speed civil transport aircraft, *J. Aircraft*, **30**, 467-479, 1993.

Olivier, J.G.J., Inventory of aircraft emissions: a review of recent literature, RIVM report 736301008, Bilthoven, The Netherlands, 1991.

Pruppacher, H.R., J.D. Klett, Microphysics of Clouds and Precipitation, D. Reidel, Norwell, Mass., 1980.

Pulles, J.W., S. Lowe, R. van Drimmelen, G. Baarse, P. McMahon, The AERO-project. Model description and status, Dutch Civil Aviation Department, Report, The Hague, 1995.

Rosen, J.M., R. McGreegor, Jet Engine Soot Emission at Altitude, *J. Aircraft*, **11**, 243-245, 1974.

Shareef, G.S., W.A. Butler, L.A. Bravo, M.B. Stockton, Air emissions species manual. Volume I. Volative Organic Compound (VOC) Species Profiles, EPA-450/2-88-003a, 1988.

Schumann, U., On the effect of emissions from aircraft engines on the state of the atmosphere, *Ann. Geophys.*, **12**, 365-384, 1994.

Schumann, U., M.E. Reinhardt, Studies on the effect of high-flying air-traffic on the atmosphere, 42nd Congr. IAF, Montreal, Canada, Paper no. IAA-91-737, Inst. Astron. Fed., Paris, 1991.

Schumann, U., P. Konopka, R. Baumann, R. Busen, T. Gerz, H. Schlager, P. Schulte, H. Volkert, Estimate of diffusion parameters of aircraft exhaust plumes near the tropopause from nitric oxide and turbulence measurements, *J. Geophys. Res.*, D **100**, 14147-14162, 1995.

Simpson, D., Long-period modelling of photochemical oxidants in Europa. Model calculations for July 1985, *Atmos. Environ.*, **26**A, 1609-1634, 1992.

Strand, A, Ø. Hov, A two-dimensional global study of tropospheric ozone production, *J. Geophys. Res.*, D **99**, 22877-22895, 1994.

Veenstra, D.L., J.P. Beck, T.H.P. The, J.G.J. Olivier, The impact of aircraft exhaust emissions on the atmosphere; scenario studies with a three dimensional global model, RIVM report 722201003, Bilthoven, The Netherlands, 1995.

Verwer, J.G. Gauss-Seidel iteration for stiff ODEs from chemical kinetic. Report NM-R9315, CWI, Amsterdam, 1993.

Wirtz, K., C. Roehl, G.D. Hayman, M.E. Jenkin, LACTOZ Steering Groupm LACTOZ Re-evaluation of the EMEP MSC-W Photo-oxidant Model, EUROTRAC report, 1994.

Weele, M. van, P.G. Duynkerke, Effects of clouds on the photodissociation of NO_2: Observation and modelling, *J. Atmos. Chem.*, **16**, 231-255, 1993.

Zhao, J., R.P. Turco, Particle nucleation in the wake of a jet aircraft in stratospheric flight, *J. Aerosol Sci.*, **26**, 779-795, 1995.

APPENDIX A: CHEMICAL MECHANISM

The chemical mechanism used in PARANOX is a combination of the EMEP scheme adapted from Strand and Hov (1994) with incorporated SO_2 oxidation and nine heterogeneous reactions. All gas-phase reactions are updated according to DeMore *at al.* (1994). The photolysis rates are derived from calculations by Van Weele and Duynkerke (1993). The species denoted in lower case letters are assumed to have constant concentrations.

Bimolecular reactions

Name	Reaction	Rate constant ($cm^3molec^{-1}s^{-1}$)
n11	$O_3 + NO \rightarrow NO_2 + o_2$	2.0e-12 * exp(-1400./T)
n12	$O_3 + NO_2 \rightarrow NO_3 + o_2$	1.2e-13 * exp(-2450./T)
n13	$O_3 + OH \rightarrow HO_2 + o_2$	1.6e-12*exp(-940./T)
n14	$O_3 + HO_2 \rightarrow OH + 2o_2$	1.1e-14*exp(-500./T)
n15	$NO + NO_3 \rightarrow 2NO_2$	1.5e-11*exp(170./T)
n17	$NO + HO_2 \rightarrow NO_2 + OH$	3.7e-12*exp(250./T)
n19	$NO_2 + NO_3 \rightarrow NO + NO_2 + o_2$	4.5e-14*exp(-1260./T)
n24	$OH + HO_2NO_2 \rightarrow NO_2 + h_2o$	1.3e-12 * exp(380./T)
n30	$OH + HO_2 \rightarrow h_2o + o_2$	4.8e-11*exp(250./T)
n31	$OH + H_2O_2 \rightarrow HO_2 + h_2o$	2.9e-12*exp(-160./T)
n33	$OH + h_2 \rightarrow HO_2 + h_2o$	5.5e-12*exp(-2000./T)
n35	$OH + HNO_3 \rightarrow NO_3 + h_2o$	7.2e-15*exp(785/T)+1.9e-33 * (725/T)*M/(1+1.9e-33* (725/T)*M* 4.1e-16*exp(1440/T))
n36	$HO_2 + HO_2 \rightarrow H_2O_2 + o_2$	(2.3e-13*exp(600./T)+1.7e-33*M* exp(1000./T))* (1+ 1.4e-21 * H_2O *exp(2200./T))
n42	$N_2O_5 + h_2o \rightarrow 2HNO_3$	1.3e-21
n59	$OH + CH_4 \rightarrow h_2o + CH_3O_2$	2.9e-12 * exp(-1820./T)
n60	$CH_3O_2 + NO \rightarrow HCHO + HO_2 + NO_2$	4.2e-12 * exp(180./T)
n61	$CH_3O_2 + CH_3O_2 \rightarrow 2HCHO + 2HO_2 + o_2$	3.0e-14*exp(416./T)
n62	$CH_3O_2 + CH_3O_2 \rightarrow 2HCHO + HO_2 + h_2o$	6.1e-14*exp(416./T)
n63	$HO_2 + CH_3COO_2 \rightarrow CH_3OOH + 0.25\ O_3$	4.5e-13 * exp(1000./T)
n65	$HO_2 + CH_3O_2 \rightarrow CH_3OOH + o_2$	4.1e-13*exp(790./T)
n66	$OH + HCHO \rightarrow h_2o + HO_2 + CO$	1.6e-11 * exp(-110./T)
n67	$NO_3 + HCHO \rightarrow HNO_3 + HO_2 + CO$	5.8e-16
n70	$OH + CO \rightarrow HO_2 + co_2$	1.5e-13*(1.0+0.6*P[atm])
n71	$C_2H_6 + OH \rightarrow C_2H_5O_2 + h_2o$	8.7e-12*exp(-1070./T)
n72	$C_2H_5O_2 + NO \rightarrow CH_3CHO + HO_2 + NO_2$	8.9e-12
n73	$C_2H_5O_2 + CH_3O_2 \rightarrow CH_3CHO + HCHO + 2HO_2$	2.0e-13
n75	$OH + CH_3CHO \rightarrow h_2o + CH3COO_2$	6.0e-12 * exp(250./T)
n76	$OH + PAN \rightarrow HCHO + NO_2$	1.1e-12 * exp(650./T)

n79	$CH_3COO_2 + NO \rightarrow CH_3O_2 + co_2 + NO_2$	2.0e-11
n80	$CH_3O_2 + CH_3COO_2 \rightarrow HCHO + HO_2 + CH_3O_2 + co_2$	3.1e-5*exp(-3870/T)/ ((2.2e6*exp(-3870/T)+1)
n81	$n\text{-}C_4H_{10} + OH \rightarrow sec\text{-}C4H_9O_2 + h_2o$	1.51e-17* T^2* exp(190./T)
n83	$sec\text{-}C4H_9O_2 + NO \rightarrow NO_2 + x1\ HO_2 + x1\ CH_3COC_2H_5 + x2\ CH_3CHO + x2\ C_2H_5O_2$	4.1e-12
n84	$sec\text{-}C_4H_9O_2 + CH_3O_2 \rightarrow x1\ HO_2 + x1\ CH_3COC_2H_5 + x2\ CH_3CHO + x2\ C_2H_5O_2 + HO_2$	1.0e-14
n86	$CH_3COC_2H_5 + OH \rightarrow CH_3COCHO_2CH_3 + h_2o$	1.62e-18*T^2*exp(414./T)
n90	$C_2H_5O_2 + C_2H_5O_2 \rightarrow 2CH_3CHO + 2HO_2 + o_2$	6.2e-14*exp(-100./T)
n91	$CH_3COO_2 + CH_3COO_2 \rightarrow 2CH_3O_2 + 2co_2 + o_2$	2.8e-12 * exp(530./T)
n105	$CH_3COCHO_2CH_3 + NO \rightarrow CH_3COCOCH_3 + HO_2 + NO_2$	5.0e-12
n106	$CH_3COCHO_2CH_3 + CH_3O_2 \rightarrow HCHO + HO_2 + CH_3COCOCH_3$	1.0e-14
n110	$CH_2O_2CH_2OH + NO \rightarrow 2HCHO + HO_2 + NO_2$	9.0e-12
n111	$CH_2O_2CH_2OH + CH_3O_2 \rightarrow 3HCHO + 2HO_2$	1.0e-12
n112	$C_2H_4 + O_3 \rightarrow HCHO + 0.42CO + 0.12HO_2 + 0.12h_2$	9.0e-15 * exp(-2560./T)
n123	$C_3H_6 + O_3 \rightarrow 1.05HCHO + 0.12CH_4 + 0.24CO + 0.34HO_2 + 0.19OH + 0.43\ CH3O_2$	1.0e-15*exp(-1900./T)
n124	$C_3H_6 + O_3 \rightarrow CH_3CHO + 0.42CO + 0.12HO_2 + 0.12h_2$	2.6e-15*exp(-1900./T)
n126	$CH_3CHO_2CH_2OH + NO \rightarrow CH_3CHO + HCHO + HO_2 + NO2$	9.e-12
n127	$CH_3CHO_2CH_2OH + CH_3O_2 \rightarrow CH_3CHO + 2HCHO + 2HO_2$	1.0e-14
n200	$CH_4 + NO_3 \rightarrow CH_3O_2 + HNO_3$	4.0e-19
n201	$C_2H_6 + NO_3 \rightarrow C_2H5O_2 + HNO_3$	8.0e-18
n202	$n\text{-}C_4H_{10} + NO_3 \rightarrow sec\text{-}C_4H_9O_2 + HNO_3$	5.5e-17
n203	$C_2H_4 + NO_3 = C_2OrgN$	2.0e-16
n204	$C_2OrgN + NO \rightarrow orgn + h_2o + NO_2 - HO_2$	6.0e-12
n205	$C_3H_6 + NO_3 \rightarrow C_3OrgN$	9.45e-15
n206	$C_3OrgN + NO \rightarrow orgn + NO_2$	6.0e-12
n207	$CH_3OH + NO_3 \rightarrow HCHO + HO_2 + HNO_3$	2.1e-16
n208	$CH_3CHO + NO_3 \rightarrow CH_3COO_2 + HNO_3$	2.8e-15
n209	$C_5H_8 + NO_3 \rightarrow C_5OrgN$	9.0e-13
n210	$C_5OrgN + NO \rightarrow orgn + NO_2$	6.0e-12
n211	$C_8H_{10} + NO_3 \rightarrow C_6H_4CH_3CH_2O_2 + HNO_3$	3.7e-16
n212	$C_6H_4CH_3CH_2O_2 + NO = orgn$	6.0e-12
n221	$HCOCHO + OH \rightarrow HO_2 + 2CO + h_2o$	1.15e-11
n222	$CH_3COCHO \rightarrow CH_3COO_2 + CO + h_2o$	1.7e-11
n230	$C_8H_{10} + OH \rightarrow OXYL1$	1.1e-11
n231	$OXYL1 + NO \rightarrow CH_3COCHO + CH_3COCHCHCHO + HO_2 + NO_2$	3.1e-13

n232	$CH_3COCHCHCHO + OH \rightarrow CH_3COCHOHCHO_2CHO$	2.0e-11
n233	$CH_3COCHOHCHO_2CHO + NO \rightarrow CH_3COCHO + HCOCHO + HO_2 + NO_2$	6.0e-12
n251	$C_5H_8 + OH \rightarrow OC_5H_8O_2$	7.7e-11
n252	$OC_5H8O_2 + NO \rightarrow CH_3COCHCH_2 + HCHO + NO_2$	3.0e-13
n253	$CH_3COCHCH_2 + OH \rightarrow OHCH_3COCHCH_2O_2$	2.0e-11
n254	$OHCH_3COCHCH_2O_2 + NO \rightarrow CH_3COCHO + HCHO + HO_2 + NO_2$	3.0e-13

Termolecular reactions

Name	Reaction	Rate constant ($cm^6molec^{-2}s^{-1}$)
n20	$NO_2 + NO_3 + m \rightarrow N_2O_5 + m$	$k_0=2.2e-30*(T/300)^{-3.2}$
		$k_\infty=1.5e-12*(T/300)^{-0.7}$
n21	$NO_2 + OH + m \rightarrow HNO_3 + m$	$k_0=2.6e-30*(T/300)^{-3.2}$
		$k_\infty=2.4e-11*(T/300)^{-1.3}$
n22	$NO_2 + HO_2 + m \rightarrow HO_2NO_2$	$k_0=1.8e-31*(T/300)^{-3.2}$
		$k_\infty=4.7e-12*(T/300)^{-1.4}$
n23	$HO_2NO_2 + m \rightarrow NO_2 + HO_2$	$K_{eq}=4.8e26*exp(-10900./T)$
n29	$N_2O_5 \rightarrow NO_2 + NO_3$	$K_{eq}=2.5e+26*exp(-10930./T)$
n39	$OH + SO + m \rightarrow h_2so_4 + m$	$k_0=3.0e-31*(T/300)^{-3.3}$
		$k_\infty=1.5e-12$
n77	$CH_2COO_2 + NO_2 + m \rightarrow PAN + m$	$k_0=2.7e-28*(T/298)^{-7.1}$
		$k_\infty=1.2e-11*(T/298)^{-0.9}$
n78	$PAN + m \rightarrow CH_3COO_2 + NO_2 + m$	$k_0=5.5e-3*exp(-12064/T)$
		$k_\infty=3.9e16*exp(-13628/T)$
		$F_c=0.3$
n109	$C_2H_4 + OH + m \rightarrow CH_2O_2CH_2OH + m$	$k_0=1.0e-28*(T/300)^{-0.8}$
		$k_\infty=8.8e-12$
n125	$C_3H_6 + OH + m \rightarrow CH_3CHO_2CH_2OH$	$k_0=3.0e-27*(T/298)^{-3.0}$
		$k_\infty=2.8e-11*(T/298)^{-1.3}$

The overall rate constants k ($cm^3molec^{-1}s^{-1}$) for termolecular reactions are given by the expression:

$$k = \frac{k_0 M}{1 + \frac{k_0}{k_\infty} M} F_c^{\{1+\ln^2(k_0 M/k_\infty)\}^{-1}}$$

where k_0 and k_∞ are stated above, M is the air density (molec cm^{-3}) and F_c is constant at 0.6, unless otherwise named, as above.

Photolysis reactions

Name	Reaction
nj1	$O_3 + hv \rightarrow x3\ OH + x4\ O_3 + o_2$
nj3	$NO_2 + hv \rightarrow NO + O_3$
nj4a	$H_2O_2 + hv \rightarrow 2OH$
nj4b	$HO_2NO_2 + hv \rightarrow HO_2 + NO_2$
nj5	$HNO_3 + hv \rightarrow NO_2 + OH$
nj6	$HCHO + hv \rightarrow CO + 2HO_2$
nj7	$HCHO + hv \rightarrow h_2 + CO$
nj8	$CH_3CHO + hv \rightarrow CH_3O_2 + HO_2 + CO$
nj9	$CH_3COC_2H_5 + hv \rightarrow CH_3COO_2 + C_2H5O_2$
nj10	$CH_3COCOCH_3 + hv \rightarrow 2CH_3COO_2$
nj11	$CH_3COCHO + hv \rightarrow CO + CH_3CHO$
nj12	$HCOCHO + hv \rightarrow HCHO + CO$
nj13	$NO_3 + hv \rightarrow NO_2 + O_3$
nj14	$NO_3 + hv \rightarrow NO + o_2$
nj15	$N_2O_5 + hv \rightarrow NO_2 + NO_3$
nj16	$CH_3OOH + hv \rightarrow HCHO + HO_2 + OH$

Heterogeneous reactions

Name	Reaction
nh1	$N_2O_5 + H_2O(\text{sulphate aerosol}) \rightarrow 2HNO_3$
nh2	$N_2O_5 + H_2O(\text{soot aerosol}) \rightarrow 2HNO_3$
nh3	$N_2O_5 + H_2O(\text{ice particle}) \rightarrow 2HNO_3(\text{solid})$
nh4	$HNO_3 + H_2O(a) \rightarrow \text{product}$
nh5	$H_2O_2 + H_2O(a) \rightarrow \text{product}$
nh6	$CH_3OOH + H_2O(a) \rightarrow \text{product}$
nh7	$HCHO + H_2O(a) \rightarrow \text{product}$
nh8	$CH_3CHO + H_2O(a) \rightarrow \text{product}$
nh9	$PAN + H_2O(a) \rightarrow \text{product}$

Stoichiometric constants

Name	Definition
x1	$1.8e\text{-}14*\exp(-260/T)*O_2$
x2	x1/(x1+4.5e3)
x3	$4.4e\text{-}10*H_2O/(2.2e\text{-}10*H_2O+3.2e\text{-}11*\exp(70/T)*O_2+1.8e\text{-}11*\exp(110/T)*N_2$
x4	1-x3

APPENDIX B: FILES

All files that are part of PARANOX are listed. The source code files contain the routines with equal names, except for "output.f", which contains all output routines and debugging routines. All plots of results for the global domain are generated by an IDL script "paranox.pro".

Source code files:

ambcon.f	dispers.f	findfile.f	hetreac.f
initconc.f	initplume.f	iter.f	julday.f
lusispar.f	nozfracs.f	output.f	paranox.f
photolysis.f	plume.f	rateconst.f	readmeteo.f
release.f	ringflux.f	rk3b.f	settings.f
sigmat.f	twostepp.f		

Include files:

indices.inc	reacind.inc

Inputfiles:

ambcon2D.dat	hetchem.dat	jvalmvw.dat	meteo2D.dat

Run-parameter inputfile:
param

IDL utility:
paranox.pro

APPENDIX C: FIGURES

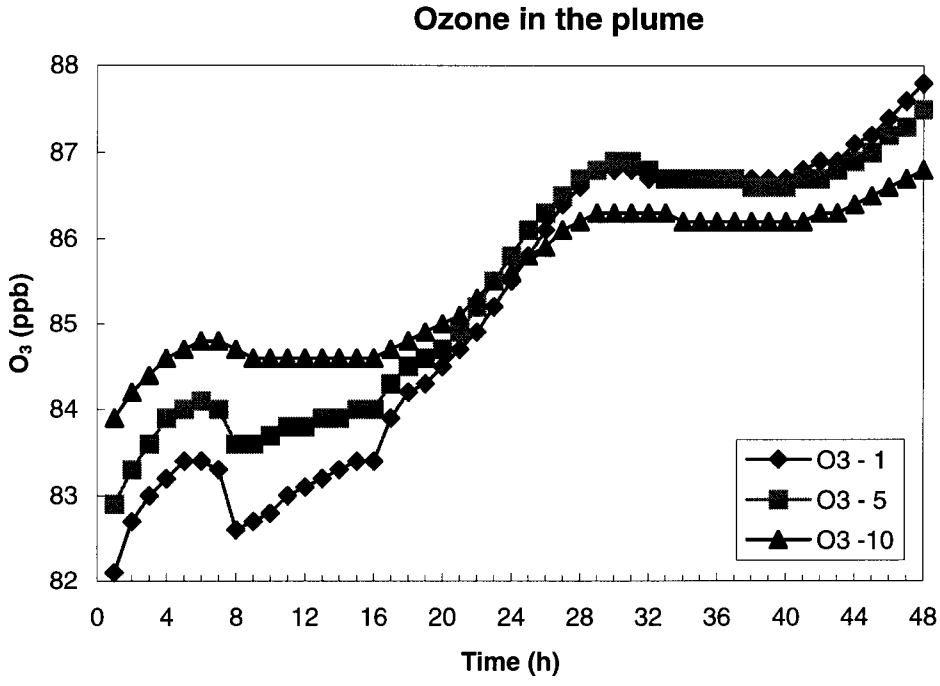

Figure 1. Time evolution over a 48-h period of the ozone concentration in the inner (1), middle (5) and outer (10) ring of a plume in the NAFC (50°N, 10 km altitude). Emissions took place at noon in July (summer). The background concentration is 85 ppbv.

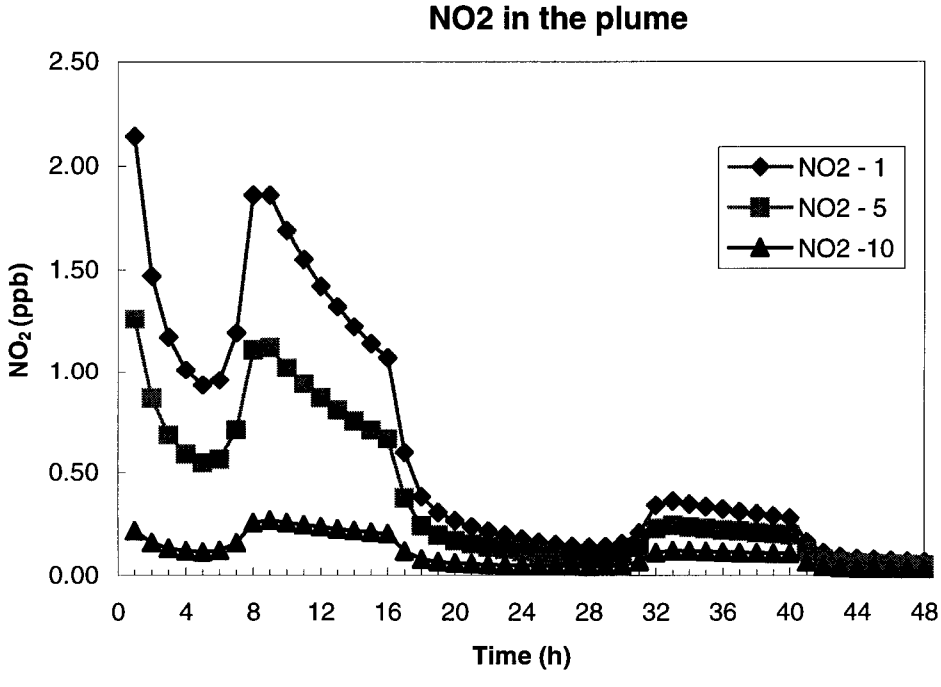

Figure 2. Time evolution over a 48-h period of the NO_2 concentration in the inner (1), middle (5) and outer (10) ring of a plume in the NAFC. Emissions took place at noon in July (summer). The background concentration of NO_x is 0.05 ppbv.

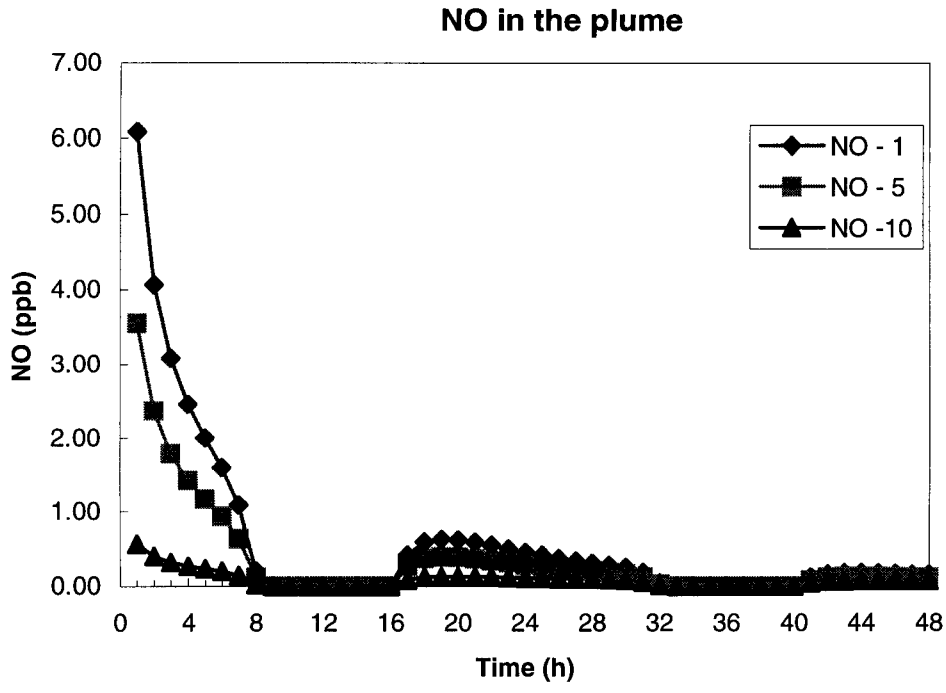

Figure 3. Time evolution over a 48-h period of the NO concentration in the inner (1), middle (5) and outer (10) ring of a plume in the NAFC. Emissions took place at noon in July (summer). The background concentration of NO_x is 0.05 ppbv.

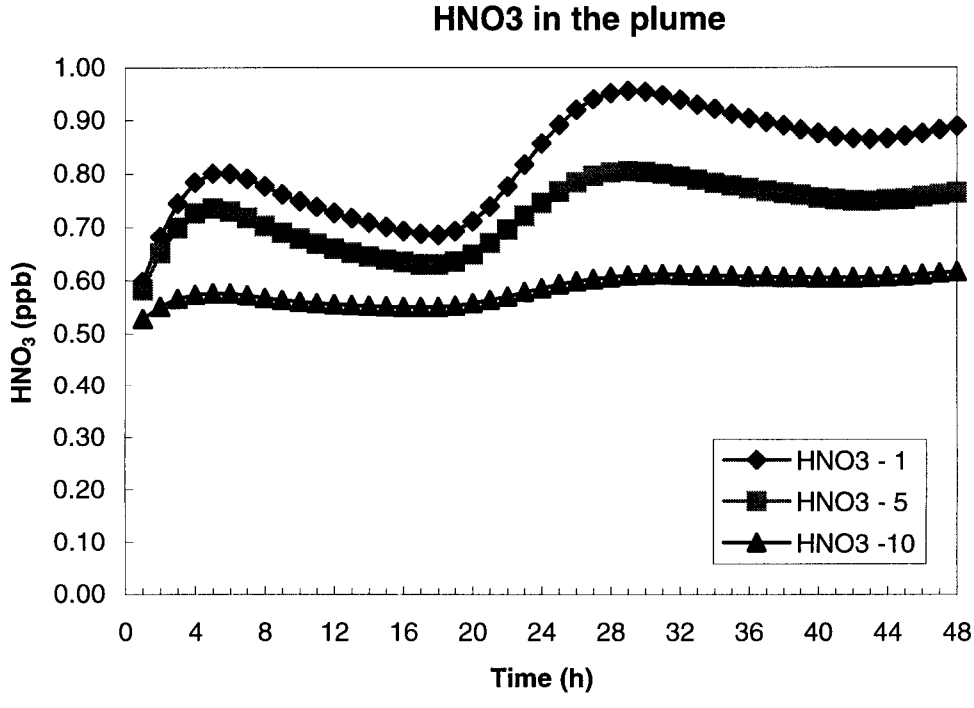

Figure 4. Time evolution over a 48-h period of the HNO_3 concentration in the inner (1), middle (5) and outer (10) ring of a plume in the NAFC. Emissions took place at noon in July (summer). The background concentration is 0.5 ppbv.

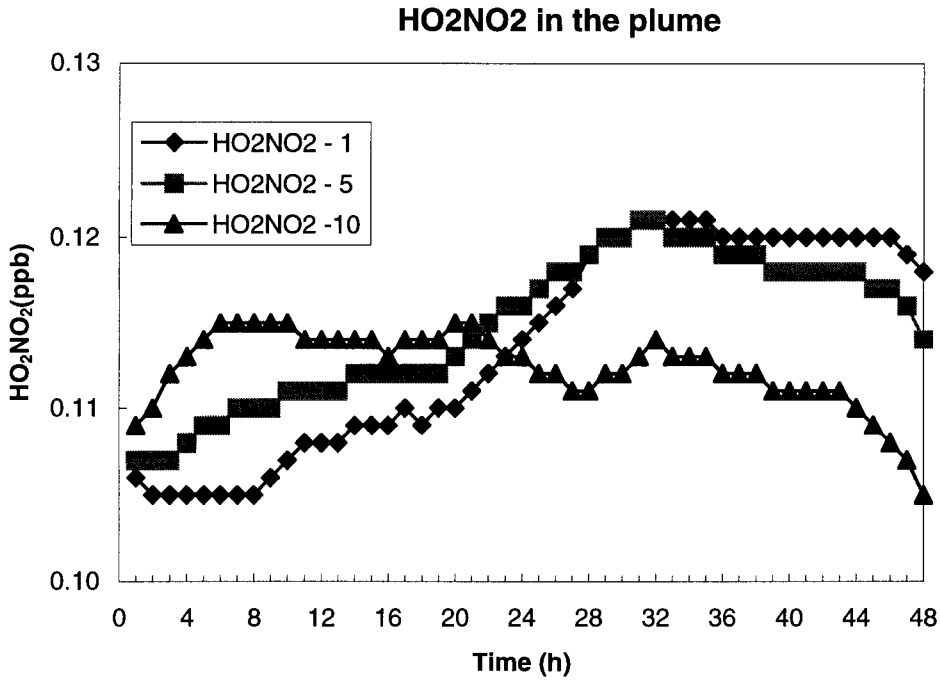

Figure 5. Time evolution over a 48-h period of the HO_2NO_2 concentration in the inner (1), middle (5) and outer (10) ring of a plume in the NAFC. Emissions took place at noon in July (summer). The background concentration of is 0.1 ppbv.

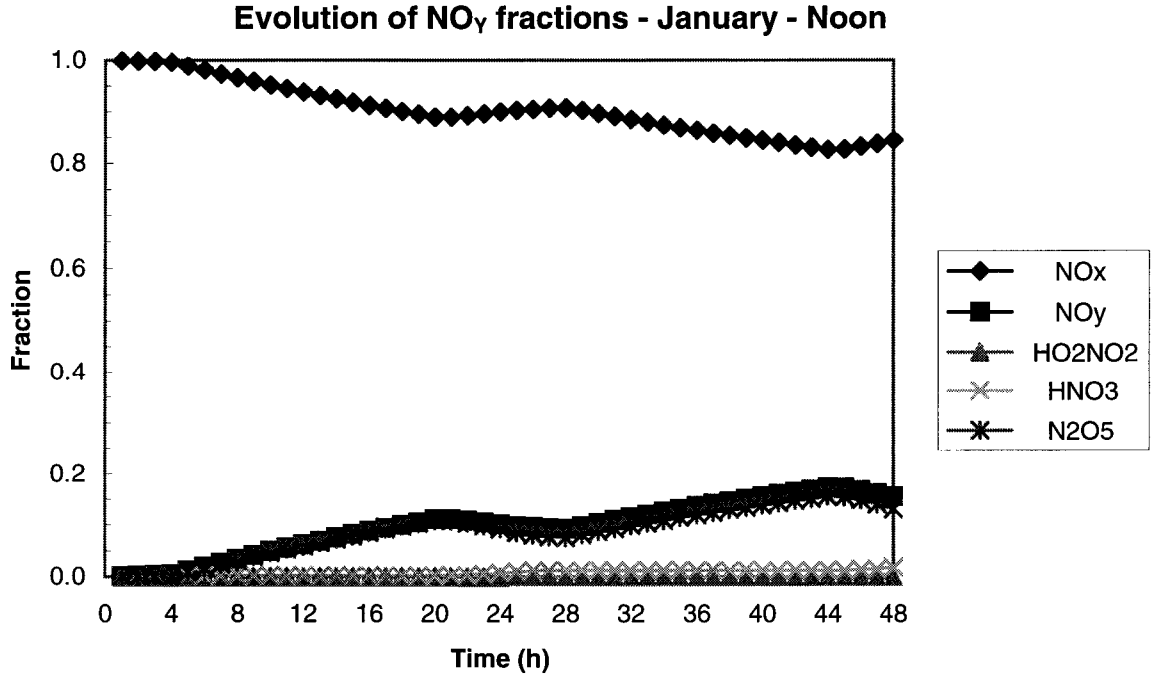

Figure 6. Time evolutions of the fractions of specific reactive nitrogen compounds compared with the sum of all reactive nitrogen compounds (emitted at noon in the NAFC in January (winter). The concentration represents the average over all rings in the plume. NO_y is defined as the sum of all reactive nitrogen compounds minus NO_x ($NO_x + NO_y = 1$).

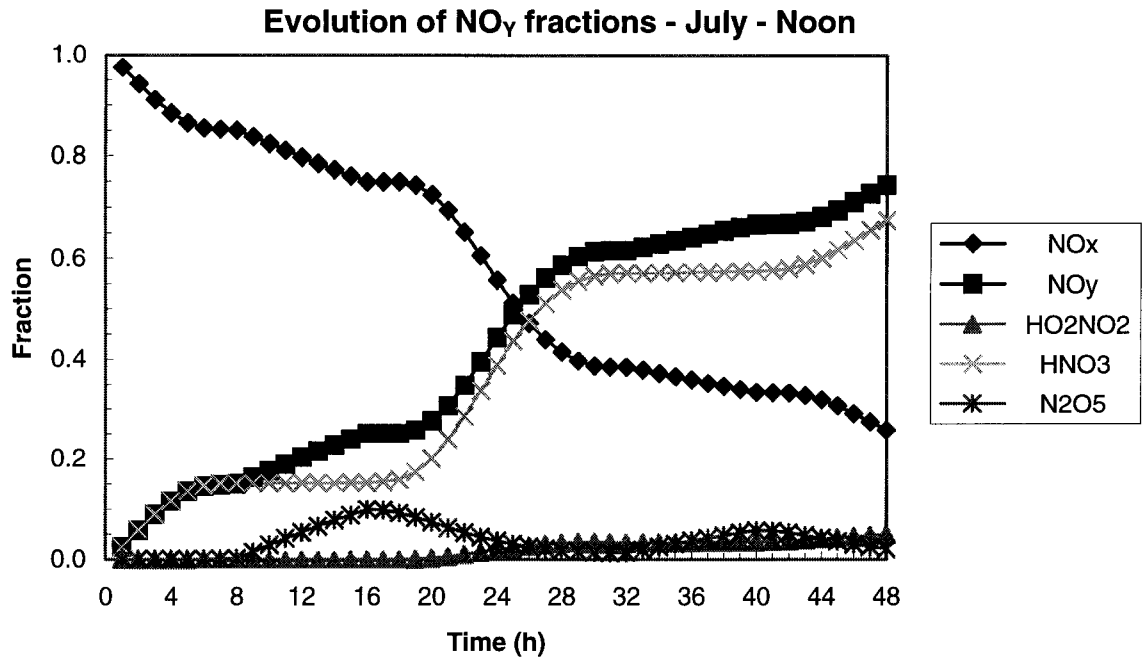

Figure 7. Time evolutions of fractions of the reactive nitrogen compounds emitted at noon in the NAFC in July (summer).

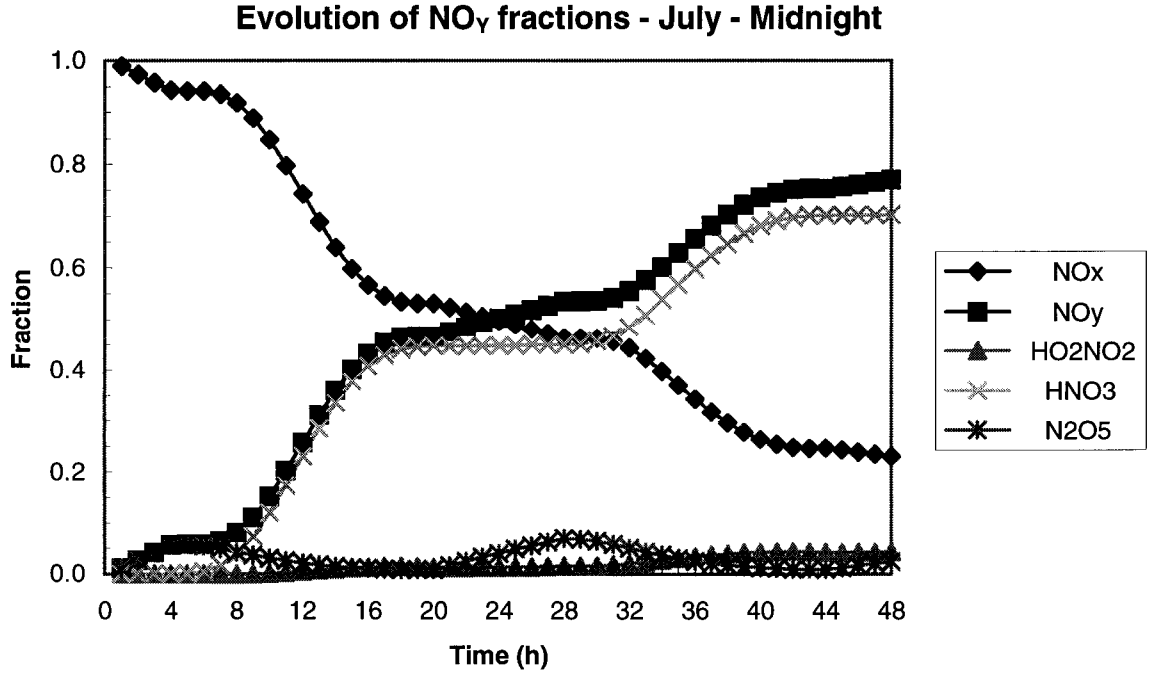

Figure 8. Time evolutions of the fractions of the reactive nitrogen compounds emitted at midnight in the NAFC in July (summer).

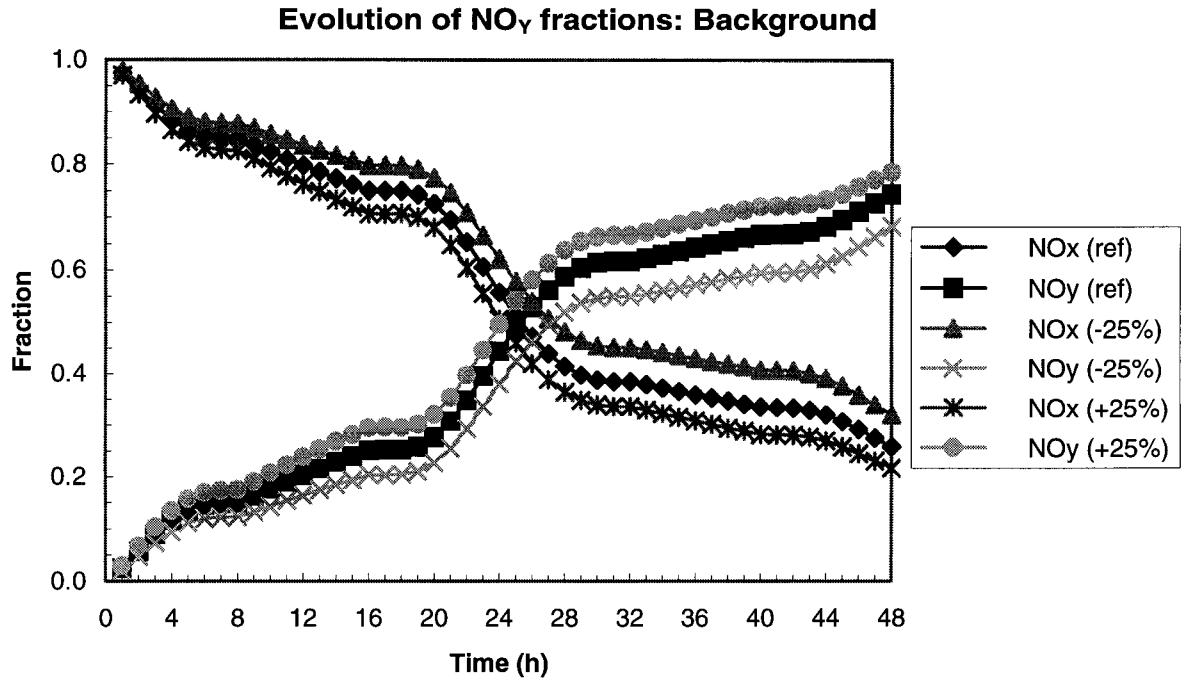

Figure 9. Time evolutions of the fractions of reactive nitrogen compounds emitted at noon in the NAFC in July (summer), for different background concentrations (-25%, normal, +25%).

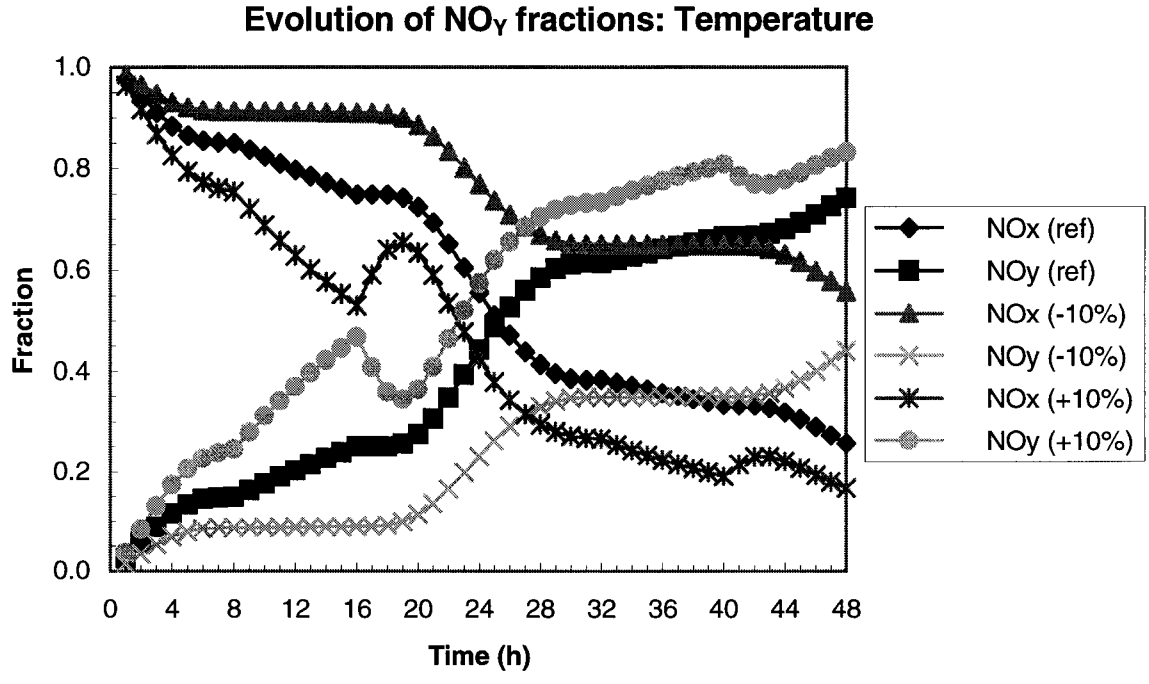

Figure 10. Time evolutions of the fractions of reactive nitrogen compounds emitted at noon in the NAFC in July (summer) for different background temperatures (-10%, normal, +10%).

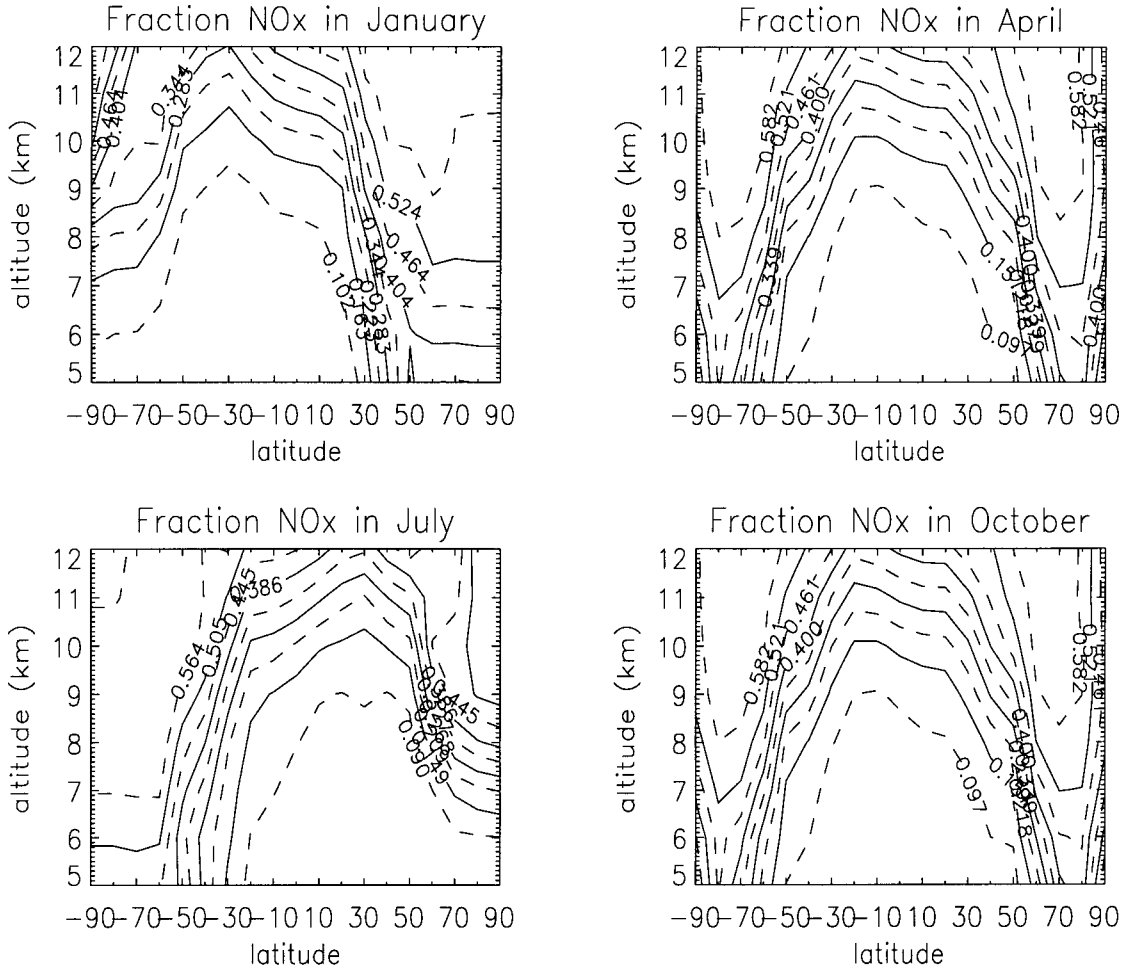

Figure 11. Fractions of NO_x, relative to the sum of all reactive nitrogen compounds, for the global domain after 48 h plume simulation, in January, April, July and October.

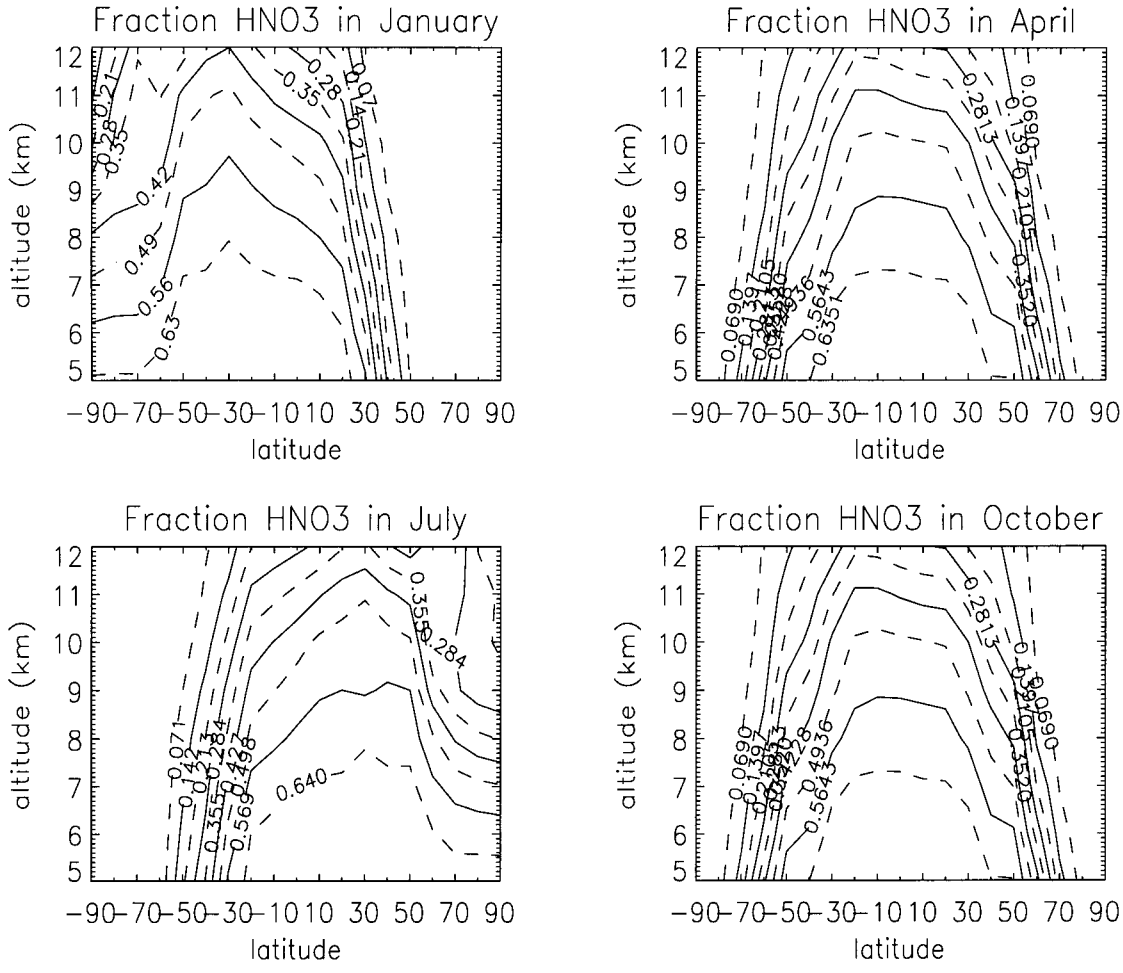

Figure 12. Fractions of HNO_3, relative to the sum of all reactive nitrogen compounds, for the global domain after 48 h plume simulation, for January, April, July and October. The fractions are averaged over emissions at 0.00, 6.00, 12.00 and 18.00.

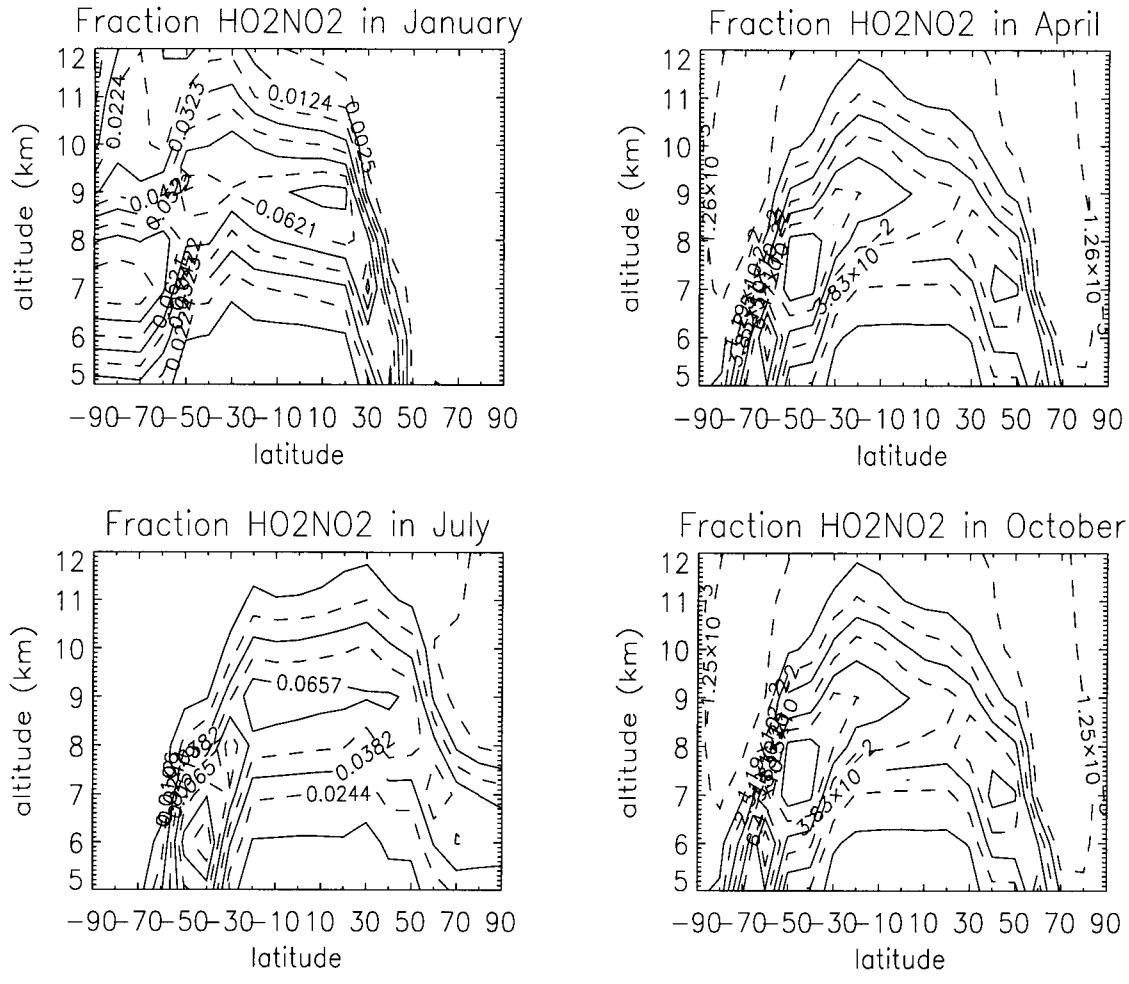

Figure 13. Fractions of HO_2NO_2, relative to the sum of all reactive nitrogen compounds, for the global domain after 48 h plume simulation, for January, April, July and October. The fractions are averaged over emissions at 0.00, 6.00, 12.00 and 18.00.

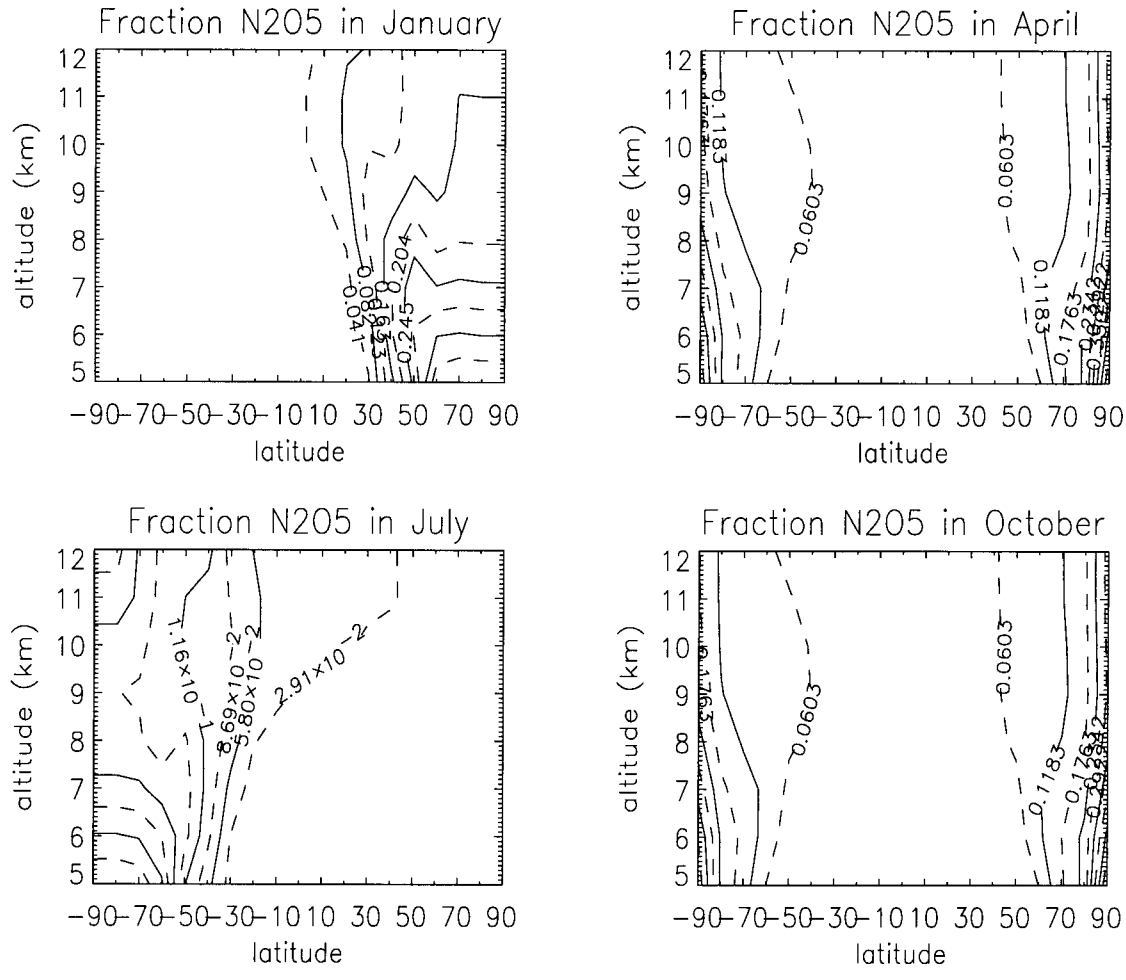

Figure 14. Fractions of N_2O_5, relative to the sum of all reactive nitrogen compounds, for the global domain after 48 h plume simulation, for January, April, July and October. The fractions are averaged over emissions at 0.00, 6.00, 12.00 and 18.00.

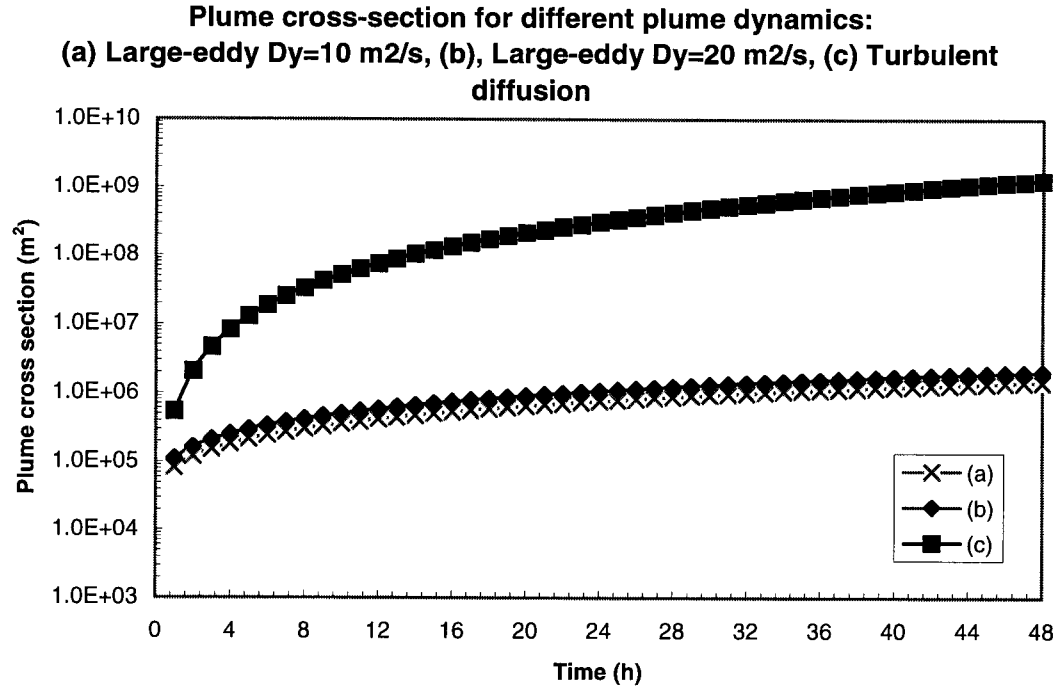

Figure 15. Cross-sections of the plume as a function of time for the three cases of plume dynamics: (a) large-scale turbulence dominated diffusion with $D_y = 10\ m^2s^{-1}$ and $D_z = 0.15\ m^2s^{-1}$; (b) large-scale turbulence dominated diffusion with $D_y = 20\ m^2s^{-1}$ and $D_z = 0.15\ m^2s^{-1}$; (c) scale-dependent diffusion. Emissions at noon at 10 km altitude, 50°N in July.

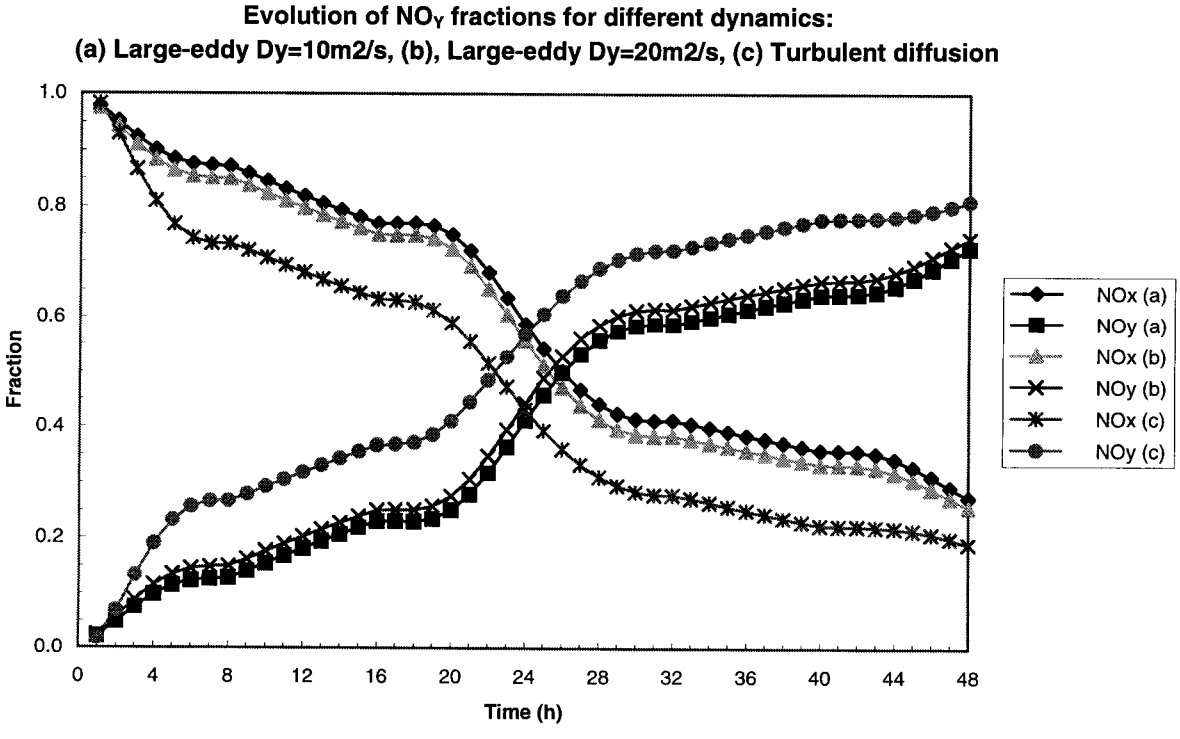

Figure 16. Fractions of NO_x and NO_y as a function of time for the three cases of plume dynamics. See Fig. 15.

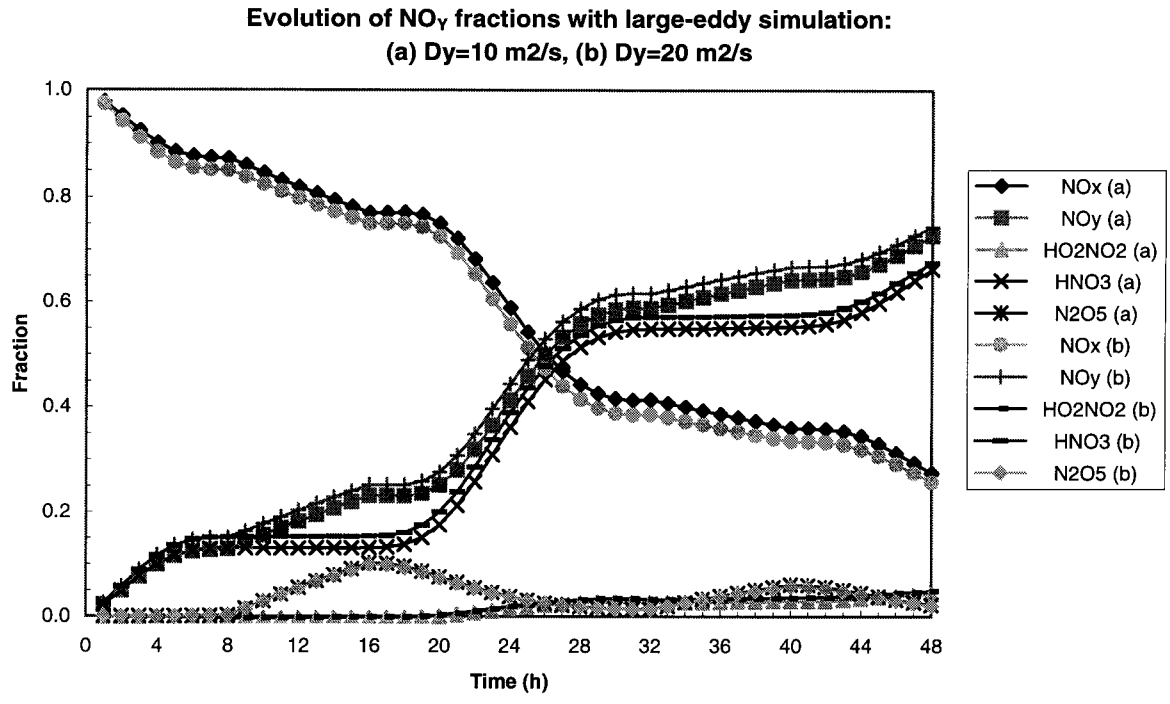

Figure 17. Fractions of NO_x, NO_y, HNO_3, HO_2NO_2 and N_2O_5 for the plume dynamics dominated by diffusion (cases a and b). See Fig. 15.

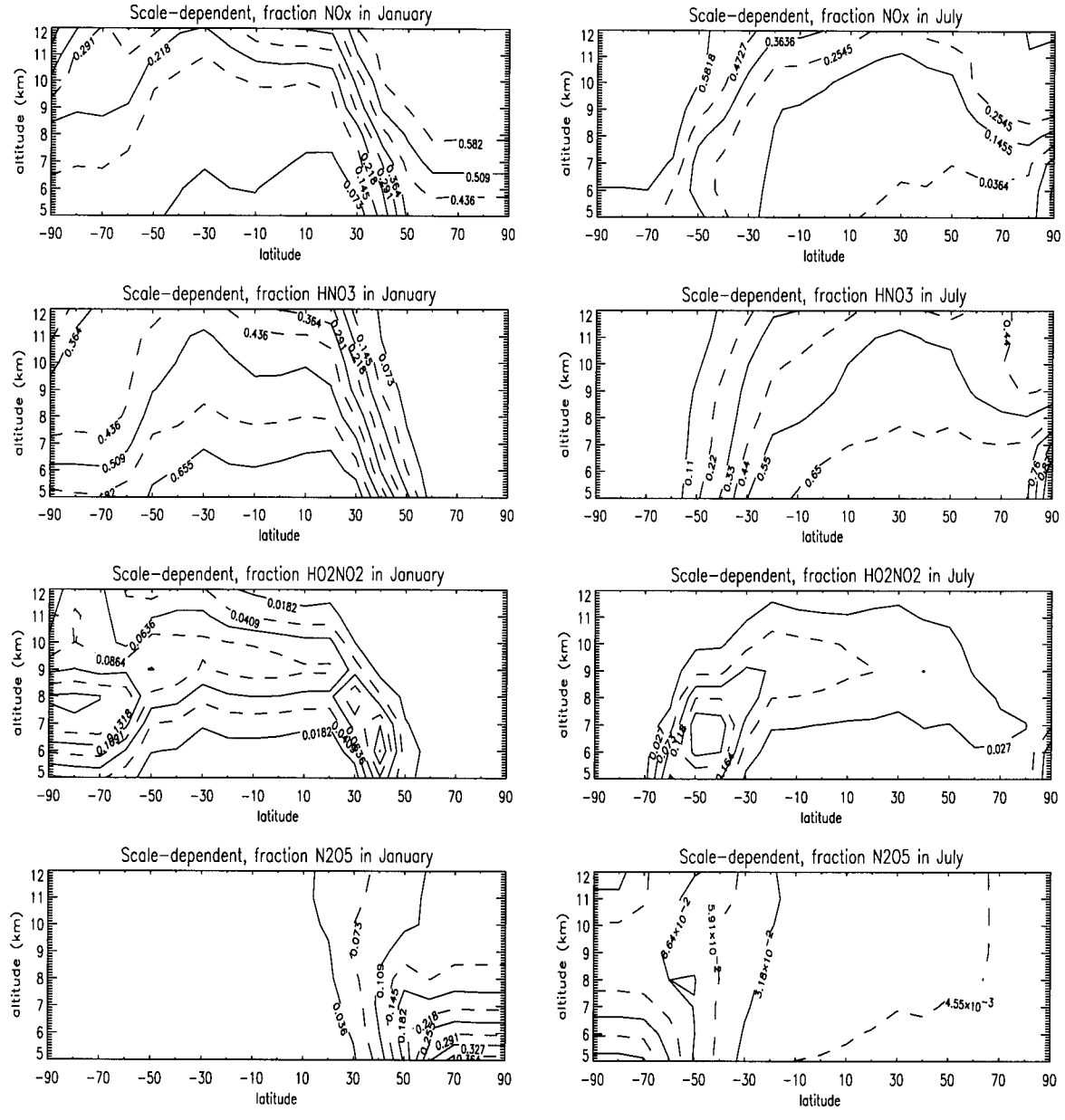

Figure 18. Fractions after 48 h of NO_x, HO_2NO_2, N_2O_5 and HNO_3 for January and July for the global domain in the case with scale-dependent diffusion (c).

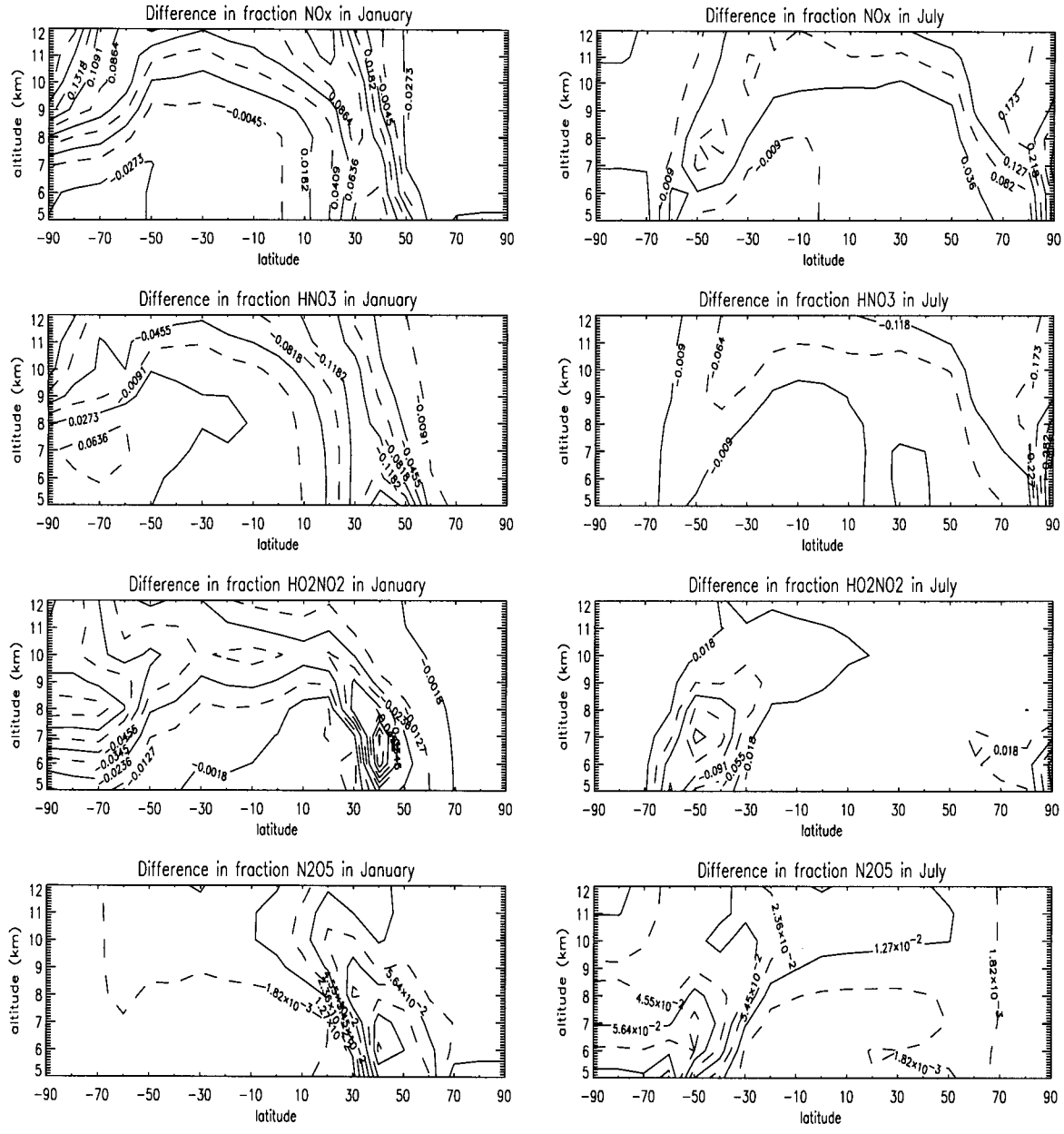

Figure 19. Difference (c-b) between the reactive nitrogen compounds fractions of the case with scale-dependent diffusion (c) and with large-scale diffusion(b). Differences of the fractions of NO_x, HNO_3, HO_2NO_2, N_2O_5 for January and July for the global domain.

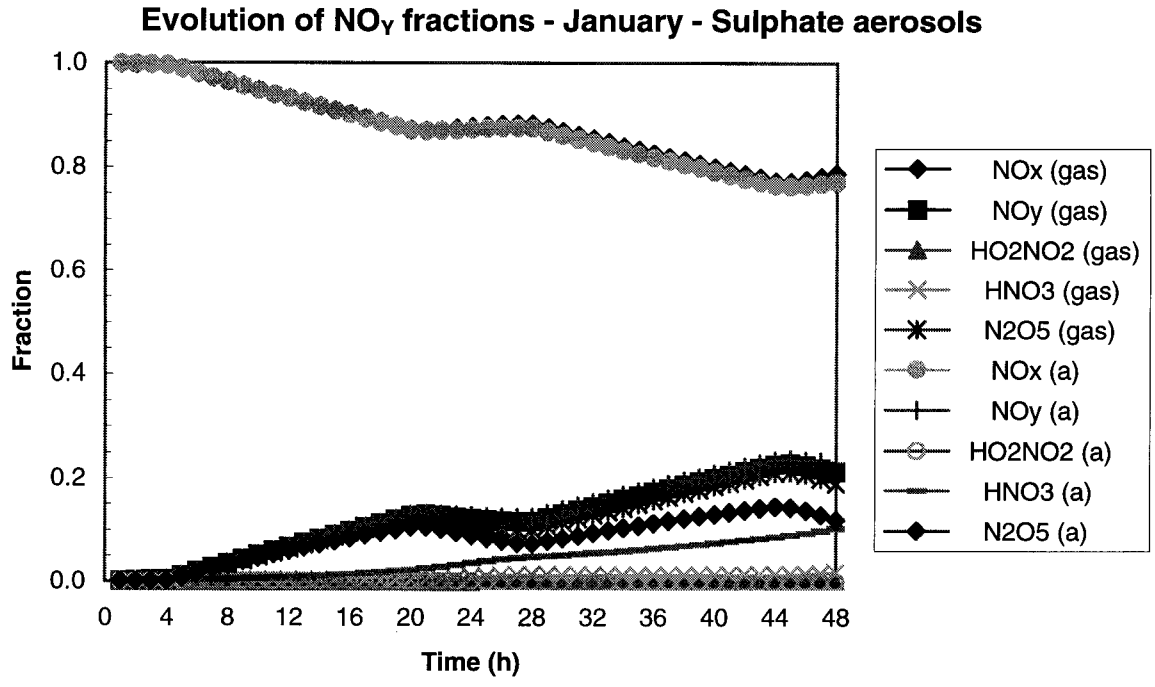

Figure 20. Time evolutions of the fraction of reactive nitrogen compounds for the heterogeneous reaction of N_2O_5 on sulphate aerosol (a) and only gas-phase chemistry. Emissions at noon in January in the NAFC (50°N, 10 km altitude).

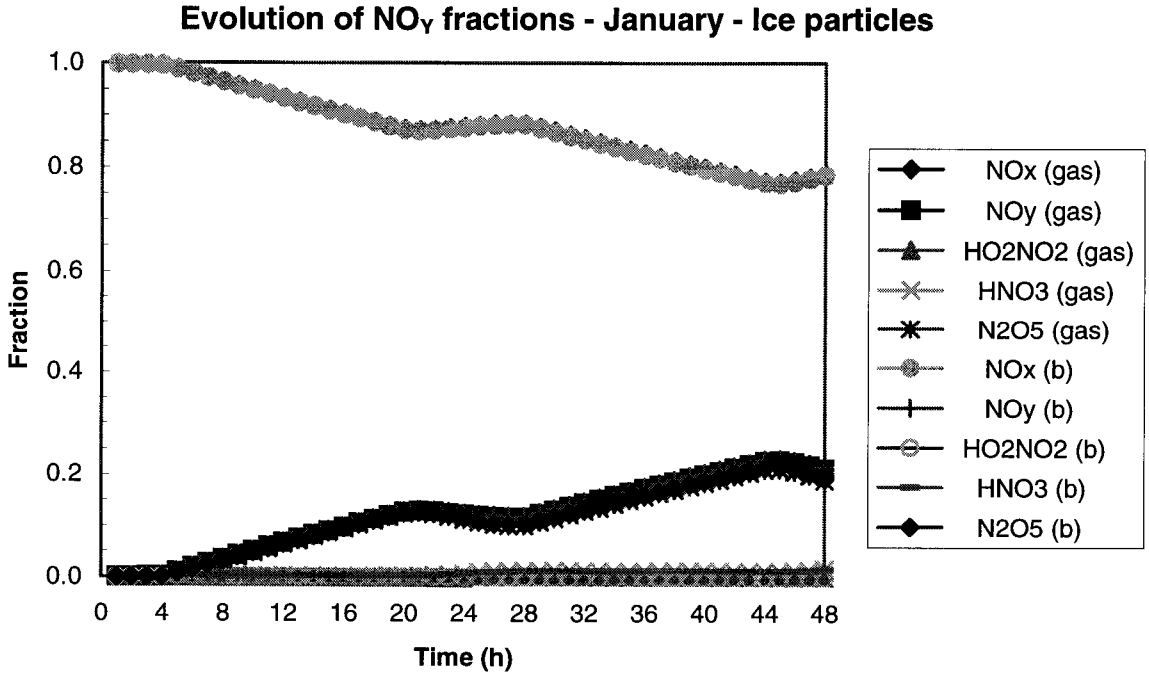

Figure 21. Time evolutions of the fraction of reactive nitrogen compounds for the heterogeneous reaction of N_2O_5 on ice particles (b) and only gas-phase chemistry. Emissions at noon in January in the NAFC.

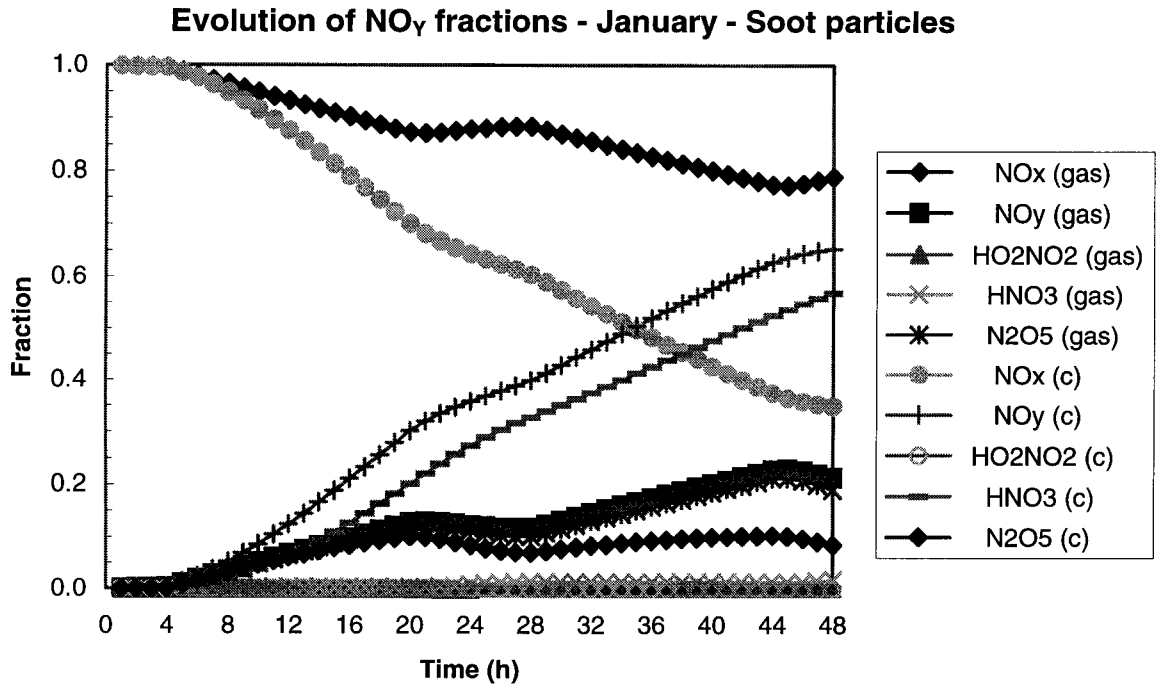

Figure 22. Time evolutions of the fraction of reactive nitrogen compounds for the heterogeneous reaction of N_2O_5 on wetted soot particles (c) and only gas-phase chemistry. Emissions at noon in January in the NAFC.

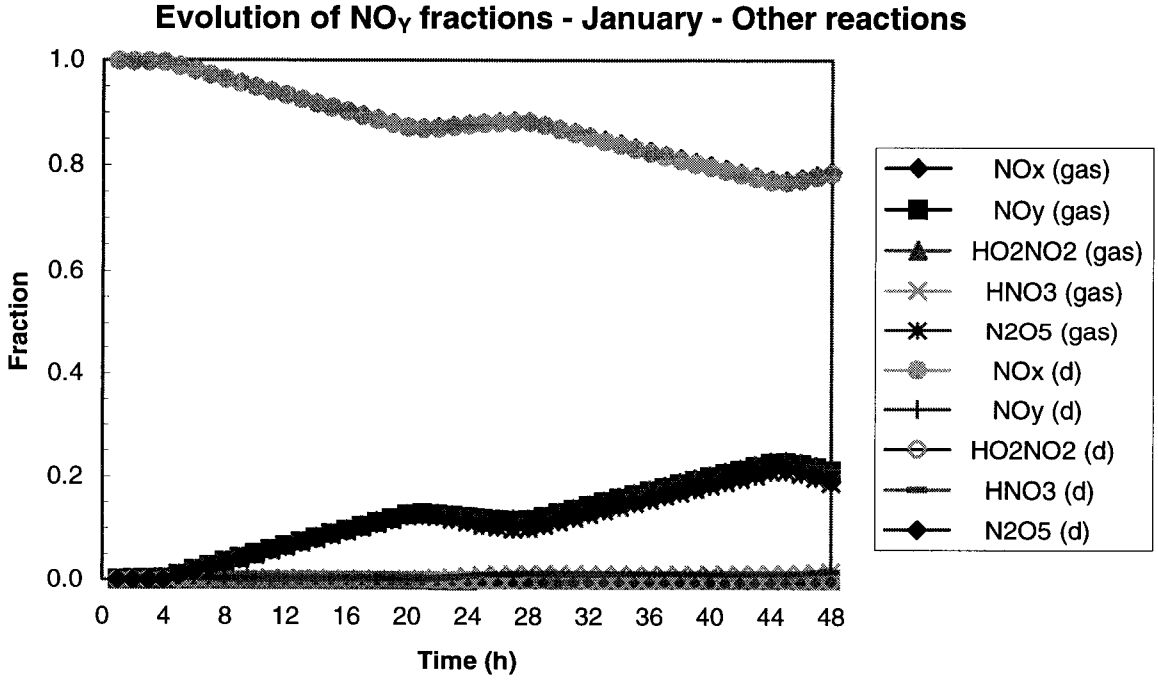

Figure 23. Time evolutions of the fraction of reactive nitrogen compounds for all other heterogeneous reactions (d) and only gas-phase chemistry. Emissions at noon in January in the NAFC.

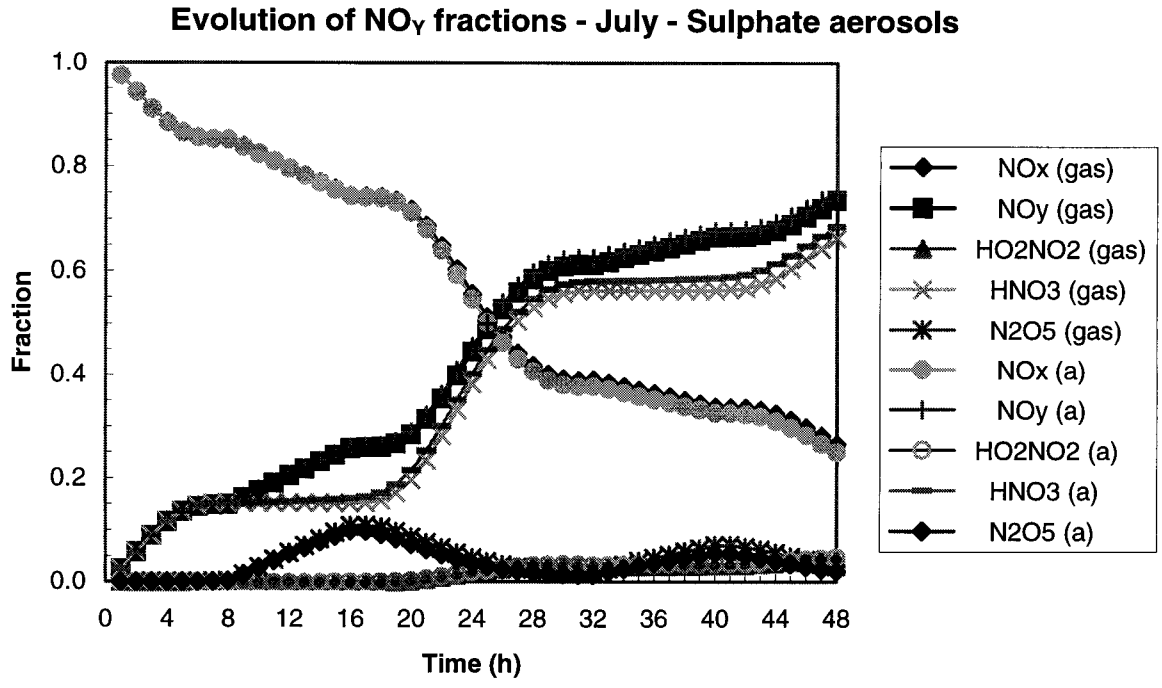

Figure 24. Time evolutions of the fraction of reactive nitrogen compounds for the heterogeneous reaction of N_2O_5 on sulphate aerosol (a) and with only gas-phase chemistry. Emissions at noon in July in the NAFC (50°N, 10 km altitude).

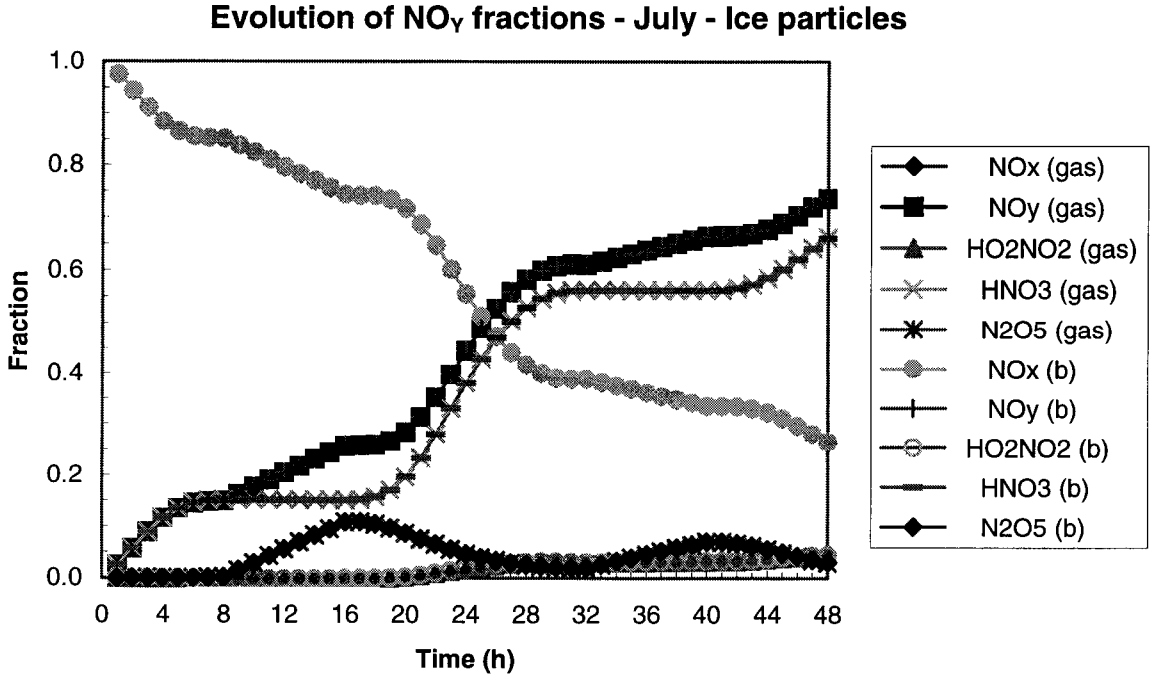

Figure 25. Time evolutions of the fraction of reactive nitrogen compounds for the heterogeneous reaction of N_2O_5 on ice particles (b) and only gas-phase chemistry. Emissions at noon in July in the NAFC.

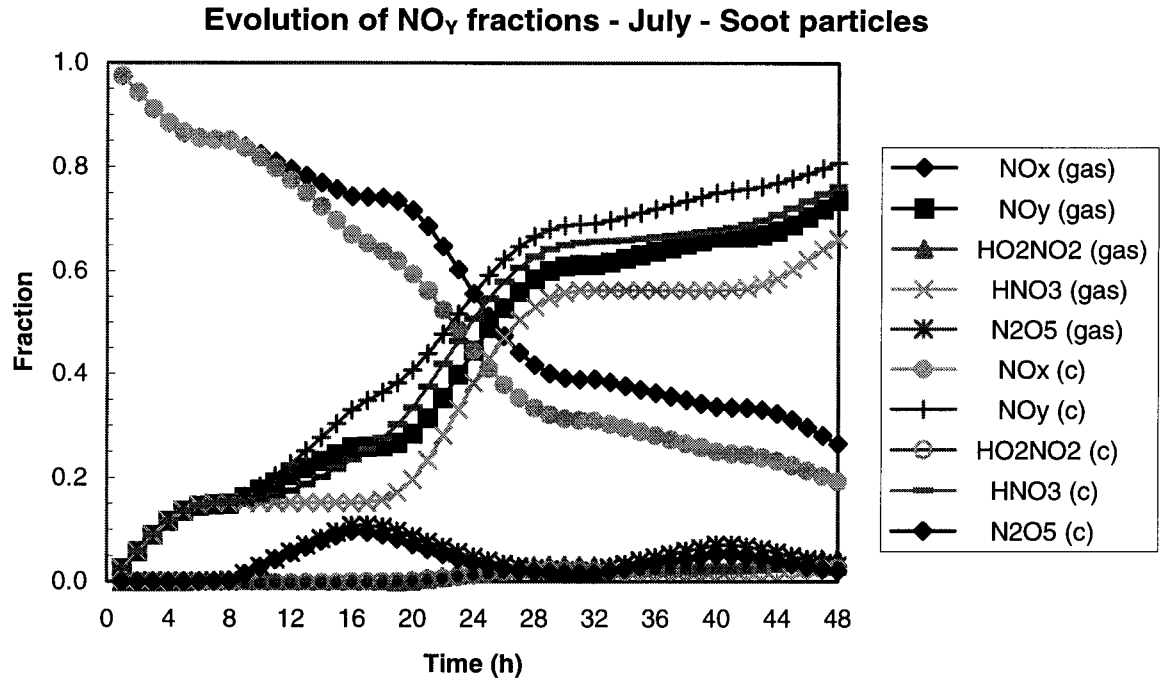

Figure 26. Time evolutions of the fraction of reactive nitrogen compounds for the heterogeneous reaction of N_2O_5 on wetted soot particles (c) and only gas-phase chemistry. Emissions at noon in July in the NAFC.

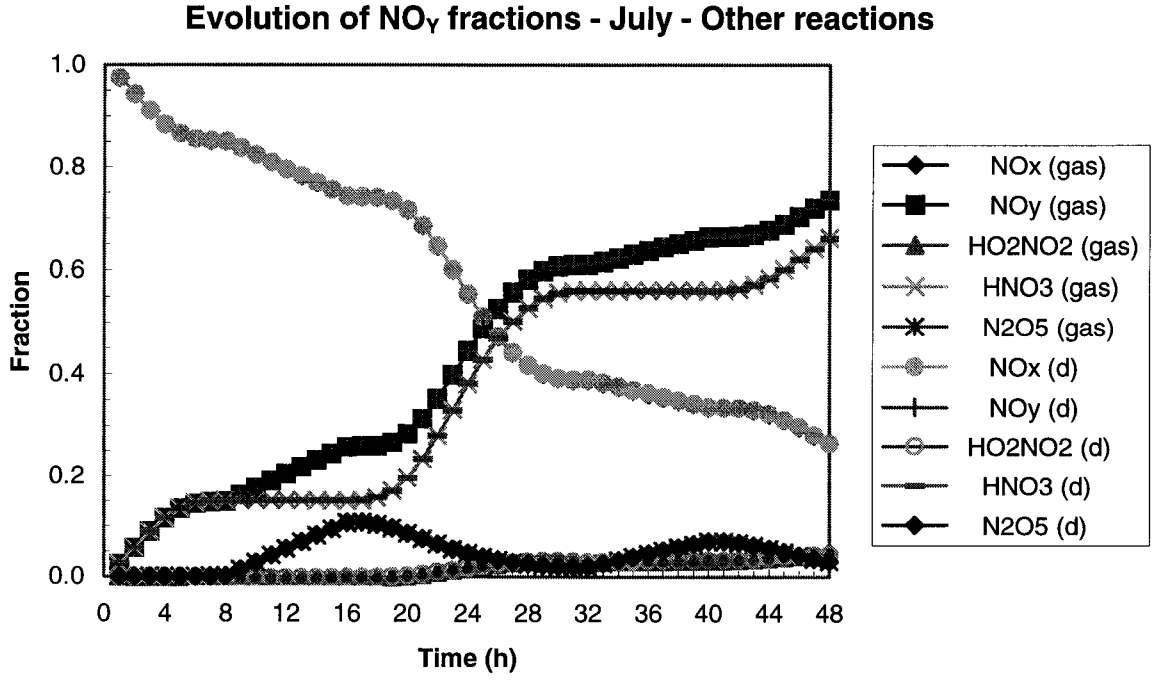

Figure 27. Time evolutions of the fraction of reactive nitrogen compounds for all other heterogeneous reactions (d) and only gas-phase chemistry. Emissions at noon in July in the NAFC.

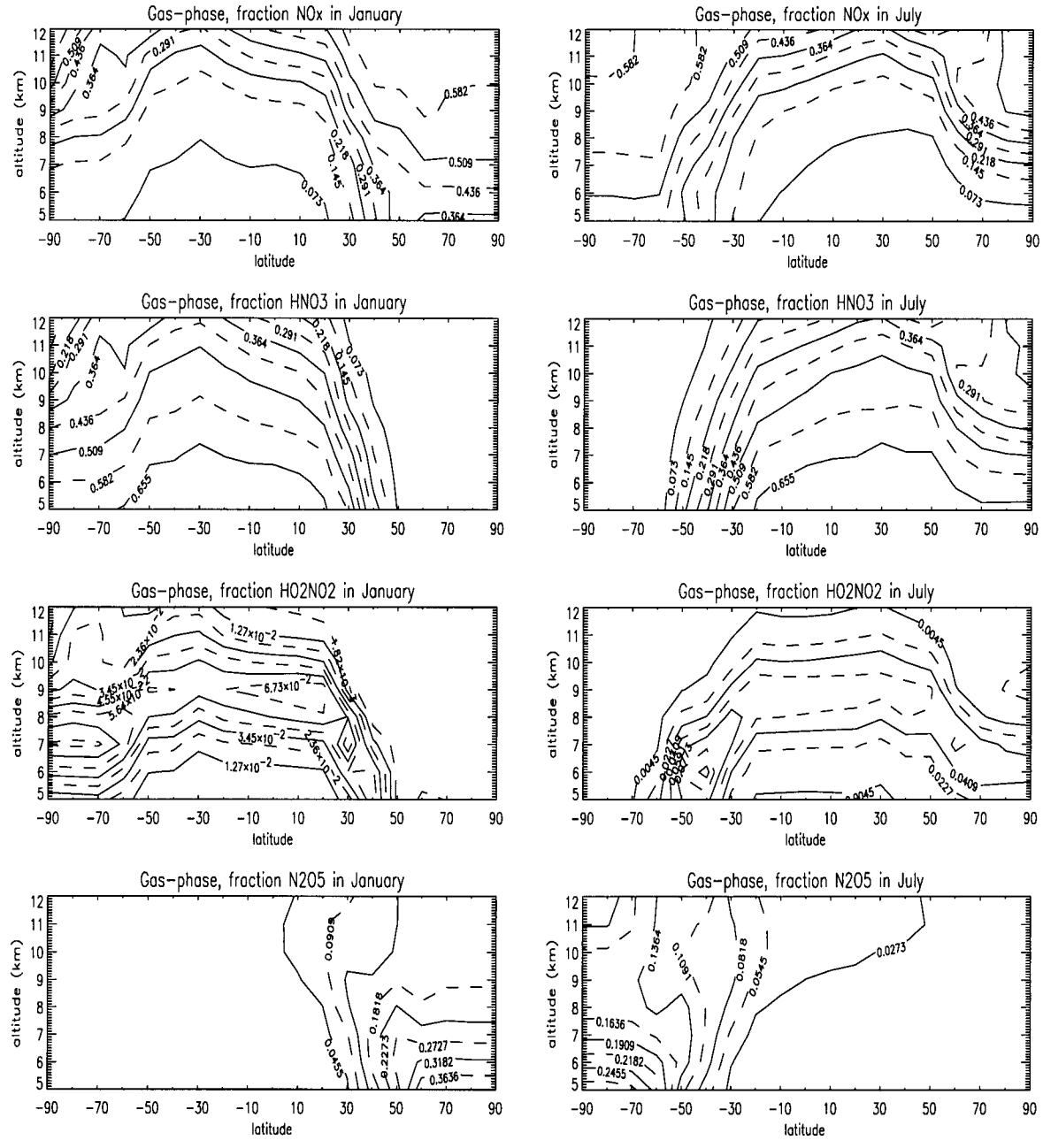

Figure 28. The fractions of NO_x, HNO_3, HO_2NO_2, and N_2O_5 for January and July for the global domain with only gas-phase chemistry (after 48 h). Fractions averaged over emissions at 0.00, 6.00, 12.00 and 18.00.

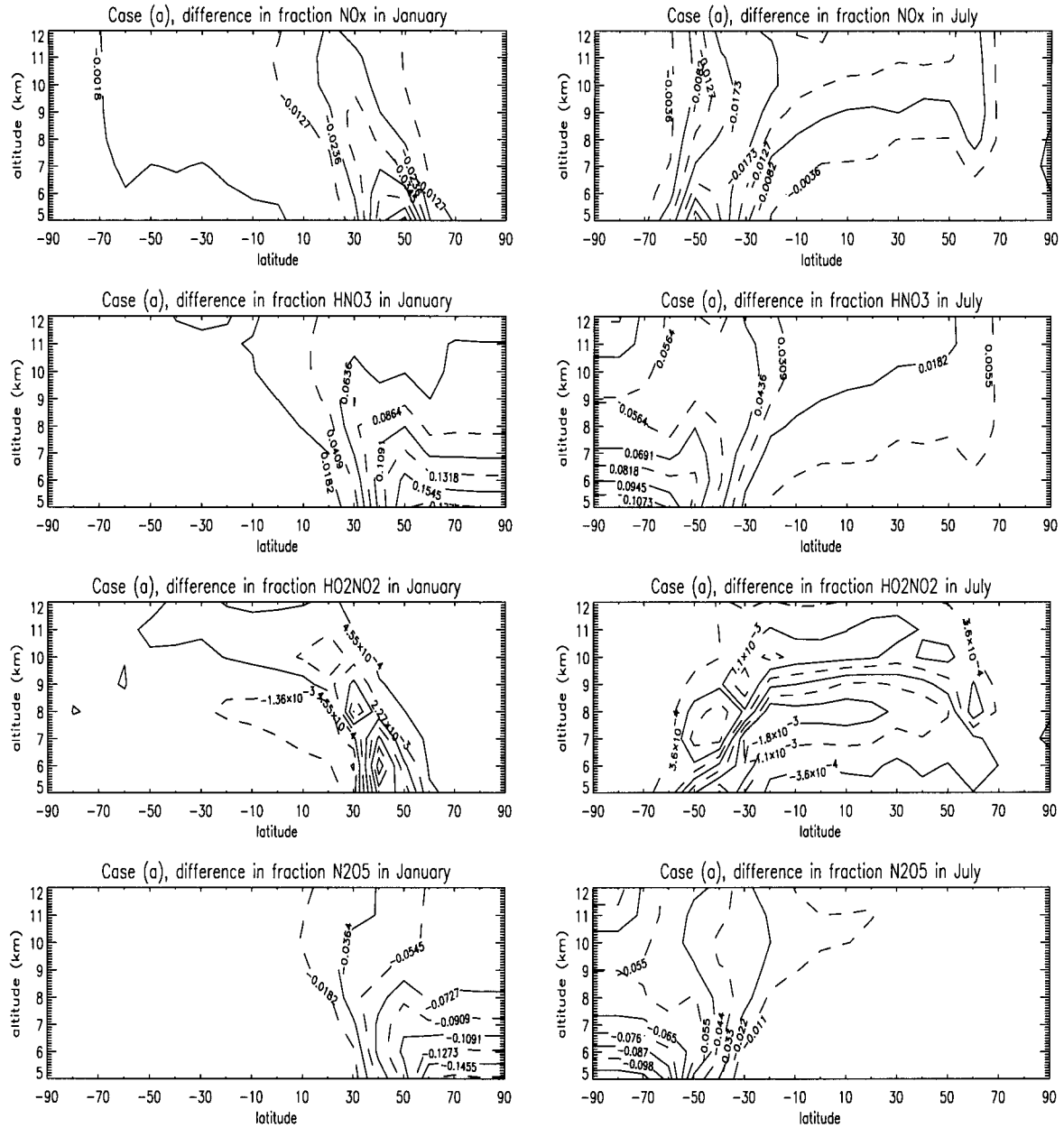

Figure 29. Differences (= case a - gas) in reactive nitrogen compound fractions (NO_x, HNO_3, HO_2NO_2, N_2O_5) between the case with the heterogeneous reaction of N_2O_5 on sulphate aerosol (a) and only gas-phase chemistry the for January and July (after 48 h).

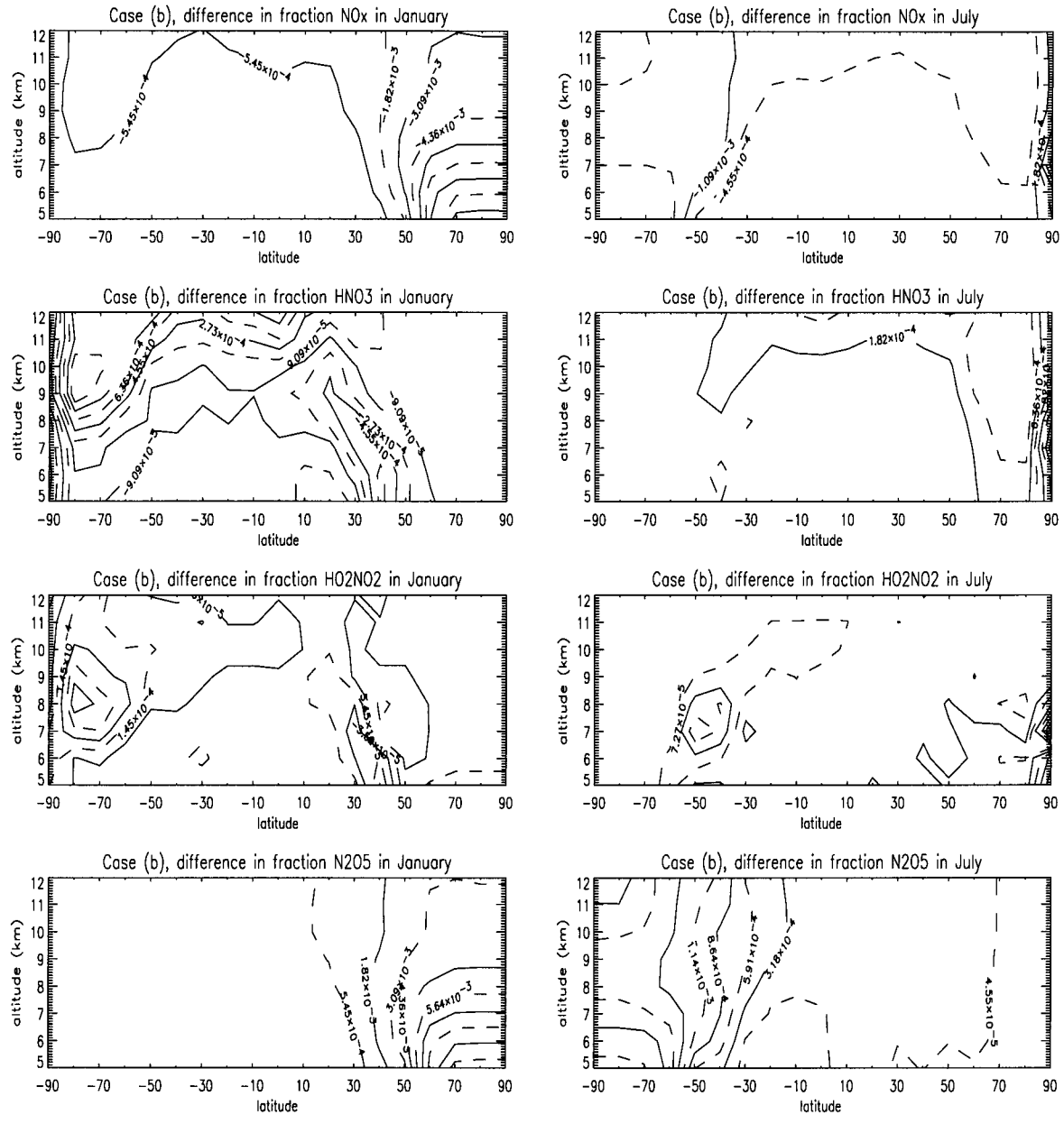

Figure 30. Differences (= case b - gas) in reactive nitrogen compound fractions (NO_x, HNO_3, HO_2NO_2, N_2O_5) between the case with the heterogeneous reaction of N_2O_5 on ice particles (b) and only gas-phase chemistry for January and July (after 48 h).

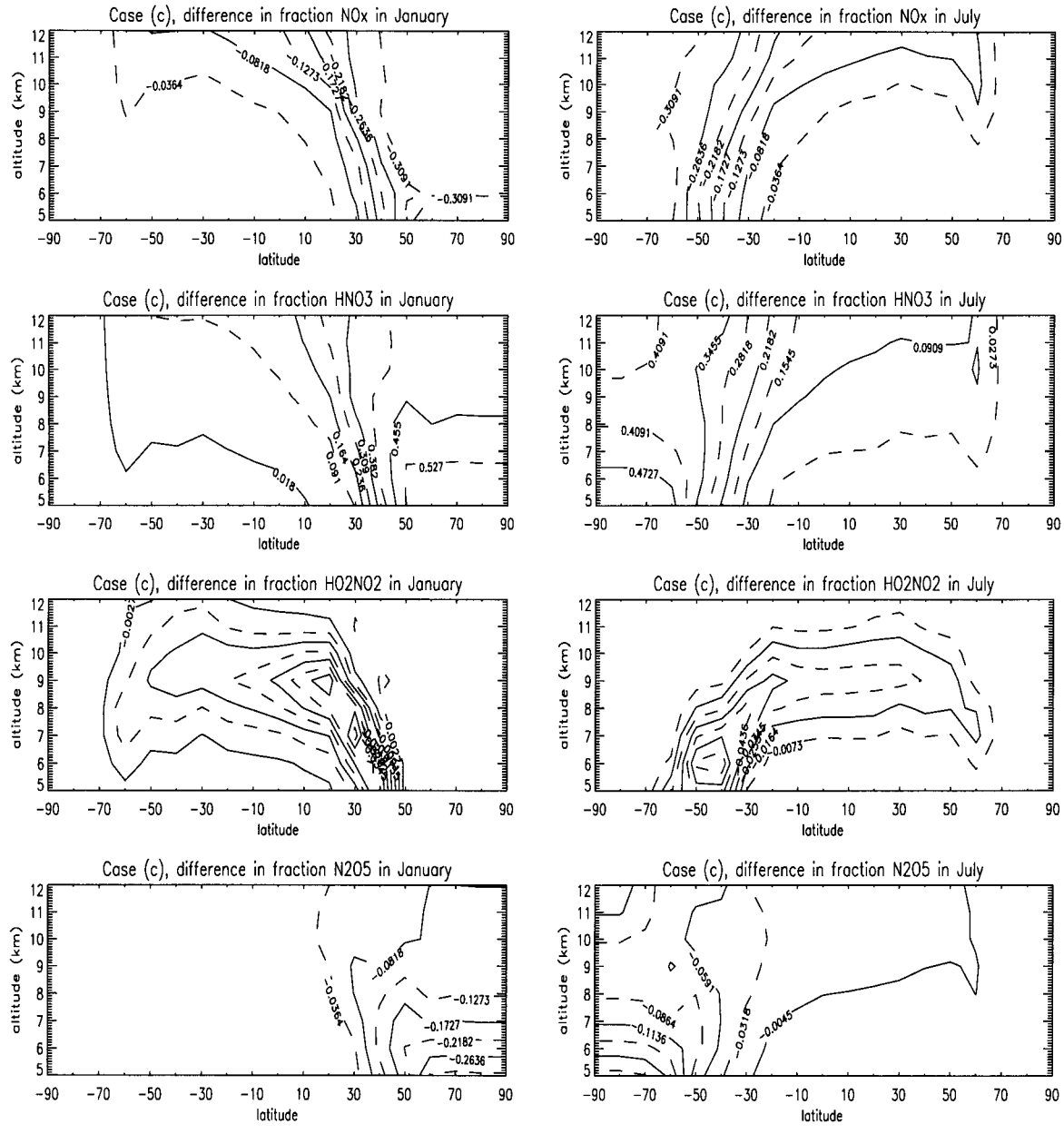

Figure 31. Differences (= case c - gas) in reactive nitrogen compound fractions (NO_x, HNO_3, HO_2NO_2, N_2O_5) between the case with the heterogeneous reaction of N_2O_5 on wetted soot aerosol (c) and only gas-phase chemistry for January and July (after 48 h).

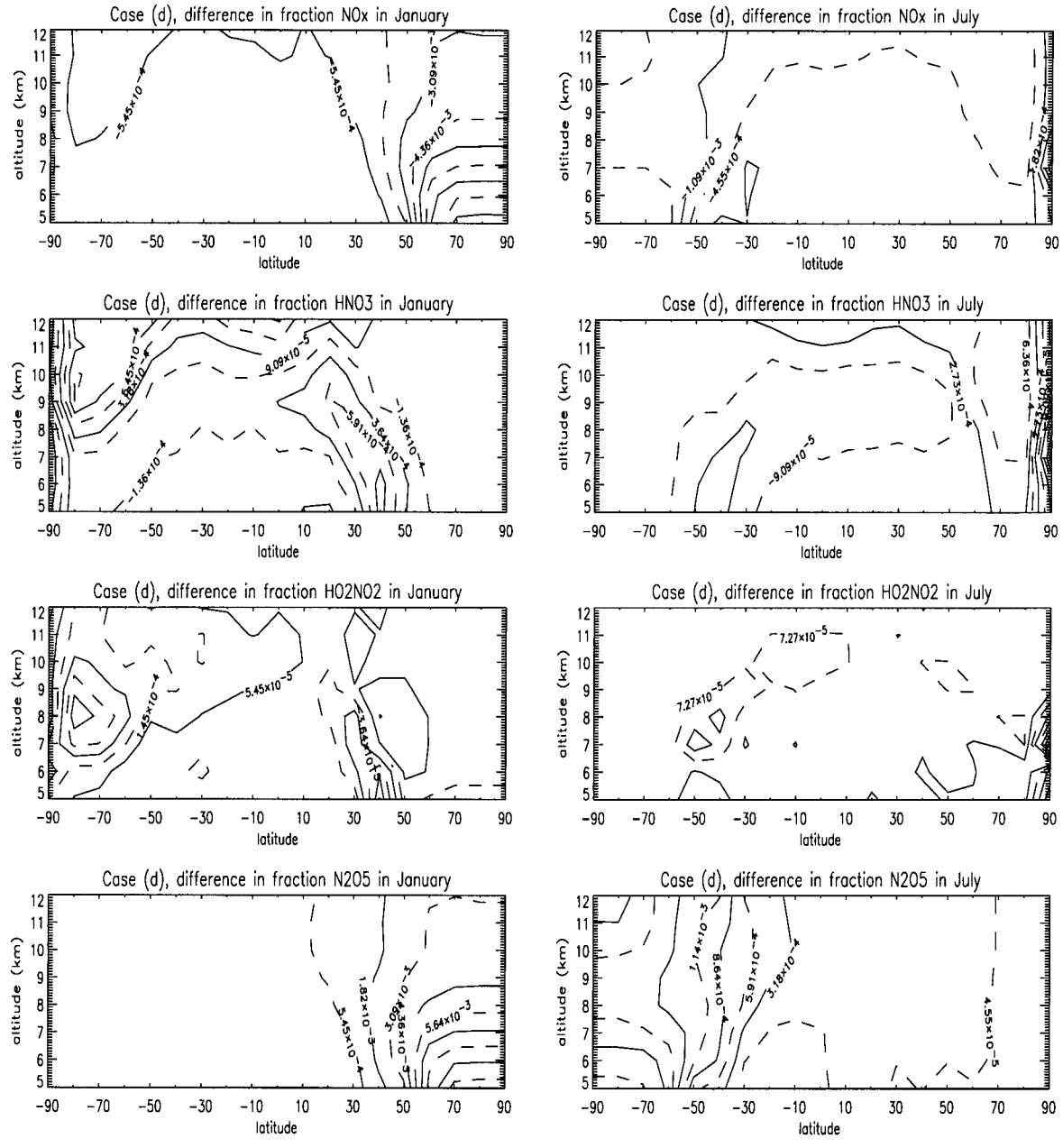

Figure 32. Differences (= case d - gas) in reactive nitrogen compounds fractions (NO_x, HNO_3, HO_2NO_2, N_2O_5) between the case with all other heterogeneous reactions on sulphate aerosol (d) and only gas-phase chemistry for January and July (after 48 h).

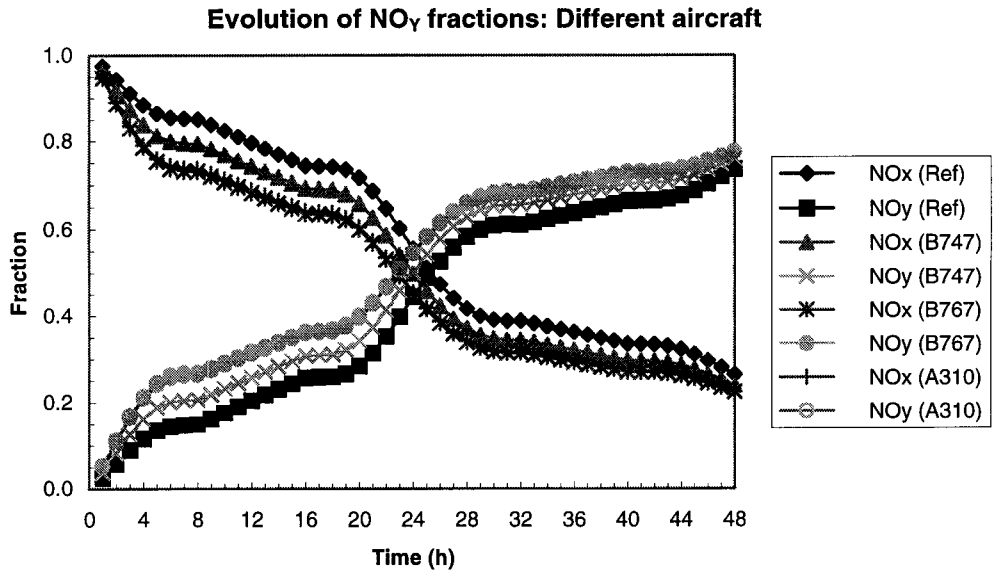

Figure 33. Fractions NO_x and NO_y of emission of different aircraft in the NAFC in July: Reference point forms the B747-400 RIVM emission data, the other aircraft emission data (B747-400, B767-300, A310-200) is from NLR. Emissions occur at noon.

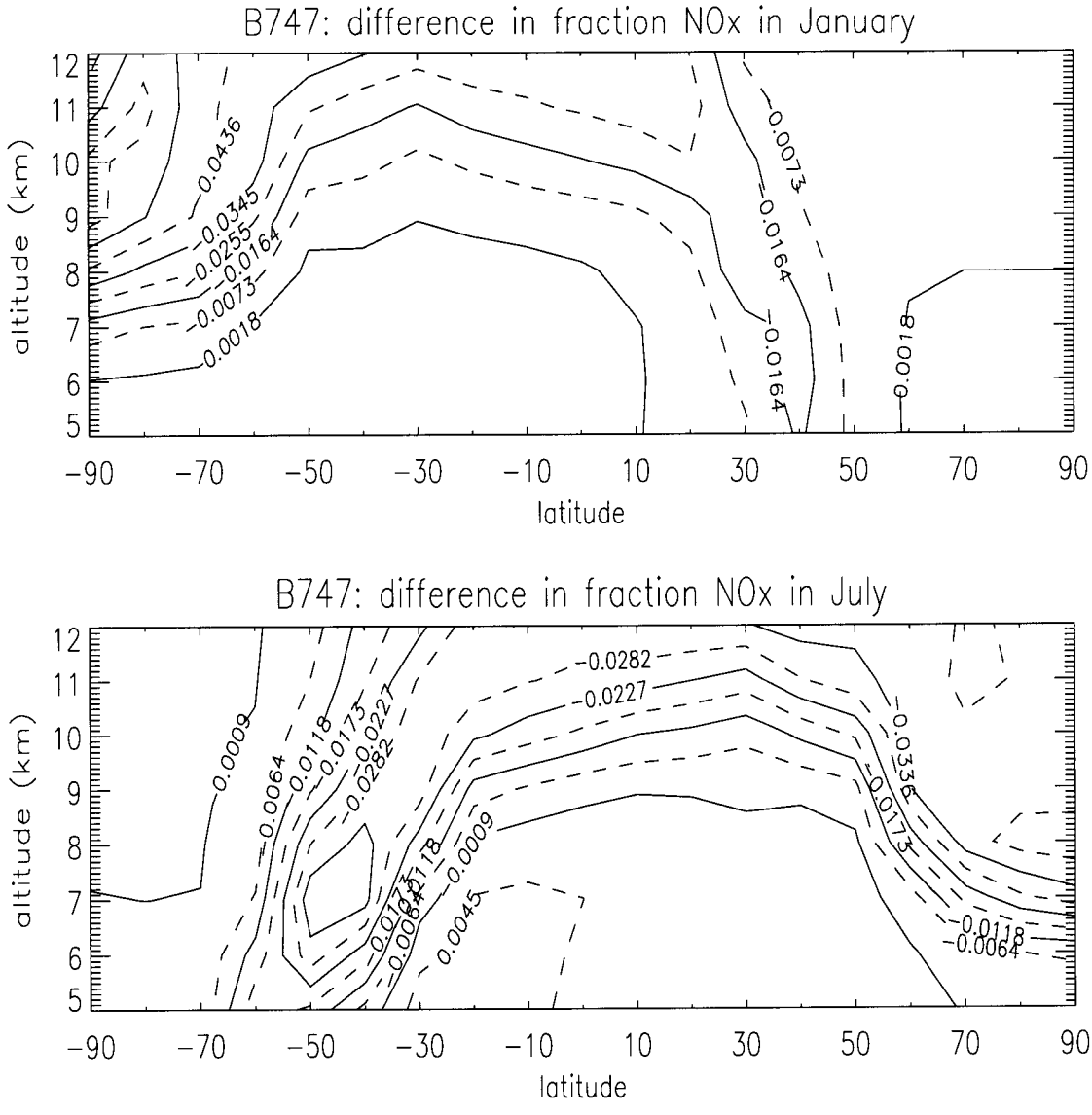

Figure 34. Differences (= RIVM - NLR) in NO_x fractions for January and July calculated with emission data of a B747-400 from RIVM and NLR, after 48 h plume simulation.

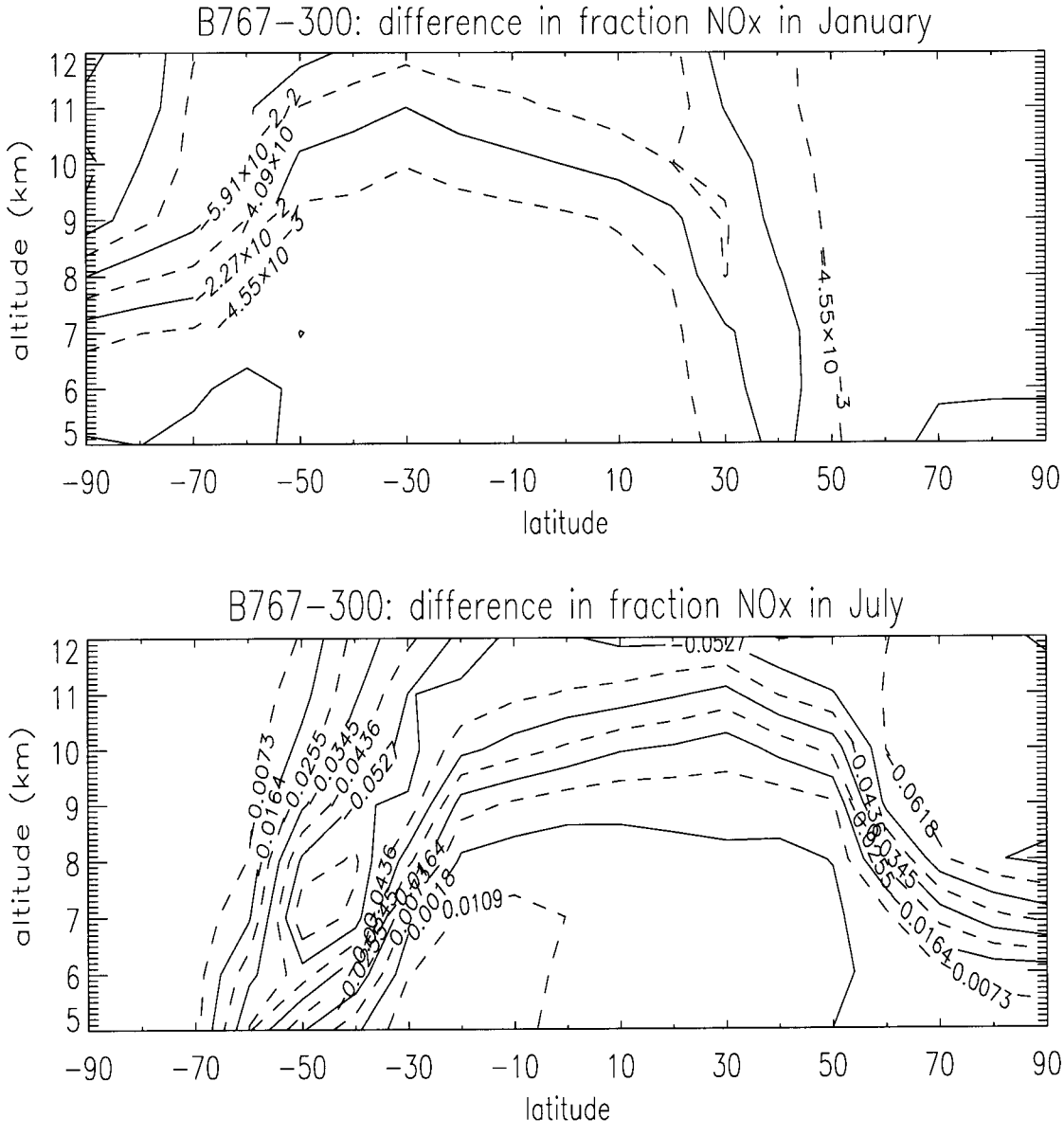

Figure 35. Differences (= B747-400 - B767-300) in NO_x fractions for January and July calculated with emission data of a B747-400 (RIVM) and a B767-300 (NLR), after 48 h plume simulation.

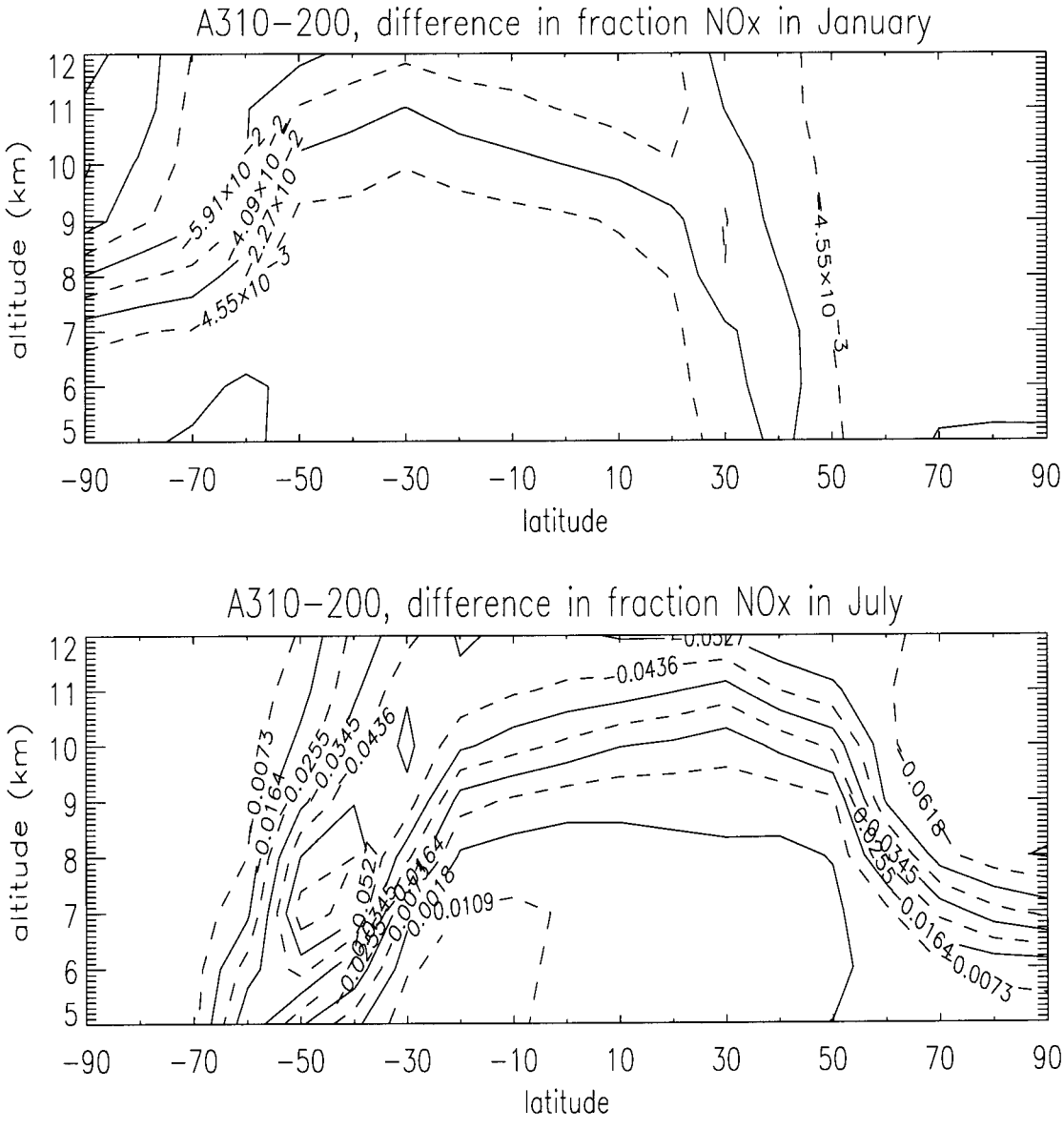

Figure 36. Differences (= B747-400 - A310-200) in NO_x fractions for January and July calculated with emission data of a B747-400 (RIVM) and a A310-200 (NLR), after 48 h plume simulation.